Understanding evolving urban air pollution sources with emissions measurement applications

Samuel J. Cliff

Doctor of Philosophy

University of York

Chemistry

October, 2023

Abstract

Air pollution continues to be a critical issue of concern for the environment and human health. The human response to improve air quality requires accurate data in the form of up-to-date emissions inventories. This thesis describes the measurement and analysis of two unique data sets characterising real-world emissions of air pollutants that address uncertainties in sources of emerging importance. Specifically, an urban eddy covariance application measured long-term (2020-2023) NO_x and CO_2 fluxes from a tall tower in central London. The measurements showed the first transition from road transport-dominated to commercial-heating-dominated NO_x emissions in a megacity. It was calculated that the heat and power generation sector now contributes 76 ± 17 % of NO_x emissions in the central London area. Despite this, European emissions inventories were determined to overestimate commercial NO_x emissions by an average of 53 % due to outdated emissions factors. The observations showed that the heat and power generation sector will require some policy consideration if World Health Organisation guidelines are to be achieved in densely populated urban environments. However, very low concentrations of NO_2 are possible provided the correct infrastructure pathways are provided as part of urban decarbonisation. The use of a mobile laboratory facilitated the application of advanced mass spectrometric instrumentation in the field and the discovery of a large source of NMVOCs missing from international road transport emissions inventories. The non-fuel-related source was attributed to screenwash application and was greater than the total of all VOCs emitted from vehicle exhausts and their associated evaporative fuel losses. In contrast to predictions, vehicle VOC emissions may increase given a predicted growth in total vehicle kilometers driven and the missing source being independent of the vehicle energy/propulsion system. Overall, improvements to current emissions inventories are recommended, and it is hoped that the findings will positively influence future air quality policy strategies.

Contents

List of figures

List of tables

Acknowledgements

The completion of my Doctor of Philosophy programme took support from a number of parties. I would like to thank the National Environmental Research Council (NERC) for funding this research via the Panorama Doctoral Training Partnership and the Integrated Research Observation System for Clean Air (OSCA). I thank my supervisors James Lee, Sarah Moller and Marvin Shaw for the opportunity to undertake this PhD and for their guidance during my time at the Wolfson Atmospheric Chemistry Laboratories (WACL). I would like to additionally thank Ally Lewis for his constant stream of ideas, and Will Drysdale for the hours of flux-related chat he has endured with me. These last three years have been made very enjoyable by the rest of my colleagues at WACL and the wider Chemistry Department at the University of York. Finally, I would like to thank my friends and family, in particular Rhianna Evans, for their support and encouragement in everything that I do.

Author's declaration

I declare that this thesis is a presentation of original work and I am the sole author. This work has not previously been presented for an award at this, or any other, University. All sources are acknowledged as References. Chapters 2 and 4 are based on peer-reviewed publications of which I am the lead author. Chapter 3 has been prepared for submission to Atmospheric Chemistry and Physics. Details of these publications are:

Cliff, S. J., Drysdale, W., Lee, J. D., Helfter, C., Nemitz, E., Metzger, S., and Barlow, J. F. Pandemic restrictions in 2020 highlight the significance of non-road NO_x sources in central London, *Atmospheric Chemistry and Physics*, 23, 2315-2330, 2023. DOI: https://doi.org/10.5194/acp-23-2315-2023.

Cliff, S. J., Drysdale, W., Lewis, A. C., Moller, S. J., Helfter, C., Nemitz, E., Metzger, S., Liddard, R., Barlow, J.F., Beevers, S., Carslaw, D., and Lee, J. D. Commercial space heating is the largest source of NO_x in central London. *Prepared for Atmospheric Chemistry and Physics*.

Cliff, S. J., Lewis, A. C., Shaw, M. D., Lee, J. D., Flynn, M., Andrews, S. J., Hopkins, J. R., Purvis, R. M., and Yeoman, A. M. Unreported VOC emissions from road transport including from electric vehicles, *Environmental Science & Technology*, 57, 8026-8034, 2023. DOI: https://doi.org/10.1021/acs.est.3c00845.

Chapter 1

Introduction

1.1 The atmosphere

The earth's dry atmosphere, which excludes highly variable water vapour levels, is approximately 78.08% nitrogen, 20.95% oxygen, and 0.93% argon by volume. The remaining 0.04% corresponds to a mix of compounds known as trace gases. Although trace gases exist in small amounts in the atmosphere, they play an essential role in sustaining life on Earth and directly or indirectly influence all atmospheric processes. The bulk of the trace gas volume can be seen in Figure 1.1 and is mostly made up of carbon dioxide (CO_2), with additional contributions from the noble gases Ne, He, Kr, and H_2, as well as CH_4.[1] A final component of the atmospheric trace gases are gaseous air pollutants which are typically another 1-6 orders of magnitude smaller in relative volume. An air pollutant is defined as a contamination of the indoor or outdoor environment by any chemical, physical or biological agent that modifies the natural characteristics of the atmosphere. As such, the definition is not limited to the gaseous phase and includes suspensions of both liquid and solid particulate matter. Air pollution has a high spatial and temporal variability around the globe and is thought to be the largest environmental risk to human health.[2]

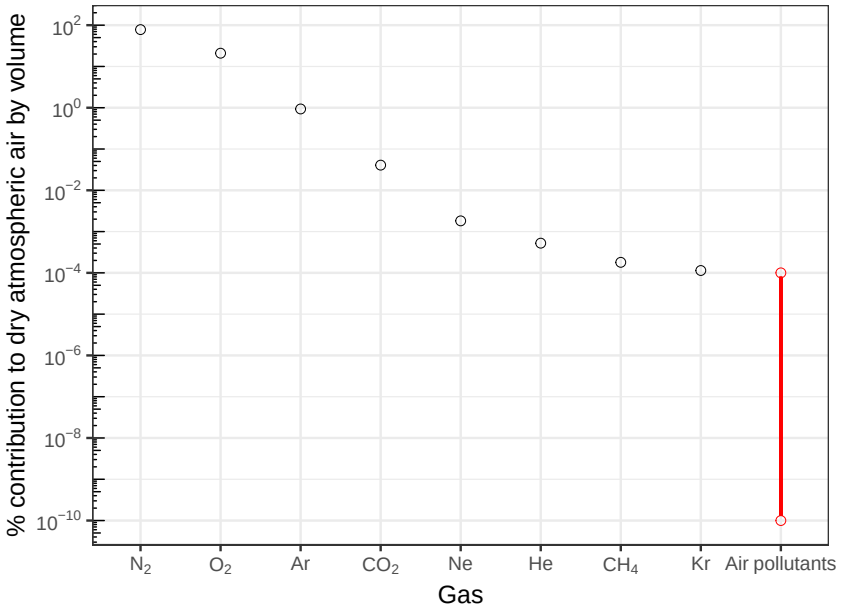

Figure 1.1: The approximate composition by volume of different gases in the atmosphere. Air pollutants are expressed as a range due to their short atmospheric lifetimes and high variability.

1.2 A brief history of air pollution

Air pollution has been a topic of concern since the early ages of human civilisation with references in writings dating back as far as ancient Greece and the Roman Empire.[3] These early references describe potential threats to human health around the use of fire and its release of smoke and other pollutants into the air. As human civilisation advanced, and the mass combustion of coal facilitated the Industrial Revolution, there was a large increase in the emission of pollutants to the atmosphere (see Fig. 1.2).[4] This led to the accumulation of emissions around population centres and thus widespread air pollution in major cities around the world. In the early 20th century, the invention of the automobile and subsequent use of leaded gasoline produced a new era of air pollution through the formation of smog.[5] This was particularly evident in developed cities such as London and Los Angeles where the use of the automobile was greatest and the meteorology

favoured smog formation.[6] Present-day estimates assign the 1952 smog episodes in London to the premature mortality of 12000 people.[7] In response, the UK introduced the first major air pollution reduction measures in the form of the Clean Air Act of 1956.[8] The US closely followed suit introducing its own clean air legislation in 1963.[9] This legislation ordered the reduction of emissions of pollutants from different applications and thus began efforts to reduce the impact of poor air quality. Global knowledge and awareness about the impacts of air pollution on human health and the environment rapidly increased in the following decades. Emissions standards for specific polluting applications became widespread in developed countries' legislation and many industrial activities were moved out of dense population centres.

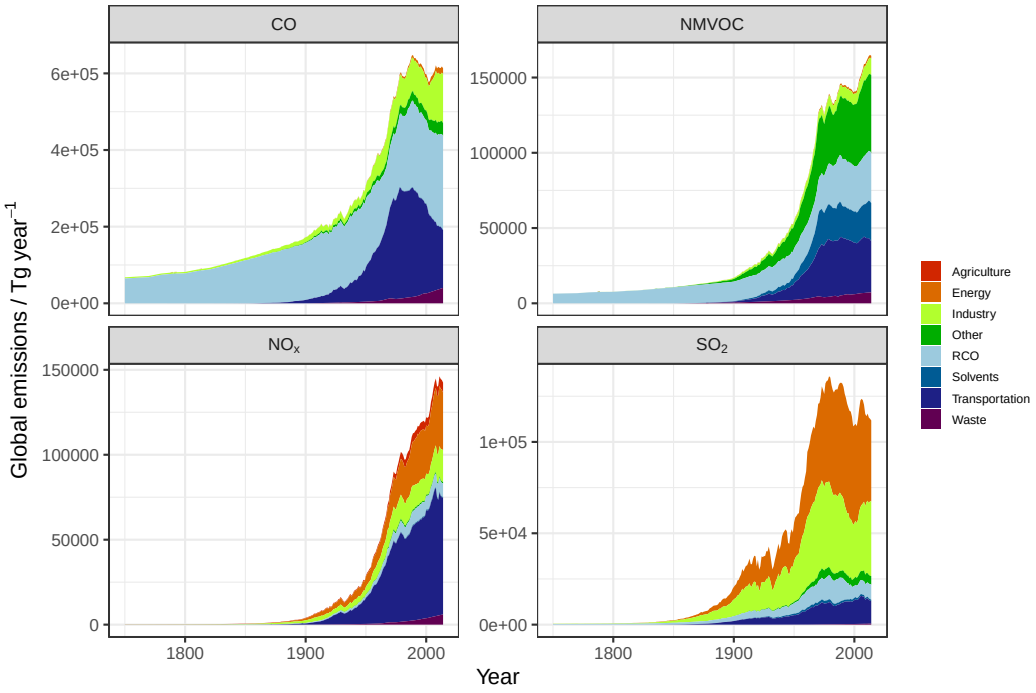

Figure 1.2: Historical global emissions of four gaseous air pollutants (CO, NMVOCs, NO_x and SO_2) from 1750-2014. Data was adapted from Hoesly et al. [4].

Despite now international efforts to reduce air pollution, it remains a

global problem. The burning of fossil fuels, industrial processes, and transportation continue to release large amounts of pollutants into the atmosphere. In the present day, it is estimated that 99% of the global population breathes air that exceeds the World Health Organisation's (WHO) guidelines and that approximately 4.5 million premature deaths occur each year as a result of outdoor air pollution exposure.[10]

1.3 Where is the science at now?

The overarching goal surrounding air pollution is to reduce the negative environmental and public health effects that arise from it. This can be most effectively done using a feedback loop of accurate information on the different factors at play. A DPSIR (Drivers-Pressures-State-Impact-Responses) framework (see Figure 1.3) is a simple breakdown to describe this loop within which areas of air pollution science can be contextualised by their importance to society.

Essential human activities demand energy, transport, food and materials. Each of these leads to the production of air pollution and so can be thought of as the **drivers**. The individual air pollutants themselves are the **pressures** in the system since they lead to negative **impacts** on the environment and human health. This is via the alteration of the atmospheric **state** of the system, namely in the concentrations of the pollutants. A consequence of the negative impacts is the human **response** which aims to minimise the damage. This is typically through regulatory action and the implementation of air quality policy. Improving our knowledge of each segment and our understanding of the interlinking variables is essential for successfully reducing the negative impacts of air pollution. The following sections discuss each segment in more detail based on current understanding in the literature.

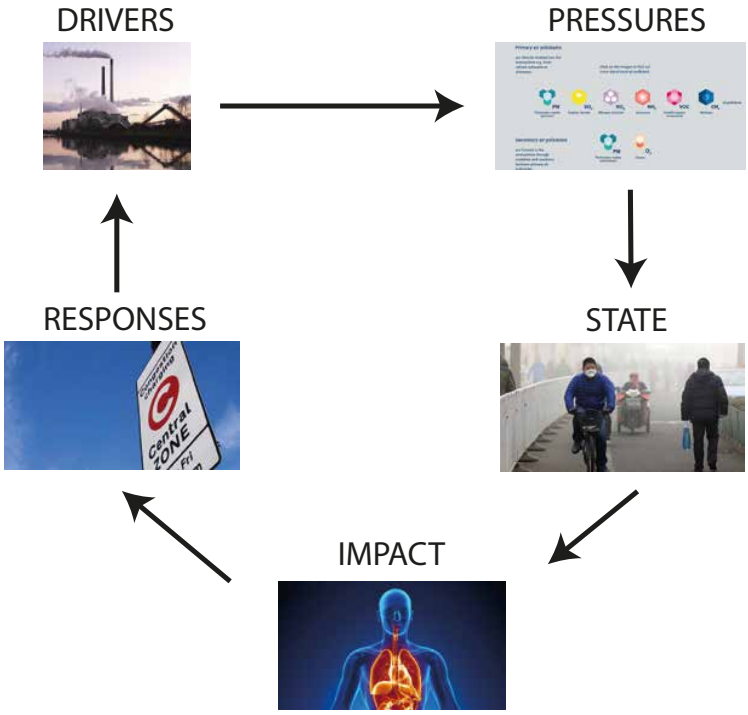

Figure 1.3: DPSIR framework for the air pollution global issue

1.3.1 Pressures: Major air pollutants

The World Health Organisation (WHO) lists five pollutants of major public health concern: particulate matter (PM), carbon monoxide (CO), nitrogen dioxide (NO_2), ozone (O_3), and sulfur dioxide (SO_2).[11] PM is typically broken down into different size brackets (PM_{10}, $PM_{2.5}$ and $PM_{0.1}$) which account for all particles up to a given diameter in microns. NO_2 is a component of the nitrogen oxides class herein referred to as NO_x (or NO + NO_2). While NO_x, CO, SO_2, and primary PM are all directly emitted from natural and anthropogenic sources, secondary PM and O_3 are produced via secondary chemical reactions in the atmosphere. The chemistry of formation of O_3 and secondary PM is summarised in Figure 1.4 and described in further detail below.

Tropospheric O_3, not to be confused with that in the stratospheric O_3 layer, is formed photochemically via the reaction of Volatile Organic Compounds (VOCs, also referred to as non-methane (NM) VOCs) with NO_x in

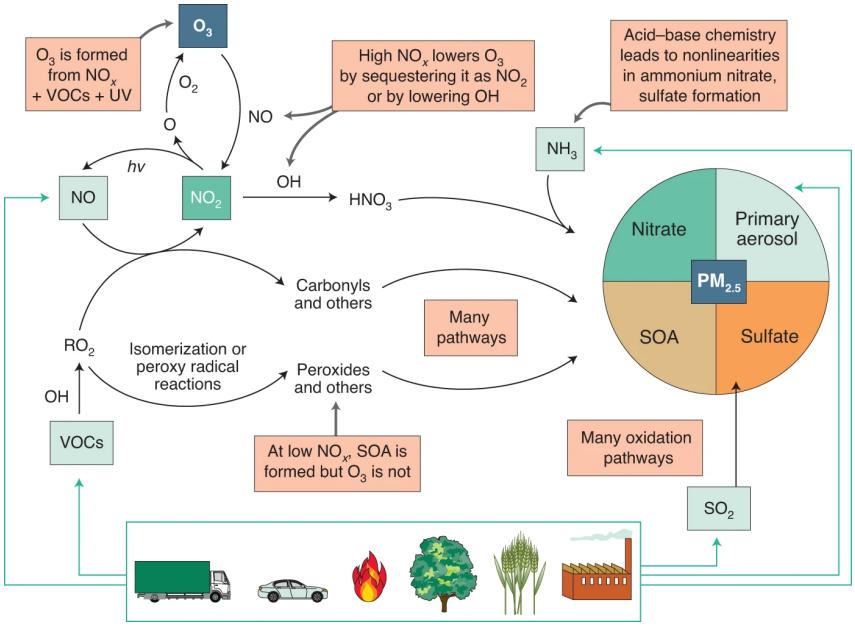

Figure 1.4: Chemistry overview for the chemical formation of secondary air pollutants in the atmosphere. Taken from Kroll et al. [12].

the presence of sunlight. The chemical reactions are described in Reactions 1.1 - 1.4 where R herein represents a hydrocarbon (or VOC) or H.[13] Initially, a VOC is oxidised by the hydroxyl radical (OH) to produce a peroxy radical (RO_2). The RO_2 species then oxidises NO to NO_2. NO_2 is photolysed back to NO and atomic oxygen (O) by sunlight < 420 nm.[14] The single oxygen atom then reacts with O_2 to form O_3.

$$VOC + OH \rightarrow RO_2 + H_2O \tag{1.1}$$

$$RO_2 + NO \rightarrow NO_2 + RO \tag{1.2}$$

$$NO_2 + h\nu \rightarrow NO + O \tag{1.3}$$

$$O + O_2 + M \rightarrow O_3 + M \tag{1.4}$$

O_3 responses to NO_x and VOC chemistry are highly non-linear. The rate of O_3 production depends on the relative balance of VOCs and NO_x in the local environment and most locations worldwide fit into two different regimes. Each regime is described by the dominant radical termination pathway in Reactions 1.5-1.6 and named after the species in which reduced concentrations would reduce the level of O_3 formation.

$$RO_2 + RO_2 + M \rightarrow R_2O_2 + O_2 + M \tag{1.5}$$

$$OH + NO_2 + M \rightarrow HNO_3 + M \tag{1.6}$$

A NO_x-limited regime occurs when peroxides (Reaction 1.5) represent the dominant radical sink. Here, the rate of O_3 formation is determined by Reaction 1.2 which increases with increasing NO_x concentration. A VOC-limited (or NO_x-saturated) regime occurs when nitric acid (Reaction 1.6) represents the dominant radical sink. Here, the rate of O_3 formation is determined by Reaction 1.1 which increases with increasing VOC concentration. It has recently been suggested that a third aerosol-inhibited regime has been identified where reactive uptake of hydroperoxyl radicals onto aerosol particles dominates.[15]

Secondary PM is formed via complex chemical reactions of volatile compounds in the atmosphere to produce both secondary organic and inorganic aerosol (SOA and SIA). SOA is formed via the multi-generational oxidation of VOCs and semi-volatile VOCs (SVOCs) via hydroxyl and nitrate radicals, O_3 and chlorine atoms. These oxidation products are lower in volatility and can either condense to form new particles or are reactively uptaken onto existing particles.[16] SIA mainly consists of sulfate, nitrate, and ammonium (also known as SNA) compounds occurring as ammonium sulfate ($(NH_4)_2SO_4$) and ammonium nitrate (NH_4NO_3).[17] These are formed via the neutralisation of sulfuric acid and nitric acid with ammonia (NH_3) via

complex gas phase, aqueous phase, and heterogeneous chemistry.

Since NH_3 and VOCs are key precursors to the formation of O_3 and secondary PM, in the context of emissions they are commonly also considered as pollutants of concern.

1.3.2 Impacts: Health and environmental effects

Short and long-term exposure to air pollution has been linked to a range of negative health effects. Air pollution mainly gains access to the body via inhalation and the respiratory tract. Once in the body, there are various mechanisms that result in disease formation including inflammation, oxidative stress, immunosuppression, and mutagenicity in cells.[18–21] Since the cardiovascular system is responsible for the method of air pollution ingestion, it suffers the highest burden of negative impacts.

The damage to cellular tissues by gaseous air pollutants largely depends on their oxidizing capacity, concentration and water solubility. SO_2 is highly soluble and tends to damage the upper airways.[23] NO_2 and O_3 are less soluble and therefore able to penetrate deeper into the lungs.[24] CO is non-irritating and easily passes into the bloodstream. Its toxicity results from out-competing O_2 in binding to haemoglobin and the resulting hypoxia.[25] The damage resulting from particulate matter depends on both composition and particle size. Toxic elements and compounds within the particle can directly harm organ tissues and cause inflammation and oxidative stress.[26] Smaller particles are able to penetrate deeper into the body and hence have greater toxicity.

Short-term effects are associated with COPD (Chronic Obstructive Pulmonary Disease), cough, shortness of breath, wheezing, asthma, respiratory disease, and high rates of hospitalization.[27] Long-term effects are associated with diseases affecting almost every organ in the body. A selection of the vast range of medical conditions associated with air pollution exposure

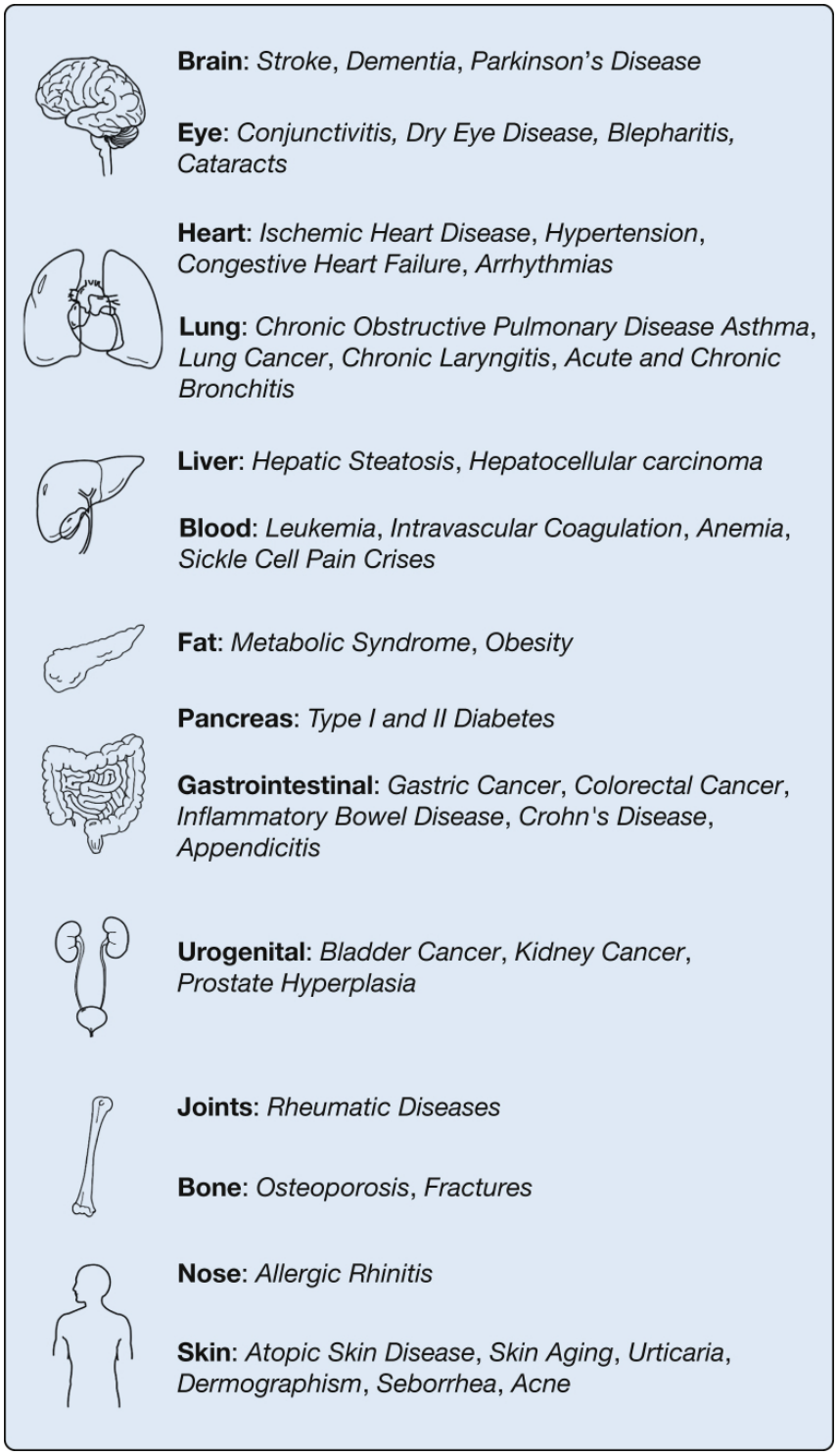

Figure 1.5: Medical conditions associated with air pollution exposure for each organ system. Taken from Schraufnagel et al. [22].

is presented in Figure 1.5 by organ system. All of the diseases directly affect society via reduced life expectancy, loss of population productivity and cost to health services. The number of premature deaths associated with outdoor air pollution is currently estimated at 4.5 million[10] and is thought to rise to 6-9 million by 2060 in the absence of more stringent policies.[28] The annual number of lost working days, which affects labour productivity, is currently around 1.2 billion (2015 estimate) and is projected to reach 3.7 billion by 2060.[28] Finally, global welfare costs are currently $3.3 trillion (2015 estimate) and predicted to rise to $20-27 trillion by 2060.[28]

In addition, emerging research has assigned $PM_{2.5}$ as a key vector for the dissemination of antibiotic-resistant bacteria and genes.[29] As a severe global issue, antibiotic resistance is thought to result in millions of further premature deaths worldwide every year.[30]

Outside of direct human health impacts, air pollution damages the environment. Tropospheric O_3 damages plants and trees by entering leaf stomata and oxidizing plant tissue during respiration. This can cause stomata to close and block CO_2 transfer, reducing photosynthesis.[31] It is also thought to reduce the survivability of seedlings and increase plant susceptibility to disease, pests, and other environmental stresses. Estimates for 2030 have global relative yield losses of 11-16% for wheat, 6.5-16.5% for soybean, 4.7-5.7% for rice, and 3.2-5.2% for maize as a result of air pollution exposure.[32] NO_x and SO_2 react with water and O_2 to form acidic compounds in the atmosphere. The deposition of these compounds to the surface is known as acid rain which causes deforestation and water body acidification.[33]

Finally, it should be noted that air pollution and climate change are closely related. Air pollutants and greenhouse gases (GHGs) have the same major sources with most air pollutants having either a direct or indirect role in the retention of heat in the atmosphere. A discussion of the potentially catastrophic health and environmental impacts associated with climate change is out of the scope of this thesis. However, a consideration of

the health and environmental impacts of air pollution would not be complete without at least their mention.

1.3.3 Drivers: Emissions sources

Emissions of air pollutants come from a range of different sectors but the majority are centered around the use of fossil fuels and their combustion. An emissions inventory is a database that lists, by source, the amount of air pollutants emitted into the atmosphere over a given time period, typically a year. They play a critical role in collating information on the emissions of air pollutants and are used for informed decision-making on the best solutions to reduce the impact of air pollution. They can additionally be used for emissions reporting to track progress towards regulatory emissions targets. Emissions inventories are generally constructed bottom-up using emissions factors and corresponding activity numbers from the emissions drivers. Global emissions inventories include the Community Emissions Data System (CEDS) and the Emissions Database for Global Atmospheric Research (EDGAR).[4,34] The UK has the annually commissioned National Atmospheric Emissions Inventory (NAEI) as well as other, more local inventories such as the London Atmospheric Emissions Inventory (LAEI).[35,36] A summary of the key sectors responsible for UK emissions of each air pollutant for the past 30 years is presented in Figure 1.6, and briefly discussed below.

Anthropogenic NO_x, SO_2 and CO are produced as by-products of the high-temperature combustion of fossil fuels. The majority of NO_x emissions arise from what is known as thermal NO_x which is the combination of nitrogen and oxygen atoms that are present in the air fueling the combustion.[37] SO_2 and smaller amounts of NO_x are produced by the oxidation of atomic sulfur and nitrogen contained within the fuel source itself during combustion. CO is a product of incomplete combustion when insuffi-

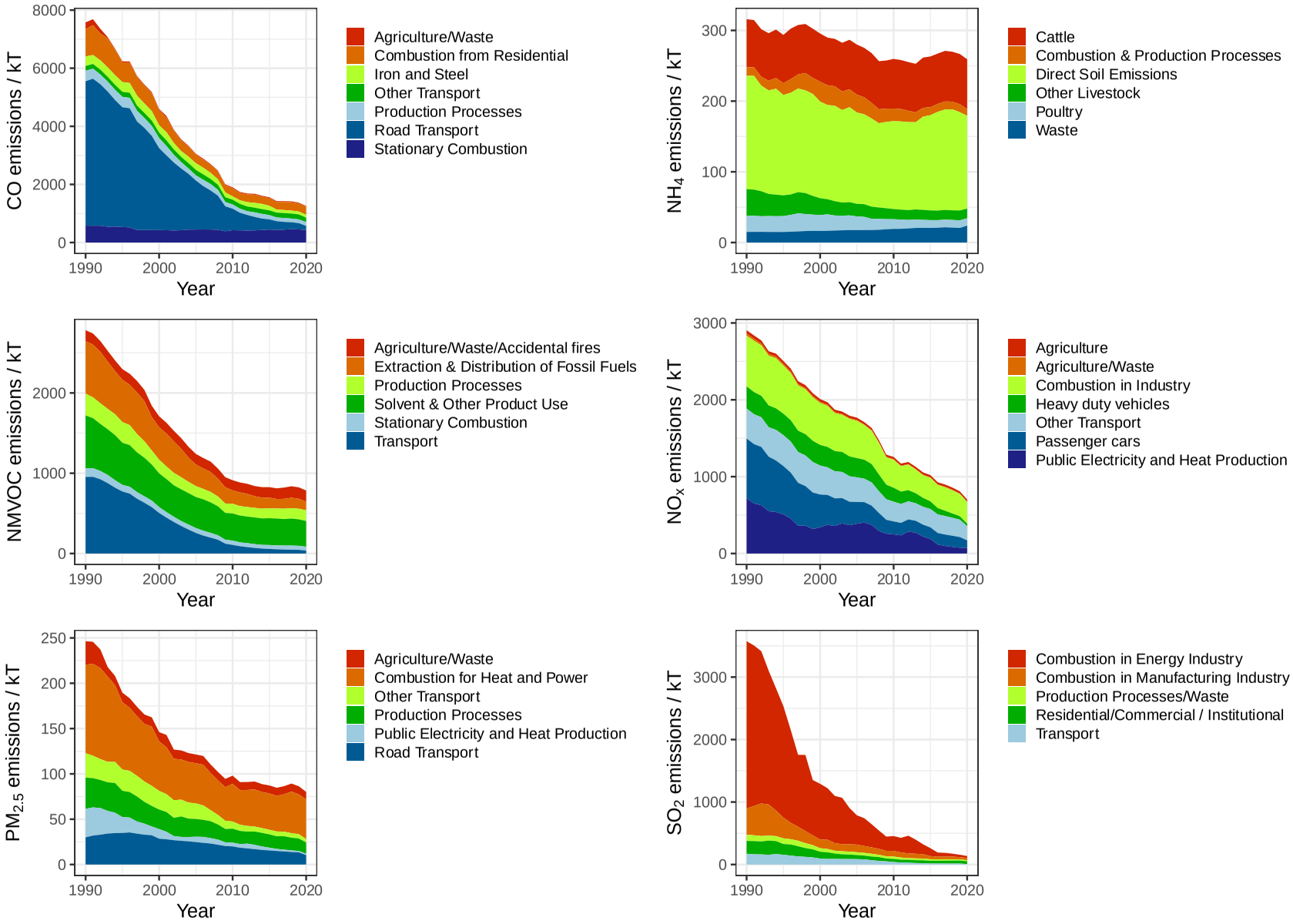

Figure 1.6: NAEI air pollutant emissions for the UK from 1990-2020

cient O_2 is present to fully oxidise carbonaceous material into CO_2. VOCs are released into the atmosphere via the volatilisation of chemicals present within fuels and other chemical products. This is either via evaporation at ambient or combustion temperatures or during the use of the chemical product. Key sectors for the combustion of fossil fuels are the energy (both heat and power), transport and industrial sectors. Uncontrolled emissions of each typically depend on the type of fossil fuel burned, the temperature of combustion, and the air-to-fuel ratio. Ammonia is released into the atmosphere via vaporisation from livestock urea decomposition and manure, and the decomposition of nitrogen-based synthetic fertilisers.[38] As such, the agricultural sector dominates ammonia emissions. It is also emitted as a byproduct of exhaust treatment systems (selective catalytic reduction and three-way catalytic converters, see Section 1.3.5) for the control of NO_x, particularly in the road transport sector.[39] Primary PM has a much more complex range of sources. It is directly released from the combustion of fossil fuels and biomass (mainly solid fuels). However, it is also released from many industrial processes that produce dust, the demolition sector and road dust resuspension.[40]

In addition to dominant anthropogenic sources, natural sources of each pollutant exist. NO_x is directly emitted from soil as a result of microbial activity and is formed during lightning strikes.[41] SO_2 emissions arise as a result of volcanic activity and from activity in marine ecosystems.[42,43] CO, NO_x, SO_2 and PM are all released from natural biomass burning (i.e. fires started via stimuli such as lightning).[44] Natural PM is introduced to the atmosphere from sea salt and dust suspension via the wind.[45] Finally, natural ammonia comes from wildlife and the decomposition of organic matter.[46]

1.3.4 State: Atmospheric concentrations

The negative impacts of air pollution are directly related to the concentration the environment or an individual is exposed to. Atmospheric concentrations are not only driven by emissions but also by atmospheric transport and air pollutant lifetimes. Complex interactions between meteorology and chemistry drive each of these, and whilst they cannot be controlled, it is important to understand how they influence concentrations for the estimation of population exposure and the areas or times of greatest concern.

The dispersion of an air pollutant away from the emission source directly influences its concentration. **Wind speed and direction** are key factors here since higher wind speeds can spread a pollutant out over a larger area reducing concentrations, whereas lower wind speeds can lead to the stagnation and accumulation of the pollutant. Similarly, the **planetary boundary layer height (PBLH)** influences dispersion by often representing the volume in which a pollutant can be diluted. The planetary boundary layer (PBL) is the lowest part of the atmosphere and is defined as the part that directly feels the effect of the earth's surface; that is the area in which turbulence created by wind shear over the rough surface and thermal heating from the earth dominates atmospheric transport.[47] The boundary layer is contained by a capping inversion which restricts vertical transport to the free troposphere. As such, pollutants released from the surface are mostly contained within this height. The development of the daytime PBL is closely related to the level of solar radiation reaching the surface with greater heating leading to a greater PBLH and increased dilution of pollutants.[48] Therefore, PBLH is typically higher in summer than in winter which results in higher winter concentrations for the same emissions and chemistry. The rate of vertical transport of a pollutant is determined by **atmospheric stability**.[49] Stable atmospheric conditions are associated with poor air quality since vertical transport and thus dispersion are re-

stricted. Conversely, unstable atmospheric conditions have unrestricted vertical transport, a high level of dispersion and lower pollutant concentrations. Atmospheric stability is often influenced by weather fronts and **atmospheric pressure systems**. The anticyclonic behaviour observed in a high-pressure system is associated with a stable atmosphere, poor dispersion and stagnant air. Conversely, cyclonic behaviour is associated with an unstable atmosphere, high winds and rainy conditions.[50] Finally, from a dispersion point of view, topography plays an important role. Cities within valleys or surrounded by mountainous regions have reduced dispersion of pollution irrespective of wind conditions due to the physical topographic barriers. A good example here is Mexico City which sits in a mountain-rimmed basin and regularly experiences high air pollutant concentrations.[51]

An air pollutant's lifetime is determined by its rate of loss from the atmosphere. Air pollutant sinks can be broken down into the chemical transformation into something else and/or the deposition of the pollutant to the earth's surface. Gas phase pollutants (i.e. O_3, CO, SO_2 and NO_x) typically have a dominant chemical sink. O_3 is mostly lost via photolysis followed by the reaction of $O(^1D)$ with H_2O in Reaction 1.7 - 1.8.[52] Additional loss occurs via reactions with HO_2 radicals and OH in Reaction 1.9 - 1.10.

$$O_3 + h\nu \rightarrow O(^1D) + O_2 \tag{1.7}$$

$$O(^1D) + H_2O \rightarrow 2OH \tag{1.8}$$

$$HO_2 + O_3 \rightarrow OH + 2O_2 \tag{1.9}$$

$$OH + O_3 \rightarrow HO_2 + O_2 \tag{1.10}$$

CO is mainly lost via oxidation by OH to form carbon dioxide in Reaction 1.11.[53] Although this reaction is relatively slow and thus CO has a greater

lifetime and background concentration compared to other pollutants.

$$CO + OH \rightarrow CO_2 + H \tag{1.11}$$

SO_2 and NO_x chemical loss usually occurs via conversion to a highly soluble acid (H_2SO_4 or HNO_3), followed by wet deposition as acid rain, or the formation of new particles as discussed in Section 1.3.1.[54]

$$SO_2 + OH \rightarrow HSO_3 \tag{1.12}$$

$$HSO_3 + O_2 \rightarrow HO_2 + SO_3 \tag{1.13}$$

$$SO_3 + H_2O \rightarrow H_2SO_4 \tag{1.14}$$

$$OH + NO_2 + M \rightarrow HNO_3 \tag{1.15}$$

The kinetics of these reactions are influenced by the level of solar radiation, temperature and humidity. This results in pollutant lifetimes with high spatial and temporal variability.

PM, and indeed each of the gaseous pollutants, can be removed from the atmosphere via deposition. Wet deposition occurs when the pollutants mix with water in the atmosphere before being washed out through rain, snow and fog. Dry deposition is the direct uptake of air pollutants to the surface, usually by sedimentation mechanisms.[55]

1.3.5 Responses: Emissions control

Human responses to reduce air pollutant emissions have the ultimate goal of reducing atmospheric concentrations down to "safe" levels, such that the negative impacts are minimised. The WHO publishes recommended guidelines for air pollutant concentrations for short-term (24-hour) and long-

term (annual) exposure (presented in Table 1.1).[11] These are continuously reviewed as new evidence supporting the health and environmental effects becomes available. Developed nations typically have legally binding targets for pollutant concentrations based on achieving these guidelines, although usually via intermediate targets. Since meteorological processes cannot be controlled, the human response to improve air quality falls under the reduction of emissions. As such, these targets are often in conjunction with national emissions ceilings for pollutants that will help achieve them (e.g. the National Emissions Ceilings Directive for EU nations).[56] The SIMPLEST way to reduce air pollutant emissions is to reduce the activity that produces them. However, this is often not EASY since all of the activities are embedded in human society and increase with an ever-increasing population. An alternative option would be to change the fuel type driving the activity to one that is cleaner. This could be a partial emissions control (i.e. the recent legislation to lower the maximum percentage of sulphur from 3.5% to 0.5% for all ships operating worldwide),[57] or a full emissions control (i.e. replacement of a coal-fired power station with a wind farm). The third option is the integration of technologies that reduce emissions at the source chemically or by other means.

Some of the recent trends in emissions can be attributed to the gradual phase-out of coal as a source of energy, to be replaced by gas, biomass and increasingly renewable sources.[35] The transition to cleaner fuels is expected to play an important role in reducing air pollution in the coming decades as a result of global pledges to reduce greenhouse gas emissions.[58] However, the implementation of emissions standards for polluting applications and the subsequent development of emissions control technologies have likely been the most effective measures in the past for reducing emissions. Key regulatory examples include standards in the Euro classes, China classes, and the US Tier system for the road transport sector,[59–61] the International Maritime Organization control of SO_2 emissions

Table 1.1: WHO guidelines for each of the six criteria air pollutants

Pollutant ($\mu g\ m^{-3}$)	Averaging time	WHO AQG level
$PM_{2.5}$	Annual	5
	24-hour	15
PM_{10}	Annual	15
	24-hour	45
O_3	Annual	60
	24-hour	100
NO_2	Annual	10
	24-hour	25
SO_2	Annual	40
	24-hour	4
CO	Annual	-
	24-hour	4000

from shipping,[57] and Ecodesign directives for control of emissions from boiler applications.[62] These regulations continuously evolve to include increasingly stringent standards. This forces the continuous improvement of emissions control technologies and the use of more effective control systems. A brief summary of these technologies is given below.

The prevalence of air pollutant emissions from the road transport sector and the proximity of their release to human populations means that a significant proportion of regulatory action has been dedicated to it. VOC, CO and NO_x emissions from gasoline-powered vehicles have shown large reductions in recent decades as a result of the **3-way catalytic converter**. First introduced in the 1970s in response to clean air legislation targeting photochemical smog, the 3-way catalytic converter uses simple redox (Reactions 1.16 - 1.19) reactions to both oxidise CO and VOCs to CO_2 and H_2O, and reduce NO_x to molecular nitrogen.[63]

$$2CO + O_2 \rightarrow 2CO_2 \tag{1.16}$$

$$NO_2 + CO \rightarrow NO + CO_2 \tag{1.17}$$

$$(8n + 2m)NO + 4H_mC_n \rightarrow (4n + m)N_2 + 2mH_2O + 4nCO_2 \tag{1.18}$$

$$2NO + 2CO \rightarrow N_2 + 2CO_2 \tag{1.19}$$

The catalysts typically use a combination of platinum, palladium and rhodium metals coated onto a ceramic honeycomb structure to catalyse Reactions 1.16 - 1.19 from the engine-out exhaust gas. In addition, **carbon canister** technology has been used on all gasoline vehicles for the past few decades which reduces the evaporative VOC emissions from the fuel tank. Upon heating (either ambient or operationally induced), gaseous vapours

are absorbed into activated charcoal, before being redirected into the engine for combustion during operation.

Catalytic removal of pollutants from diesel exhaust is slightly different to those in gasoline exhaust. Platinum-based oxidation catalysts are still used for reducing VOC and CO emissions, although the nature of diesel fuel itself, which is less volatile than gasoline, means these emissions are not as prevalent. However, the lower exhaust temperature and different air-fuel ratios make NO_x reduction challenging.[63] Gasoline engines are fuel-rich and operate near a stoichiometric ratio. This is within a range in which Reactions 1.17 - 1.19 proceed efficiently. Diesel engines operate under fuel-lean conditions which are ineffective for the reduction of NO_x. Therefore, additional technology is required with the two common options being **lean NO_x traps (LNT)** and **selective catalytic reduction (SCR)** systems.

An LNT works by chemically trapping NO_x during fuel-lean (normal) operation. NO_2 is adsorbed onto an alkaline metal (M) to form a stable nitrate (Reaction 1.21).[64] This is via the oxidation of all NO to NO_2 with a platinum catalyst (Reaction 1.20). Once the adsorbing material is saturated, the engine is temporarily switched to fuel-rich conditions which cause the decomposition of the metal nitrate, the regeneration of NO_2, and facilitates the efficient reduction of NO_x via Reaction 1.17 - 1.19 in the presence of rhodium.[64]

$$2NO + O_2 \rightarrow 2NO_2 \tag{1.20}$$

$$2NO_2 + MCO_3 + 0.5O_2 \rightarrow M(NO_3)_2 + CO_2 \tag{1.21}$$

$$M(NO_3)_2 + 2CO \rightarrow MCO_3 + NO_2 + NO + CO_2 \tag{1.22}$$

Selective Catalytic Reduction (SCR) chemically reduces the NO_x molecule into molecular nitrogen and water vapour using ammonia.[65] The ammo-

nia is usually supplied via urea injection into the hot exhaust upstream of the SCR catalyst which decomposes by Reaction 1.23.[63] Ammonia then proceeds to reduce NO_x in Reactions 1.24 and 1.25 via a catalyst (typically vanadium oxide supported on titanium oxide, Fe-exchanged zeolites, or Cu-exchanged zeolites).[66]

$$(NH_2)_2CO + H_2O \rightarrow 2NH_3 + CO_2 \tag{1.23}$$

$$4NH_3 + 4NO + O_2 \rightarrow 4N_2 + 6H_2O \tag{1.24}$$

$$4NH_3 + 2NO + 2NO_2 \rightarrow 4N_2 + 6H_2O \tag{1.25}$$

Diesel particulate filters (DPF) have been used to reduce particles from diesel vehicles since around 2010. In simple terms, a DPF is a porous substrate that traps engine-out particulates but allows gas to pass through. In doing so, issues arise with the build-up of pressure that degrades engine performance. Therefore, a process of regeneration occurs in which PM (denoted as [C] in Reaction 1.27) is oxidised to CO_2 at temperatures higher than that of normal engine operation.[67] The high temperatures are usually achieved by increasing fuel combustion in the engine.[68]

$$2NO + O_2 \rightarrow 2NO_2 \tag{1.26}$$

$$[C] + 2NO_2 \rightarrow CO_2 + 2NO \tag{1.27}$$

Flue gas desulfurisation (FGD) has been the major influence on reducing SO_2 emissions from power plants. The process of wet scrubbing typically utilizes an alkaline-based slurry of lime to scrub gases.[69] A shower of lime slurry is then sprayed into a flue gas scrubber, where the SO_2 is absorbed into the spray and becomes a wet calcium sulfite (see Reaction 1.28).

$$SO_2 + CaCO_3 \rightarrow CaSO_3 + CO_2 \tag{1.28}$$

Flue gas recirculation (FGR) is commonly used to reduce NO_x emissions from boiler applications. As discussed in Section 1.3.3, NO_x is formed during high-temperature combustion via the combination of N_2 and O_2 in the air. FGR works by recirculating exhaust gases into the combustion chamber as a way of diluting the oxygen content present. In doing so, NO_x formation is limited by the concentration of oxygen and reduced flame temperatures.[70]

In some locations with the resources to do so, policies that speed up the transition to cleaner technologies are becoming increasingly common. In particular, the implementation of low emissions zones incentivises the use of up-to-date emissions control technology in the road transport sector by charging the use of non-compliant vehicles within the specified area.[71] Although difficult, attempts to reduce activity have seen some success. For example, the number of vehicles on the road can be reduced via congestion charging zones which are similar to a low emissions zone, except they charge any vehicle to enter.[72] This can also be done via the incentivisation of public transport or green methods of travel (e.g. walking or cycling).[73] Additionally, the improvement in the energy efficiency of buildings has reduced energy use per unit floor area. However, the number of buildings is ever increasing and so total energy use has in fact risen.[74]

1.4 How does this research contribute?

The 2020s mark a critical decade for the control of emissions. Decisions made over the next few years will determine the pathways followed in response to the Paris Agreement and international pledges to achieve net zero greenhouse gas emissions. Greenhouse gas and air pollutant emission sources are closely related meaning these pathways will have a significant

impact on air quality. It is a common opinion in air pollution research that the adoption of a pathway which does not also maximise air quality improvements would be a missed opportunity. Strategies aimed at reducing the impact of air pollution can only be as good as the data that informs it. This is typically data related to the atmospheric state of the system in combination with the magnitude of the different emissions drivers. Long-term national concentration measurements are required for the identification of the main pollutants of concern in each region/location. In the UK, these air quality monitoring sites make up what is known as the Automatic Rural and Urban Network (AURN). In total, this constitutes 174 sites distributed across different pollution environments in the UK; their locations are presented in Figure 1.7. Once the pollutant and location of concern are identified, the emissions inventories discussed in Section 1.3.3 play a critical role in providing information on which emission sources should be targeted. The monitoring network can then be used to track the effectiveness of the chosen intervention measures.

National monitoring networks are limited by the number of monitoring locations and the complexity of the instrumentation used for measurements. Speciated measurements of PM and VOCs provide important source apportionment information. However, the cost and amount of skilled labour required to perform these measurements is highly impractical on a national scale. Additionally, while reductions in concentrations are what is ultimately desired, they are heavily influenced by meteorology (see Section 1.3.4). Therefore, the meteorological factors at play can make their study in response to emissions reduction strategies challenging to interpret (although this has become easier with the recent development of meteorological normalisation machine learning methods).[76]

Emissions inventories are often produced using laboratory-derived emission factors and activity estimates. These emission factors may not be equivalent to those in the real world (e.g. the diesel-gate scandal in 2015) and

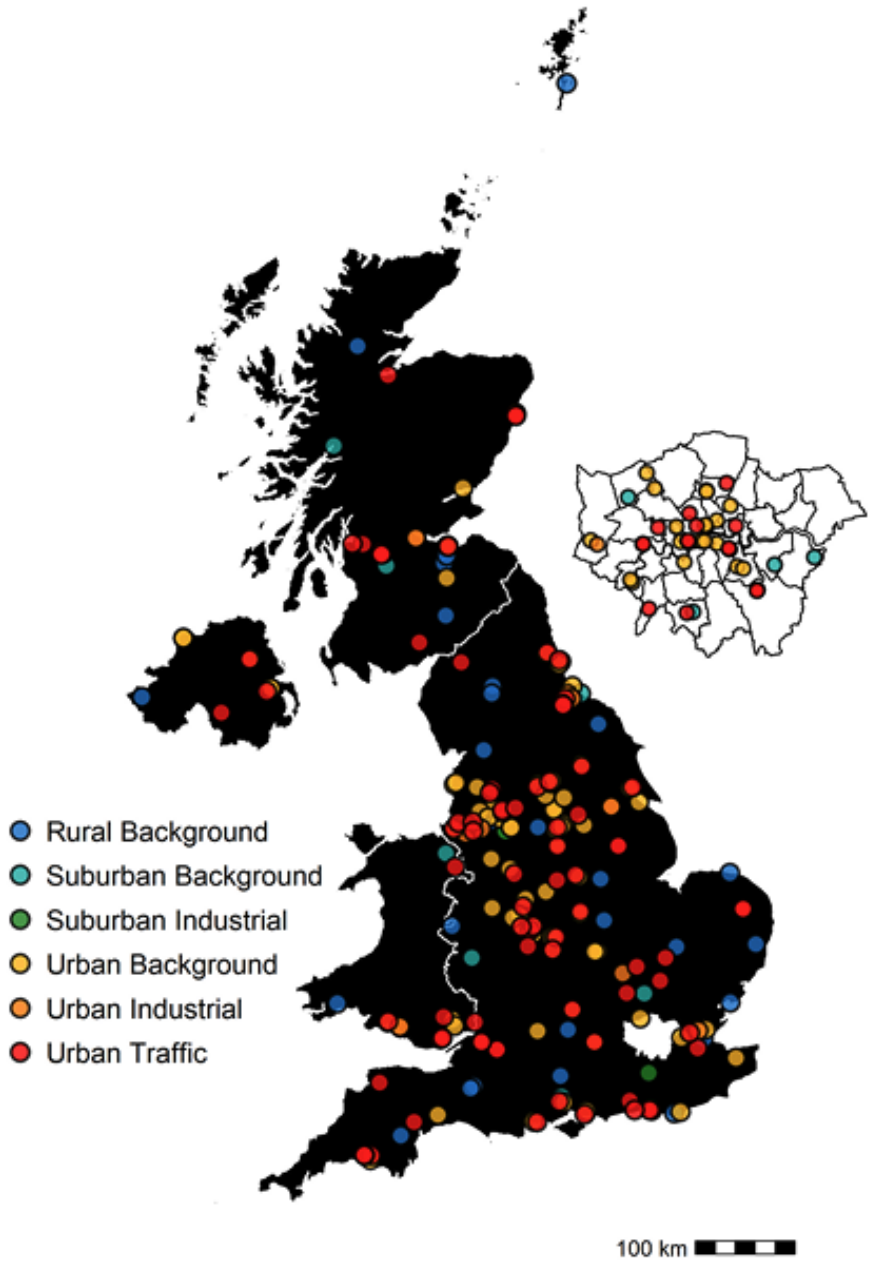

Figure 1.7: AURN monitoring site locations in the UK. Taken from [75].

emissions sources are continuously evolving.[77] As emissions from the dominant sources are reduced, previously minor sources increase in their relative importance. However, by nature of being minor in the past, these other sources have usually received less attention and are prone to larger uncertainties. As such, the science on which the inventory is based can be inaccurate or become outdated. It is therefore essential to continuously verify and update emissions inventories to ensure they are sufficiently accurate to identify the most critical sources for policy intervention.

The direct measurement of emissions produces an output that facilitates simple inventory verification. Additionally, the success of policy intervention measures at reducing emissions can be quantified by emissions measurements with reduced interference from meteorology. This thesis presents two unique emissions measurement applications for the study of evolving urban air pollution sources. The aims of the research were to a) assess the accuracy of emissions inventories and b) quantify the success of some air quality policies introduced in the UK, with the overall aim of improving the quality of the data informing subsequent air pollution decision-making.

Eddy covariance (EC) is a measurement technique that directly calculates vertical turbulent fluxes (or emissions) in the PBL. It is regularly used for measuring the biospheric exchange of CO_2, CH_4, H_2O and energy between the earth's surface and the atmosphere to improve understanding of the global carbon budget.[78] A number of flux measurement networks are now established as an alternate source of information to traditional concentration monitoring (e.g. FLUXNET, AmeriFLux, ICOS).[79–81] Recently, the use of EC has transitioned to the urban environment and to air pollutant exchange.[82–84] However, the number of studies is limited due to the extra challenges this environment brings. Urban EC measurements require sampling atop a tower that is much larger than the surrounding buildings and instrumentation that can acquire air pollution concentration data at a

very fast time resolution while maintaining high precision. In the first part of this thesis, long-term measurements of NO_x and CO_2 fluxes from a tall tower in central London are presented. The measurements are of particular air quality interest as they are the only measurements of their type in a megacity in the world, and are situated within an area that has seen local government take an international lead in traffic air quality policy. Assessment of the success of these policies at reducing road transport emissions and the characterisation of increasingly important sources in their absence was carried out here.

An additional area of developing air pollutant research is the use of mobile laboratories for assessing pollutant emissions and/or concentrations at a greater spatial extent.[85,86] Here, field measurements can be made in locations not covered by national monitoring, and utilise more specialist instrumentation to measure a greater range of compounds. The second part of this thesis presents emissions measurements made in the field with a mobile laboratory that facilitates the detection of compounds not routinely monitored in the UK by the AURN. Emissions factors of speciated VOCs from road transport were identified as an area of emissions inventory uncertainty and verified here in the real world. This represents the application of an emissions measurement in a more targeted approach to a specific air pollution source.

1.5 Thesis outline

This thesis is presented in the journal-style format using three articles as stand-alone chapters, with details of each given in the thesis's declaration. The contents of the chapters are faithful to the accepted and published articles, however, minor formatting changes have been made to section headings, figures and captions, citations and reference styles, and the inclusion of supplementary material for the sake of completeness and consistency.

Chapter 2 focuses on the first year (Sept. 2020 - Sept. 2021) of the long-term flux measurements in central London. This year was heavily impacted by restrictions associated with the coronavirus pandemic and represented a unique opportunity to study emissions scenarios under reduced activity. It was found that NO_x emissions had reduced by 73 % since 2017. Novel analysis techniques were developed to source apportion this reduction which determined that traffic NO_x emissions reduced by 73 - 100 % since 2017. This was a result of COVID-19 restrictions, the Ultra Low Emissions Zone and the natural fleet transition to cleaner vehicles. The findings from this work gave the first indication that the heat and power generation sector would be important for future urban NO_x emissions.

Chapter 3 studies the following two years (Sept. 2021 - Sept. 2023) of flux measurements in central London. It was shown that NO_x emissions did not recover post-lifting of the pandemic restrictions. Use of NO_x/CO_2 emission ratios assigned 76 ± 17 % of NO_x emissions for the 2021-2023 period to the heat and power generation sector, the majority of which is made up of natural gas combustion in the commercial sector for space heating. Measurements were compared to the UK's emissions inventories which, despite this change in the dominant source, actually suggest an overestimation of commercial heating NO_x emissions of 53 %. This was assigned to outdated emission factors that did not account for recent legislation regulating NO_x emissions from gas-fired boilers. Future emissions scenarios are then discussed including the role of net zero pledges in the possible achievement of WHO air quality guidelines for NO_2.

Chapter 4 presents emissions factor measurements of VOC emissions from road transport. The measurements were conducted with a mobile laboratory which facilitated the use of advanced mass spectrometric instrumentation in a complex field environment. It was shown that international road transport emissions inventories are missing a large source of alcohol-based VOCs. This was assigned to the use of screenwash (or windshield

washer fluid) through verification with industry sales statistics and laboratory headspace analysis. The implications that this source missing in emissions inventories may have on future policy and atmospheric chemistry are discussed.

Bibliography

[1] Schlesinger, W. H. and Bernhardt, E. S. Chapter 3 - The Atmosphere. *Biogeochemistry (Fourth Edition)*. Ed. by W. H. Schlesinger and E. S. Bernhardt. Fourth Edition. Academic Press, 2020, pp. 51–97. DOI: 10.1016/B978-0-12-814608-8.00003-7.

[2] Fuller, R., Landrigan, P. J., Balakrishnan, K., Bathan, G., Bose-O'Reilly, S., Brauer, M., Caravanos, J., Chiles, T., Cohen, A., Corra, L., Cropper, M., Ferraro, G., Hanna, J., Hanrahan, D., Hu, H., Hunter, D., Janata, G., Kupka, R., Lanphear, B., Lichtveld, M., Martin, K., Mustapha, A., Sanchez-Triana, E., Sandilya, K., Schaefli, L., Shaw, J., Seddon, J., Suk, W., Téllez-Rojo, M. M., and Yan, C. Pollution and health: a progress update. *The Lancet Planetary Health* 6.6 (2022), e535–e547. DOI: 10.1016/S2542-5196(22)00090-0.

[3] Fowler, D., Brimblecombe, P., Burrows, J., Heal, M. R., Grennfelt, P., Stevenson, D. S., Jowett, A., Nemitz, E., Coyle, M., Lui, X., Chang, Y., Fuller, G. W., Sutton, M. A., Klimont, Z., Unsworth, M. H., and Vieno, M. A chronology of global air quality. *Philosophical Transactions of the Royal Society A: Mathematical, Physical and Engineering Sciences* 378.2183 (2020), p. 20190314. DOI: 10.1098/rsta.2019.0314.

[4] Hoesly, R. M., Smith, S. J., Feng, L., Klimont, Z., Janssens-Maenhout, G., Pitkanen, T., Seibert, J. J., Vu, L., Andres, R. J., Bolt, R. M., Bond, T. C., Dawidowski, L., Kholod, N., Kurokawa, J.-I., Li, M., Liu, L., Lu, Z., Moura, M. C. P., O'Rourke, P. R., and Zhang, Q. Historical (1750–2014) anthropogenic emissions of reactive gases and aerosols from the Community Emissions Data

System (CEDS). *Geoscientific Model Development* 11.1 (2018), pp. 369–408. DOI: 10.5194/gmd-11-369-2018.

[5] Layne, D. A Review On Smog. *Royal Society of Health* 75.2 (1955), pp. 171–192. DOI: 10.1177/146642405507500213.

[6] Haagen-Smit, A. J. Chemistry and Physiology of Los Angeles Smog. *Industrial & Engineering Chemistry* 44.6 (1952), pp. 1342–1346. DOI: 10.1021/ie50510a045.

[7] Bell, M. L., Davis, D. L., and Fletcher, T. A retrospective assessment of mortality from the London smog episode of 1952: the role of influenza and pollution. *Environmental Health Perspectives* 112.1 (2004), pp. 6–8. DOI: 10.1289/ehp.6539.

[8] United Kingdom Government. *The Clean Air Act*. https://www.legislation.gov.uk/ukpga/Eliz2/4-5/52/enacted, accessed October 2023. 1956.

[9] US EPA. *The Clean Air Act*. https://www.epa.gov/clean-air-act-overview/clean-air-act-text, accessed October 2023. 1963.

[10] World Health Organisation. *Global health estimates 2016: deaths by cause, age, sex, by country and by region, 2000–2016*. https://www.who.int/health-topics/air-pollution#tab=tab_1, accessed October 2021. 2018.

[11] World Health Organisation. *WHO global air quality guidelines: particulate matter (PM2.5 and PM10), ozone, nitrogen dioxide, sulfur dioxide and carbon monoxide*. https://apps.who.int/iris/handle/10665/345329, accessed December 2022. 2021.

[12] Kroll, J. H., Heald, C. L., Cappa, C. D., Farmer, D. K., Fry, J. L., Murphy, J. G., and Steiner, A. L. The complex chemical effects of COVID-19 shutdowns on air quality. *Nature Chemistry* 12.9 (2020), pp. 777–779. DOI: 10.1038/s41557-020-0535-z.

[13] Crutzen, P. J. Tropospheric Ozone: An Overview. *Tropospheric Ozone: Regional and Global Scale Interactions*. Ed. by I. S. A. Isaksen. Springer Netherlands, 1988, pp. 3–32. DOI: 10.1007/978-94-009-2913-5_1.

[14] Madronich, S., Hastie, D. R., Ridley, B. A., and Schiff, H. I. Measurement of the photodissociation coefficient of NO2 in the atmosphere: I. Method and surface measurements. *Journal of Atmospheric Chemistry* 1.1 (1983), pp. 3–25. DOI: 10.1007/BF00113977.

[15] Ivatt, P. D., Evans, M. J., and Lewis, A. C. Suppression of surface ozone by an aerosol-inhibited photochemical ozone regime. *Nature Geoscience* 15 (2022), pp. 536–540. DOI: 10.1038/s41561-022-00972-9.

[16] Srivastava, D., Vu, T. V., Tong, S., Shi, Z., and Harrison, R. M. Formation of secondary organic aerosols from anthropogenic precursors in laboratory studies. *npj Climate and Atmospheric Science* 5.1 (2022), p. 22. DOI: 10.1038/s41612-022-00238-6.

[17] Wang, S., Wang, L., Fan, X., Wang, N., Ma, S., and Zhang, R. Formation pathway of secondary inorganic aerosol and its influencing factors in Northern China: Comparison between urban and rural sites. *Science of The Total Environment* 840 (2022), p. 156404. DOI: 10.1016/j.scitotenv.2022.156404.

[18] Block, M. L. and Calderon-Garciduenas, L. Air pollution: mechanisms of neuroinflammation and CNS disease. *Trends Neurosci.* 32.9 (2009), pp. 506–516. DOI: 10.1016/j.tins.2009.05.009.

[19] Lodovici, M. and Bigagli, E. Oxidative Stress and Air Pollution Exposure. *Journal of Toxicology* 2011 (2011), p. 487074. DOI: 10.1155/2011/487074.

[20] Glencross, D. A., Ho, T.-R., Camiña, N., Hawrylowicz, C. M., and Pfeffer, P. E. Air pollution and its effects on the immune system. *Free Radical Biology and Medicine* 151 (2020), pp. 56–68. DOI: 10.1016/j.freeradbiomed.2020.01.179.

[21] Mehta, M., Chen, L., Gordon, T., Rom, W., and Tang, M. Particulate matter inhibits DNA repair and enhances mutagenesis. *Mutation Research* 657.2 (2008), pp. 116–121. DOI: 10.1016/j.mrgentox.2008.08.015.

[22] Schraufnagel, D. E., Balmes, J. R., Cowl, C. T., De Matteis, S., Jung, S. H., Mortimer, K., Perez-Padilla, R., Rice, M. B., Riojas-Rodriguez, H., Sood, A., Thurston, G. D., To, T., Vanker, A., and Wuebbles, D. J. Air Pollution and

Noncommunicable Diseases. *Chest* 155.2 (2019), pp. 417–426. DOI: 10.1016/j.chest.2018.10.041.

[23] Kleinman, M. T. Sulfur Dioxide and Exercise: Relationships between Response and Absorption in Upper Airways. *Journal of the Air Pollution Control Association* 34.1 (1984), pp. 32–37. DOI: 10.1080/00022470.1984.10465720.

[24] Ko, S., Tam, W., Wong, T., Chan, D., Tung, A., Lai, C., and Hui, D. Temporal relationship between air pollutants and hospital admissions for chronic obstructive pulmonary disease in Hong Kong. *Thorax* 62 (2007), pp. 780–785. DOI: 10.1136/thx.2006.076166.

[25] Townsend, C. L. and Maynard, R. L. Effects on health of prolonged exposure to low concentrations of carbon monoxide. *Occupational and Environmental Medicine* 59.10 (2002), pp. 708–711. DOI: 10.1136/oem.59.10.708.

[26] Athanasios, V., Konstantinos, F., and Thomais, V. Airborne Particulate Matter and Human Health: Toxicological Assessment and Importance of Size and Composition of Particles for Oxidative Damage and Carcinogenic Mechanisms. *Journal of Environmental Science and Health, Part C* 26.4 (2008), pp. 339–362. DOI: 10.1080/10590500802494538.

[27] Manisalidis, I., E., S., Stavropoulos, A., and Bezirtzoglou, E. Air Pollution: A Review. *Front Public Health* 8 (2020), p. 14. DOI: 10.3389/fpubh.2020.00014.

[28] OECD. *The Economic Consequences of Outdoor Air Pollution*. 2016, p. 116. DOI: 10.1787/9789264257474-en.

[29] Zhou, Z., Shuai, X., Lin, Z., Yu, X., Ba, X., Holmes, M. A., Xiao, Y., Gu, B., and Chen, H. Association between particulate matter (PM)2·5 air pollution and clinical antibiotic resistance: a global analysis. *The Lancet Planetary Health* 7.8 (2023), e649–e659. DOI: 10.1016/S2542-5196(23)00135-3.

[30] Global burden of bacterial antimicrobial resistance in 2019: a systematic analysis. *The Lancet* 399.10325 (2022), pp. 629–655. DOI: 10.1016/S0140-6736(21)02724-0.

[31] Singh, E., Tiwari, S., and Agrawal, M. Effects of elevated ozone on photosynthesis and stomatal conductance of two soybean varieties: a case study to assess impacts of one component of predicted global climate change. *Plant Biology* 11.s1 (2009), pp. 101–108. DOI: 10.1111/j.1438-8677.2009.00263.x.

[32] Van Dingenen, R., Dentener, F. J., Raes, F., Krol, M. C., Emberson, L., and Cofala, J. The global impact of ozone on agricultural crop yields under current and future air quality legislation. *Atmospheric Environment* 43.3 (2009), pp. 604–618. DOI: 10.1016/j.atmosenv.2008.10.033.

[33] Grennfelt, G., Engleryd, A., Forsius, M., Hov, O., Rodhe, H., and Cowling, E. Acid rain and air pollution: 50 years of progress in environmental science and policy. *Ambio* 49.4 (2020), pp. 849–864. DOI: 10.1007/s13280-019-01244-4.

[34] Crippa, M., Solazzo, E., Huang, G., GGuizzardi, D., Koffi, E., Muntean, M., Schieberle, C., Friedrich, R., and Janssens-Maenhout, G. High resolution temporal profiles in the Emissions Database for Global Atmospheric Research. *Scientific Data* 7 (2020), p. 121. DOI: 10.1038/s41597-020-0462-2.

[35] Defra and BEIS. *National Atmospheric Emissions Inventory, licenced under the Open Government Licence (OGL), Crown Copyright 2020*. naei.beis.gov.uk/data/, accessed March 2022. 2019.

[36] Greater London Authority. *London Atmospheric Emissions Inventory 2016, licensed under the Open Government Licence (OGL) v2.0, Crown Copyright 2020*. https://data.london.gov.uk/dataset/london-atmospheric-emissions-inventory--laei--2016, accessed March 2022. 2016.

[37] England, G., Heap, M., Pershing, D., Nihart, R., and Martin, G. Mechanisms of NOx formation and control: Alternative and petroleum-derived liquid fuels. *Symposium (International) on Combustion* 18.1 (1981), pp. 163–174. DOI: 10.1016/S0082-0784(81)80021-5.

[38] Damme, M. V., Clarisse, L., Franco, B., Sutton, M. A., Erisman, J. W., Kruit, R. W., Zanten, M. van, Whitburn, S., Hadji-Lazaro, J., Hurtmans, D., Clerbaux, C., and Coheur, P.-F. Global, regional and national trends of atmo-

spheric ammonia derived from a decadal (2008–2018) satellite record. *Environmental Research Letters* 16.5 (2021), p. 055017. DOI: 10.1088/1748-9326/abd5e0.

[39] Farren, N. J., Davison, J., Rose, R. A., Wagner, R. L., and Carslaw, D. C. Underestimated Ammonia Emissions from Road Vehicles. *Environmental Science & Technology* 54.24 (2020), pp. 15689–15697. DOI: 10.1021/acs.est.0c05839.

[40] Hammer, M. S., Donkelaar, A. van, Bindle, L., Shah, V., Jaeglé, L., Luo, G., Yu, F., Adeniran, J. A., Lin, J., and Brauer, M. Source sector and fuel contributions to ambient PM2.5 and attributable mortality across multiple spatial scales. *Nature Communications* 12.1 (2021), p. 3594. DOI: 10.1038/s41467-021-23853-y.

[41] Delmas, R., Serca, D., and Jambert, C. Global inventory of NOx sources. *Nutrient Cycling in Agroecosystems* 48.1 (1997), pp. 51–60. DOI: 10.1023/A:1009793806086.

[42] Andreae, M. O. The Ocean as a Source of Atmospheric Sulfur Compounds. *The Role of Air-Sea Exchange in Geochemical Cycling*. Ed. by P. Buat-Ménard. Springer Netherlands, 1986, pp. 331–362. DOI: 10.1007/978-94-009-4738-2_14.

[43] Carn, S. A., Fioletov, V. E., McLinden, C. A., Li, C., and Krotkov, N. A. A decade of global volcanic SO2 emissions measured from space. *Scientific Reports* 7.1 (2017), p. 44095. DOI: 10.1038/srep44095.

[44] Andreae, M. O. Emission of trace gases and aerosols from biomass burning – an updated assessment. *Atmospheric Chemistry and Physics* 19.13 (2019), pp. 8523–8546. DOI: 10.5194/acp-19-8523-2019.

[45] McDuffie, E. E., Martin, R. V., Spadaro, J. V., Burnett, R., Smith, S. J., O'Rourke, P., Hammer, M. S., Donkelaar, A. van, Bindle, L., Shah, V., Jaeglé, L., Luo, G., Yu, F., Adeniran, J. A., Lin, J., and Brauer, M. Source sector and fuel contributions to ambient PM2.5 and attributable mortality across multiple spatial scales. *Nature Communications* 12.1 (2021), p. 3594. DOI: 10.1038/s41467-021-23853-y.

[46] Schlesinger, W. H. and Hartley, A. E. A global budget for atmospheric NH_3. *Biogeochemistry* 15.3 (1992), pp. 191–211. DOI: 10.1007/BF00002936.

[47] Stull, R. B. Mean Boundary Layer Characteristics. *An Introduction to Boundary Layer Meteorology*. Ed. by R. B. Stull. Springer Netherlands, 1988, pp. 1–27. DOI: 10.1007/978-94-009-3027-8_1.

[48] Pan, L., Xu, J., Tie, X., Mao, X., Gao, W., and Chang, L. Long-term measurements of planetary boundary layer height and interactions with PM2.5 in Shanghai, China. *Atmospheric Pollution Research* 10.3 (2019), pp. 989–996. DOI: 10.1016/j.apr.2019.01.007.

[49] Perrino, C., Pietrodangelo, A., and Febo, A. An atmospheric stability index based on radon progeny measurements for the evaluation of primary urban pollution. *Atmospheric Environment* 35.31 (2001), pp. 5235–5244. DOI: 10.1016/S1352-2310(01)00349-1.

[50] Graham, A. M., Pringle, K. J., Arnold, S. R., Pope, R. J., Vieno, M., Butt, E. W., Conibear, L., Stirling, E. L., and McQuaid, J. B. Impact of weather types on UK ambient particulate matter concentrations. *Atmospheric Environment: X* 5 (2020), p. 100061. DOI: 10.1016/j.aeaoa.2019.100061.

[51] Collins, C. O. and Scott, S. L. Air Pollution in the Valley of Mexico. *Geographical Review* 83.2 (1993), pp. 119–133. DOI: 10.2307/215250.

[52] Lu, X., Zhang, L., and Shen, L. Meteorology and Climate Influences on Tropospheric Ozone: a Review of Natural Sources, Chemistry, and Transport Patterns. *Current Pollution Reports* 5.4 (2019), pp. 238–260. DOI: 10.1007/s40726-019-00118-3.

[53] Badr, O. and Probert, S. Sinks and environmental impacts for atmospheric carbon monoxide. *Applied Energy* 50.4 (1995), pp. 339–372. DOI: 10.1016/0306-2619(95)98803-A.

[54] Stavrakou, T., Müller, J.-F., Boersma, K. F., A, R. J. van der, Kurokawa, J., Ohara, T., and Zhang, Q. Key chemical NO_x sink uncertainties and how they influence top-down emissions of nitrogen oxides. *Atmospheric Chemistry and Physics* 13.17 (2013), pp. 9057–9082. DOI: 10.5194/acp-13-9057-2013.

[55] Borrego, C., Amodio, M., Catino, S., Dambruoso, P. R., Gennaro, G. de, Di Gilio, A., Giungato, P., Laiola, E., Marzocca, A., Mazzone, A., Sardaro, A., and Tutino, M. Atmospheric Deposition: Sampling Procedures, Analytical Methods, and Main Recent Findings from the Scientific Literature. *Advances in Meteorology* 2014 (2014), p. 161730. DOI: 10.1155/2014/161730.

[56] European Parliament. *Directive (EU) 2016/2284 of the European Parliament and of the Council of 14 December 2016 on the reduction of national emissions of certain atmospheric pollutants*. https://eur-lex.europa.eu/legal-content/EN/TXT/?uri=uriserv:OJ.L_.2016.344.01.0001.01.ENG&toc=OJ:L:2016:344:TOC, accessed August 2023. 2016.

[57] European Parliament. *Directive 2012/33/EU of the European Parliament and of the Council of 21 November 2012 amending Council Directive 1999/32/EC as regards the sulphur content of marine fuels*. https://eur-lex.europa.eu/legal-content/EN/TXT/?uri=celex%3A32012L0033, accessed August 2023. 2012.

[58] United Nations Framework Convention on Climate Change. *The Paris Agreement*. https://unfccc.int/documents/184656, accessed August 2023. 2018.

[59] European Parliament. *Regulation (EC) No 715/2007 of the European Parliament and of the Council of 20 June 2007 on type approval of motor vehicles with respect to emissions from light passenger and commercial vehicles (Euro 5 and Euro 6) and on access to vehicle repair and maintenance information*. https://eur-lex.europa.eu/legal-content/EN/ALL/?uri=celex%3A32007R0715, accessed August 2023. 2007.

[60] Ministry of Environmental Protection of the PRC. *GB 18352.5-2013 National Standard of the People's Republic of China ICS 13.040.50 Z 64 Replacing GB18352.3-2005 Limits and measurement methods for emissions from light-duty vehicles (CHINA 5)*. https://www.chinesestandard.net/PDF.aspx/GB18352.5-2013, accessed August 2023. 2013.

[61] United States Environmental Protection Agency. *Control of Air Pollution from Motor Vehicles: Tier 3 Motor Vehicle Emission and Fuel Standards*. https://www.epa.gov/regulations-emissions-vehicles-and-engines/final-rule-control-air-pollution-motor-vehicles-tier-3, accessed August 2023. 2014.

[62] European Parliament. *Commission Regulation (EU) No 813/2013 of 2 August 2013 implementing Directive 2009/125/EC of the European Parliament and of the Council with regard to ecodesign requirements for space heaters and combination heaters*. legislation.gov.uk/eur/2013/813/annex/II, accessed June 2022. 2013.

[63] Twigg, M. V. Catalytic control of emissions from cars. *Catalysis Today* 163.1 (2011), pp. 33–41. DOI: 10.1016/j.cattod.2010.12.044.

[64] Gill, L. J., Blakeman, P. G., Twigg, M. V., and Walker, M. V. The Use of NOx Adsorber Catalysts on Diesel Engines. *Topics in Catalysis* 28.1 (2004), pp. 157–164. DOI: 10.1023/B:TOCA.0000024345.85369.73.

[65] Komar, I., Antoniæ, R., and Matiæ, P. Selective catalytic reduction as a secondary method to remove NOx from diesel engine exhaust gas. *IFAC Proceedings Volumes* 40.17 (2007), pp. 305–309. DOI: 10.3182/20070919-3-HR-3904.00054.

[66] Janssens, T. V. W., Falsig, H., Lundegaard Lars F. andVennestrøm, P. N. R., Rasmussen, S. B., Moses, P. G., Giordanino, F., Borfecchia, E., Lomachenko, K. A., Lamberti, C., Bordiga, S., Godiksen, A., Mossin, S., and Beato, P. A Consistent Reaction Scheme for the Selective Catalytic Reduction of Nitrogen Oxides with Ammonia. *ACS catalysis* 5.5 (2015), pp. 2832–2845. DOI: 10.1021/cs501673g.

[67] Zhang, Z., Dong, R., Lan, G., Yuan, T., and Tan, D. Diesel particulate filter regeneration mechanism of modern automobile engines and methods of reducing PM emissions: a review. *Environmental Science and Pollution Research* 10.14 (2023), pp. 39338–39376. DOI: 10.1007/s11356-023-25579-4.

[68] Fu, J., Li, J., Tang, Y., Yan, F., He, Y., and Li, Y. Recirculation zone characteristics research on a sudden expansion swirl burner for DPF regeneration. *Environmental Progress & Sustainable Energy* 37.6 (2018), pp. 2000–2009. DOI: 10.1002/ep.12884.

[69] Poullikkas, A. Review of Design, Operating, and Financial Considerations in Flue Gas Desulfurization Systems. *Energy Technology & Policy* 2.1 (2015), pp. 92–103. DOI: 10.1080/23317000.2015.1064794.

[70] Cho, E.-S. and Chung, S. H. Characteristics of NOx emission with flue gas dilution in air and fuel sides. *KSME International Journal* 18.12 (2004), pp. 2303–2309. DOI: 10.1007/BF02990235.

[71] Holman, C., Harrison, R., and Querol, X. Review of the efficacy of low emission zones to improve urban air quality in European cities. *Atmospheric Environment* 111 (2015), pp. 161–169. DOI: 10.1016/j.atmosenv.2015.04.009.

[72] Peirson, J. and Vickerman, R. The London Congestion Charging Scheme: The Evidence. Ed. by C. Jensen-Butler, B. Sloth, M. M. Larsen, B. Madsen, and O. A. Nielsen. Springer Berlin Heidelberg, 2008, pp. 79–91. DOI: 10.1007/978-3-540-77150-0_5.

[73] Punzo, G., Panarello, D., and Castellano, R. Sustainable urban mobility: evidence from three developed European countries. *Quality & Quantity* 56.5 (2022), pp. 3135–3157. DOI: 10.1007/s11135-021-01253-0.

[74] Li, C. Z., Zhang, L., Liang, X., Xiao, B., Tam, V. W., Lai, X., and Chen, Z. Advances in the research of building energy saving. *Energy and Buildings* 254 (2022), p. 111556. DOI: 10.1016/j.enbuild.2021.111556.

[75] Drysdale, W. S., Vaughan, A. R., Squires, F. A., Cliff, S. J., Metzger, S., Durden, D., Pingintha-Durden, N., Helfter, C., Nemitz, E., Grimmond, C. S. B., Barlow, J., Beevers, S., Stewart, G., Dajnak, D., Purvis, R. M., and Lee, J. D. Eddy Covariance Measurements Highlight Sources of Nitrogen Oxide Emissions Missing from Inventories for Central London. *Atmospheric Chemistry and Physics Discussions* 2022 (2022), pp. 1–35. DOI: 10.5194/acp-2021-982.

[76] Grange, S. K. and Carslaw, D. C. Using meteorological normalisation to detect interventions in air quality time series. *Science of The Total Environment* 653 (2019), pp. 578–588. DOI: 10.1016/j.scitotenv.2018.10.344.

[77] United States Environmental Protection Agency. *VW Notice of Violation, Clean Air Act*. https://www.epa.gov/sites/production/files/2015-10/documents/vw-nov-caa-09-18-15.pdf, accessed August 2023. 2015.

[78] Baldocchi, D. Assessing the eddy covariance technique for evaluating carbon dioxide exchange rates of ecosystems: past, present and future. *Global Change Biology* 9.4 (2003), pp. 479–492. DOI: 10.1046/j.1365-2486.2003.00629.x.

[79] Baldocchi, D., Falge, E., Gu, L., Olson, R., Hollinger, D., Running, S., Anthoni, P., Bernhofer, C., Davis, K., Evans, R., Fuentes, J., Goldstein, A., Katul, G., Law, B., Lee, X., Malhi, Y., Meyers, T., Munger, W., Oechel, W., U, K., Pilegaard, K., Schmid, H., Valentini, R., Verma, S., Vesala, T., Wilson, K., and Wofsy, S. FLUXNET: A new tool to study the temporal and spatial variability of ecosystem-scale carbon dioxide, water vapor, and energy flux densities. *Bulletin of the American Meteorological Society* 82.11 (2001), pp. 2415–2434. DOI: 10.1175/1520-0477(2001)082<2415:FANTTS>2.3.CO;2.

[80] Novick, K. A., Biederman, J. A., Desai, A. R., Litvak, M. E., Moore, D. J. P., Scott, R. L., and Torn, M. S. The AmeriFlux network: A coalition of the willing. *Agricultural and Forest Meteorology* 249 (2018), pp. 444–456. DOI: 10.1016/j.agrformet.2017.10.009.

[81] Rebmann, C., Aubinet, M., Schmid, H., Arriga, N., Aurela, M., Burba, G., Clement, R., De Ligne, A., Fratini, G., Gielen, B., Grace, J., Graf, A., Gross, P., Haapanala, S., Herbst, M., Hortnagl, L., Ibrom, A., Joly, L., Kljun, N., Kolle, O., Kowalski, A., Lindroth, A., Loustau, D., Mammarella, I., Mauder, M., Merbold, L., Metzger, S., Molder, M., Montagnani, L., Papale, D., Pavelka, M., Peichl, M., Roland, M., Serrano-Ortiz, P., Siebicke, L., Steinbrecher, R., Tuovinen, J.-P., Vesala, T., Wohlfahrt, G., and Franz, D. ICOS eddy covariance flux-station site setup: a review. *International Agrophysics* 32.4 (2018), pp. 471+. DOI: 10.1515/intag-2017-0044.

[82] Lee, J. D., Helfter, C., Purvis, R. M., Beevers, S. D., Carslaw, D. C., Lewis, A. C., Møller, S. J., Tremper, A., Vaughan, A., and Nemitz, E. G. Measurement of NOx Fluxes from a Tall Tower in Central London, UK and Comparison with Emissions Inventories. *Environmental Science & Technology* 49.2 (2015), pp. 1025–1034. DOI: 10.1021/es5049072.

[83] Joshi, R., Liu, D., Nemitz, E., Langford, B., Mullinger, N., Squires, F., Lee, J., Wu, Y., Pan, X., Fu, P., Kotthaus, S., Grimmond, S., Zhang, Q., Wu, R., Wild, O., Flynn, M., Coe, H., and Allan, J. Direct measurements of black carbon fluxes in central Beijing using the eddy covariance method. *Atmospheric Chemistry and Physics* 21.1 (2021), pp. 147–162. DOI: 10.5194/acp-21-147-2021.

[84] Karl, T., Lamprecht, C., Graus, M., Cede, A., Tiefengraber, M., Arellano, J. V.-G. de, Gurarie, D., and Lenschow, D. High urban NOx triggers a substantial chemical downward flux of ozone. *Science Advances* 9.3 (2023), eadd2365. DOI: 10.1126/sciadv.add2365.

[85] Vaughan, A. R., Lee, J. D., Metzger, S., Durden, D., Lewis, A. C., Shaw, M. D., Drysdale, W. S., Purvis, R. M., Davison, B., and Hewitt, C. N. Spatially and temporally resolved measurements of NO_x fluxes by airborne eddy-covariance over Greater London. *Atmospheric Chemistry and Physics* 2021 (2021), pp. 1–27. DOI: 10.5194/acp-21-15283-2021.

[86] Apte, J. S., Messier, K. P., Gani, S., Brauer, M., Kirchstetter, T. W., Lunden, M. M., Marshall, J. D., Portier, C. J., Vermeulen, R. C. H., and Hamburg, S. P. High-Resolution Air Pollution Mapping with Google Street View Cars: Exploiting Big Data. *Environmental Science & Technology* 51.12 (2017), pp. 6999–7008. DOI: 10.1021/acs.est.7b00891.

Chapter 2

Pandemic restrictions in 2020 highlight the significance of non-road NO_x sources in central London

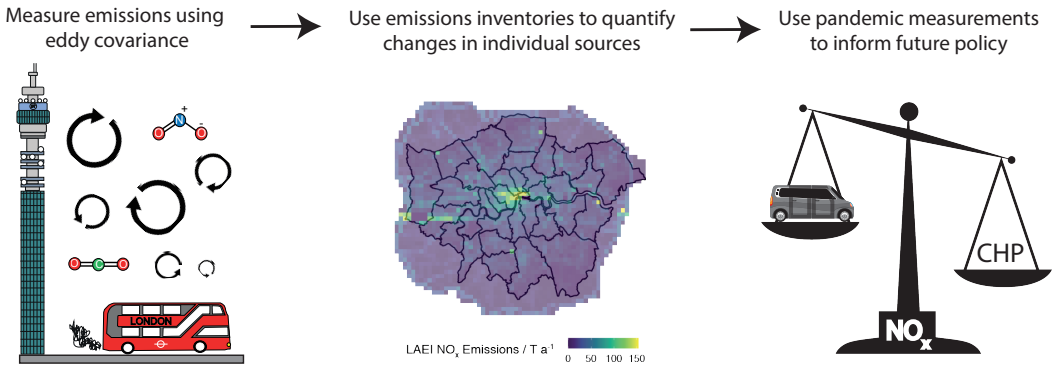

2.1 Abstract

Fluxes of nitrogen oxides (NO_x = NO + NO_2) and carbon dioxide (CO_2) were measured using eddy covariance at the British Telecommunications (BT) Tower in central London during the coronavirus pandemic. Comparing fluxes to those measured in 2017 prior to the pandemic restrictions and the introduction of the Ultra-Low Emissions Zone (ULEZ) highlighted a 73 % reduction in NO_x emissions between the two periods but only a 20 % reduction in CO_2 emissions and a 32 % reduction in traffic load. Use of a footprint model and the London Atmospheric Emissions Inventory (LAEI) identified transport and heat and power generation to be the two dominant sources of NO_x and CO_2 but with significantly different relative contributions for each species. Application of external constraints on NO_x and CO_2 emissions allowed the reductions in the different sources to be untangled identifying that transport NO_x emissions had reduced by > 73 % since 2017. This was attributed in part to the success of air quality policy in central London, but crucially due to the substantial reduction in congestion that resulted from pandemic reduced mobility. Spatial mapping of the fluxes suggests that central London was dominated by point source heat and power generation emissions during the period of reduced mobility. This will have important implications on future air quality policy for NO_2 which until now, has been primarily focused on the emissions from diesel exhausts.

2.2 Introduction

Air pollution is thought to be the world's largest environmental risk to human health causing an estimated 7 million premature deaths every year.[1] One species of pollutants of particular concern, especially in the UK, is NO_x. Formed as a by-product of high temperature combustion, NO_x is commonly emitted from the tailpipe exhaust of internal combustion engine vehicles

and through the use of fossil fuels to generate heat and energy in the residential, commercial and industrial sectors. The major component of NO_x is nitrogen dioxide (NO_2); direct exposure to which is known to contribute to respiratory infections such as bronchitis and pneumonia.[2] Indirectly, NO_x is a key component to the photochemical formation of ozone and fine particulate matter ($PM_{2.5}$). Exposure to ozone and $PM_{2.5}$ has additional adverse effects on the respiratory and cardiovascular systems.[3] Consequentially, NO_2 and $PM_{2.5}$ were estimated to cost the UK's National Health Service (NHS) and social care £1.6bn between 2017 and 2025, rising to £5.6bn if diseases with less robust evidence for an association are included.[4] This has become particularly relevant since the start of the coronavirus pandemic whereby long-term exposure to air pollution has been associated with the severity of COVID-19 cases.[5]

In 2008, countries in the EU were set legally binding limits for NO_2 concentrations in line with the World Health Organisation (WHO) recommendations. These are 40 µg m^{-3} for the annual mean with no more than 18 exceedances of the 200 µg m^{-3} hourly limit every year.[6] This target was expected to be met by 2010. In 2021, the WHO reduced the recommended annual mean limit by 75 % to 10 µg m^{-3}.[7]

London is a megacity in the UK with extensive NO_2 air quality issues. Almost all roadside locations exceeded the European Limit Value for NO_2 every year between 2010 and 2016.[8] Being in a highly developed position with significant resources, it has acted as a testing bed for policy intervention to try and curb emissions and achieve these air quality targets. These have been focused largely on traffic pollution and congestion charging and have the primary goal of reducing NO_x concentrations via reduced road transport emissions, either through reduced traffic numbers or through reduced average emission per vehicle per unit distance. Most notable is the introduction of the world's first ultra-low emissions zone (ULEZ), launched on 8th April 2019 with the zone spatially shown in Figure 2.1 a). This oper-

ates 24 hours a day, 364 days a year (excludes Christmas Day) and requires a daily payment if the vehicle driven inside the zone does not meet the most stringent emissions standards (currently Euro III for motorbikes, Euro IV for petrol cars and Euro VI for diesel cars and larger vehicles), in addition to the congestion charging payment within the same area. The ULEZ was expanded on 25th October 2021 up to the north and south circular roads in an 18-fold increase in size. In addition to policy, the coronavirus pandemic had significant implications on NO_x emissions in the UK through reduced mobility. During 2020 and 2021 the UK staged three lockdowns with "stay at home" orders. Full details on the timings and the severity of lockdown restrictions in London can be found in Figure 2.2.

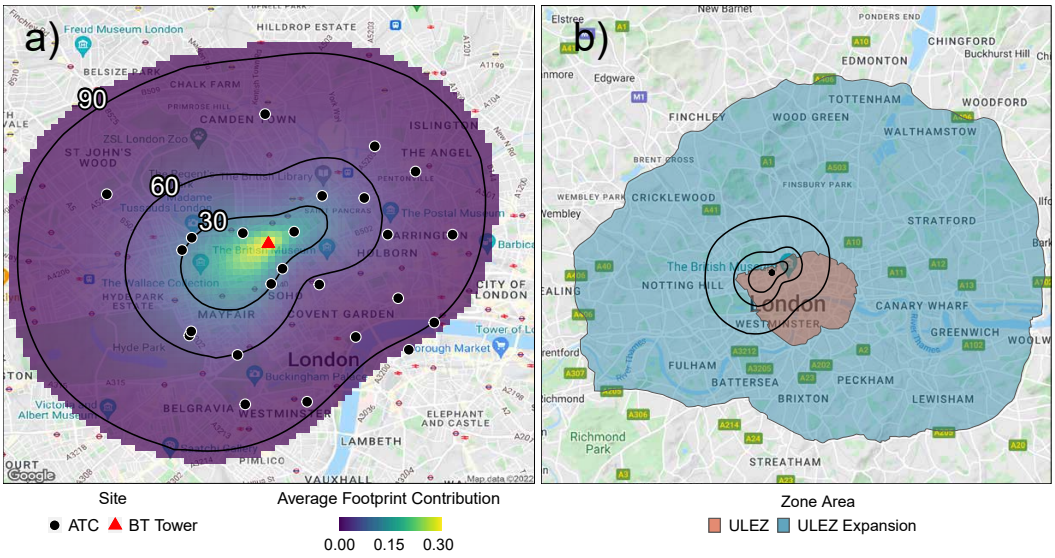

Figure 2.1: a) The average footprint climatology for the Sept 2020-Sept 2021 time period, with the 30, 60 and 90 % contribution contours and the location of the 24 ATC sites and the BT Tower site overlaid. b) Spatial boundary of the ULEZ (red) and ULEZ expansion (blue) with the same footprint contribution contours presented in a) overlaid as black lines, and the BT Tower site marked as a black dot. Maps produced from Google Maps (© Google Maps 2022) accessed using an API in R.

Assessment of the impact of policy intervention and other external stim-

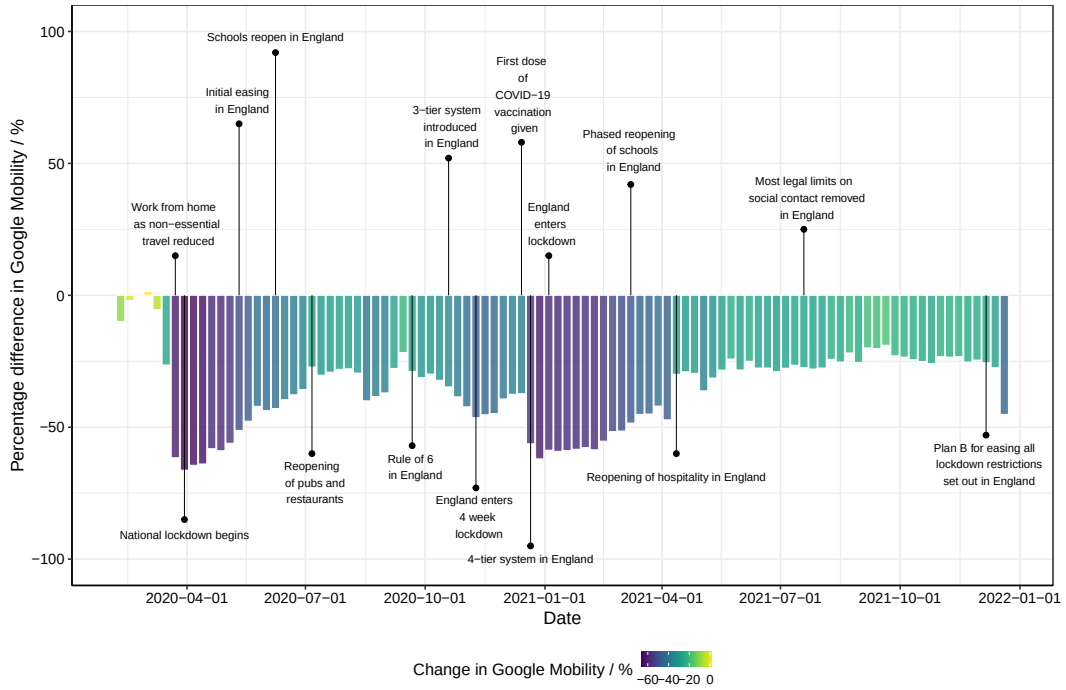

Figure 2.2: A timeline of COVID restrictions in England from the start of the COVID-19 pandemic until January 2022. Coloured bars represent the weekly change in Google Mobility across the UK.

uli like the coronavirus pandemic on NO_x emissions is crucial for the future design and implementation of air quality policy in the UK. Eddy-covariance is a technique used to quantify the surface-atmosphere exchange of an atmospheric pollutant. The calculated flux coupled with a footprint model provides information on surface emissions, allowing for changes to be studied and for direct comparison to the emissions inventories used in policy development. Whilst most frequently used for measuring carbon dioxide exchange with ecosystems from stationary towers,[9–11] the technique has been extended to the urban canopy for both greenhouse gases and air pollutants,[12–15] as well as to airborne measurements for the assessment of fluxes at a much greater spatial extent.[16–18] Recently, Lamprecht et al. [19] have used long term air pollutant emissions measurements to understand how COVID-19 restrictions have impacted different sources of NO_x in the small European city of Innsbruck, Austria. We undertake a similar analysis, but for the megacity of London. This offers the perspective of a different location where not only are emissions much higher, but contributions from different sources can vary significantly due to the nature of the activity required to support both greater population size and density. With the number of megacities consistently increasing, and expected to reach 43 in 2030 (up from 31 in 2018), improving our understanding of the air pollutant sources in them is as critical as ever.[20]

Here we present the first year of data from the long-term NO_x flux measurement programme at the BT Tower (London, UK). As the only long-term measurements of NO_x emissions from a megacity in the world this is a highly unique and potentially informative data-set. The NO_x emissions measurements are combined with additional CO_2 emissions measurements, a footprint model and the London Atmospheric Emissions Inventory (LAEI), and compared to previous measurements in 2017 to source apportion changes in emissions due to the coronavirus pandemic and the ULEZ. Resulting policy implications are inferred.

2.3 Experimental

2.3.1 Measurement Site

Instruments for measuring fluxes of urban air pollutants and greenhouse gases are situated in a small lab atop the BT Tower located in central London, UK (51°31'17.4"N, 0°8'20.04"W). The measurement height is 190 m above street level, with a mean building height of 8.8 ± 3.0 m in the 10 km radius surrounding the tower.[13] The gas inlet and ultrasonic anemometer are attached to a solid mast that extends 3 m above the top of the tower. Air is pumped down a 45 m Teflon tube (3/8" OD) in a turbulent flow of 20-25 L min^{-1} to the gas instruments, which are situated in a small air conditioned room inside the tower on the 35th floor.

2.3.2 NO_x measurements

Long-term measurements of NO and NO_2 fluxes began in September 2020 with data presented here up to September 2021. Data is compared to previous measurements made by Drysdale et al. [21] from March-August 2017. Both chemical species were measured using a dual channel chemiluminescence analyser (Air Quality Design Inc., Boulder Colorado, USA; 5 Hz) as described previously by Drysdale et al. [21] and Squires et al. [22]. The number of photons measured by the photomultiplier tube was converted into a part per trillion (ppt) mixing ratio using a five point calibration curve produced through dilutions of a 5 ppm NO in N_2 calibration standard (BOC Ltd., UK; traceable to the scale of the UK National Physical Laboratory, NPL) into NO_x free air (generated from an external Sofnofil and activated charcoal trap). NO_2 was calculated by conversion of NO_2 into NO using a photolytic blue light converter (BLC). Here, both NO and NO_2 were measured, from which NO_2 can be quantified by subtracting the NO mixing ratio and applying a correction factor for the conversion efficiency of the BLC.

The instrument was calibrated every 37 hours in addition to an hourly zero measurement to subtract the temperature dependent background signal of each channel. The uncertainty of the NO measurement is given as ± 3%, resulting from uncertainties in the sample mass flow controller, calibration gas mass flow controller and calibration gas certification. The uncertainty for the NO_2 measurement is given as ± 4.7% due to the additional uncertainty in the conversion efficiency calculation, determined in the laboratory via variation in repeated tests. The precision for each channel is calculated as 53 ppt and 184 ppt for NO and NO_2 respectively from the standard deviation in all the hourly zeros during the measurement period.

2.3.3 CO_2 measurements

Long-term measurements of CO_2 have been ongoing at the BT Tower since 2011 as part of UKCEH's National Capability programme. Dry mass fractions (1σ precision < 300 ppb) were measured initially using a cavity ring-down spectrometer (Model 1301-f, Picarro Inc., Santa Clara, California, USA; 10 Hz) as described by Helfter et al. [14]. Unfortunately, instrumental failure means data is not available between February and June 2021, after which a closed path infrared gas analyser (Li-7000, LI-COR Environmental, Lincoln, Nebraska, USA; 10 Hz) took over the CO_2 flux measurement.

2.3.4 Meteorological measurements

Meteorological measurements were made at the BT Tower as described by Lane et al. [23]. Wind speed, wind direction and sonic temperature were measured using a ultrasonic anemometer (Gill R3-50, Gill Instruments, Lymington, UK; 20 Hz), along with pressure and relative humidity measurements using a weather station (WXT520, Vaisala Corp. Helsinki, Finland; 1 Hz). For ease of processing, each chemical species is logged separately at it's maximum measurement frequency into a file with the sonic

anemometer data averaged to the same measurement frequency.

2.3.5 Flux Calculations

The flux, F, is defined in this context as the vertical transport of a chemical species per unit area per unit time. Hourly fluxes were calculated using eddy covariance theory as described by Eq. (2.1), where F is equal to the covariance between the instantaneous change in vertical wind speed, w', and the instantaneous change in species concentration, c', averaged over the hour.

$$F = \overline{w'c'} \tag{2.1}$$

Eddy-covariance calculations were performed using the modular software packages in eddy4R adopting the same processing settings described in Drysdale et al. [21] as adapted from Squires et al. [22] This was to allow a direct comparison to be made to the previous measurements made in 2017. The lag time correction was determined by maximisation of the cross-covariance between the pollutant concentration and the vertical wind component with an additional application of a high-pass filter which improves the precision of the determined lag time by an order of magnitude.[22,24] This resulted in median lag times of 7.2 s for NO, 7.6 s for NO_2 and 21 s for CO_2. Data was filtered such that the friction velocity (u*) is > 0.2 to ensure sufficiently developed turbulence and using eddy4R's quality control flagging scheme. The QA/QC process is described in detail by [25, 26]. Data is flagged as either valid or invalid based on the combination of individual flags for input data validation, homogeneity and stationarity, and development of turbulence.

2.3.6 Flux uncertainties

2.3.6.1 NO_x chemistry

Eddy covariance has traditionally only been used for relatively unreactive greenhouse gases like CO_2 with long atmospheric lifetimes. Attempting the calculation of NO_x fluxes is potentially problematic due to the greater reactivity and hence shorter lifetime of the species. If the loss rates of the reactive species is of a similar timescale to the vertical transport to the measurement height, the measured flux would be an underestimate and would not be representative of those emitted at the ground. In the case of NO_x, the major loss route to the atmosphere is via the reaction between NO_2 and OH. The rate constant for this simple association reaction can be calculated for the BT Tower specific conditions from Eq. 2.2 using mean values of temperature (T, 289 K) and pressure (P, 989 hPa).[27] This is derived from the low-pressure limiting rate constant ($k_0(T)$) and the high-pressure limiting rate constant ($k_\infty(T)$) using location specific total gas concentrations ([M]). n and m are simple exponents for the given reaction, in this case 3 and 0 respectively.

$$k_f(T,[M]) = \left\{\frac{k_\infty(T)\,k_0(T)\,[M]}{k_\infty(T)+k_0(T)\,[M]}\right\} 0.6^{\left\{1+\left[log_{10}\left(\frac{k_0(T)[M]}{k_\infty(T)}\right)\right]^2\right\}^{-1}} \tag{2.2}$$

Where:

$$k_0(T) = k_0^{298}\left(\frac{298}{T}\right)^n \tag{2.3}$$

$$k_\infty(T) = k_\infty^{298}\left(\frac{298}{T}\right)^m \tag{2.4}$$

$$[M] = \frac{PA_v}{RT} \tag{2.5}$$

Assuming a simple first order loss rate, the level of NO_x loss to the atmosphere can then be estimated from Eq. 2.6 using the previously determined

rate constant ($k_f(T,[M]) = 1.973 \times 10^{-11}$), the concentration of OH ([OH]) and the transport time to the measurement height (t).

$$\frac{[NO_x]}{[NO_x]_0} = e^{-k[OH]t} \tag{2.6}$$

Since [OH] is not routinely measured in London, a typical midday summers value 2×10^6 is used from London measurements in 2012 which would represent the maximum loss rate observed throughout the year.[28] Barlow et al. [29] estimate a typical transport time of < 10 minutes for the BT Tower, although under stable conditions this could increase to 20-50 minutes. This results in a loss of 2%, increasing up to 11% for a 50 minute transport time. The 11% loss represents the maximum loss observed at the BT Tower since it occurs under the most stable conditions during peak OH concentrations for London in Summer. In reality, this level of loss will not be observed in the data since stable conditions are filtered out in the QA/QC process and the majority of the OH concentration present throughout the year is less than that used in this calculation. Since it is much more likely to be at or below the 2% threshold, we consider NO_x reactivity to be a minor uncertainty in the flux calculations and a correction is not applied.

2.3.6.2 Vertical flux divergence

Another source of uncertainty is the size of the measurement height relative to the boundary layer. At 191 m, the sample inlet and sonic anemometer is often an appreciable portion of the boundary layer and can extend above the constant flux layer. On occasion, this results in concentration enhancements below the measurement height and an underestimation of the surface flux through vertical flux divergence. The impact of storage and vertical flux divergence at the BT Tower has been discussed previously by Helfter et al. [14] and Drysdale et al. [21], and in the absence of concentration and wind measurements at different heights up the tower, remains to be a notable

source of uncertainty in the measurement. Helfter et al. [14] speculates that venting after the onset of turbulence would capture some, if not most of the material stored below the measurement height. Drysdale et al. [21] demonstrates a correction for vertical flux divergence as a function of effective measurement height and effective entrainment height. The correction was typically around 20% for 2017, but is not applied to the data due to uncertainties in the boundary layer height data. Since this work studies relative magnitudes between two periods, the impact of VFD will likely cancel out, provided the meteorology is similar. Figure 2.3 shows that boundary layer height was on average 8% lower in 2020/21 compared to the 2017 measurement period. As such, a comparison between the VFD correction presented in Drysdale et al. [21] for both periods was conducted (see Figure 2.4. The lower boundary layer height in 2020/21 meant the correction was slightly higher at 24 %. A discussion on the impact this had on the results of this paper is given in Section 2.4.

2.3.6.3 High/low frequency loss

Due to the height of the measurement and the large eddy size above the urban roughness layer, the high frequency contributions to the fluxes are expected to be small. Drysdale et al. [21] calculated high frequency loss for NO and NO_2 at the BT Tower via co-spectra relative to temperature measured at 20 Hz. Correction factors above 1 Hz were shown to be of the order of 2 - 3 %. Losses due to low frequency can occur due to an insufficient length of averaging period. Previous studies at the BT Tower for 30 minute flux averaging periods have calculated losses due to high-pass filtering to be < 5%.[30,31] Since a 60 minute averaging period is used here, loss will be even lower. Both of these errors are considered minor and as a result no correction has been applied.

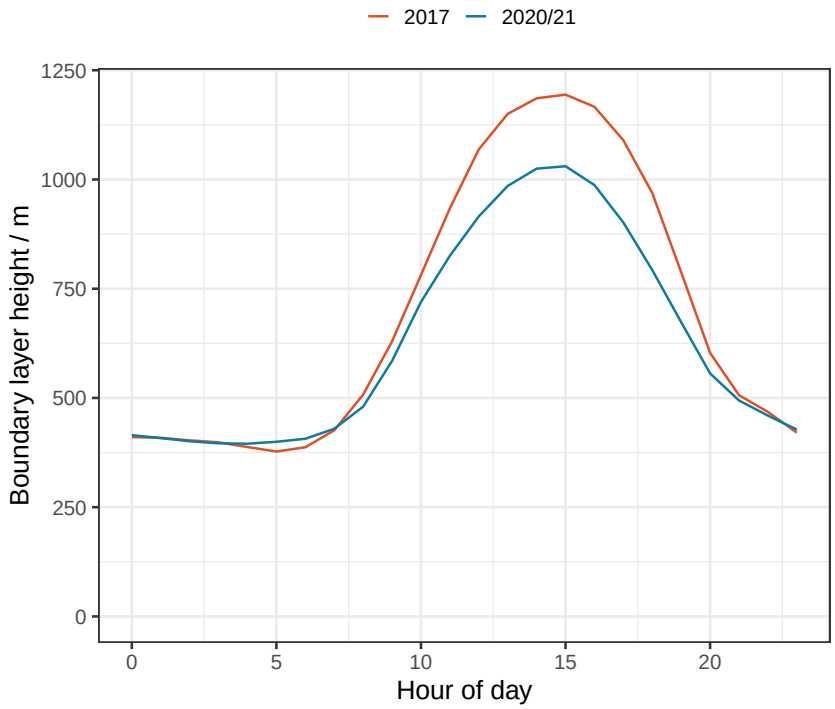

Figure 2.3: Boundary layer height comparison for 2017 and 2020/21 measurement periods

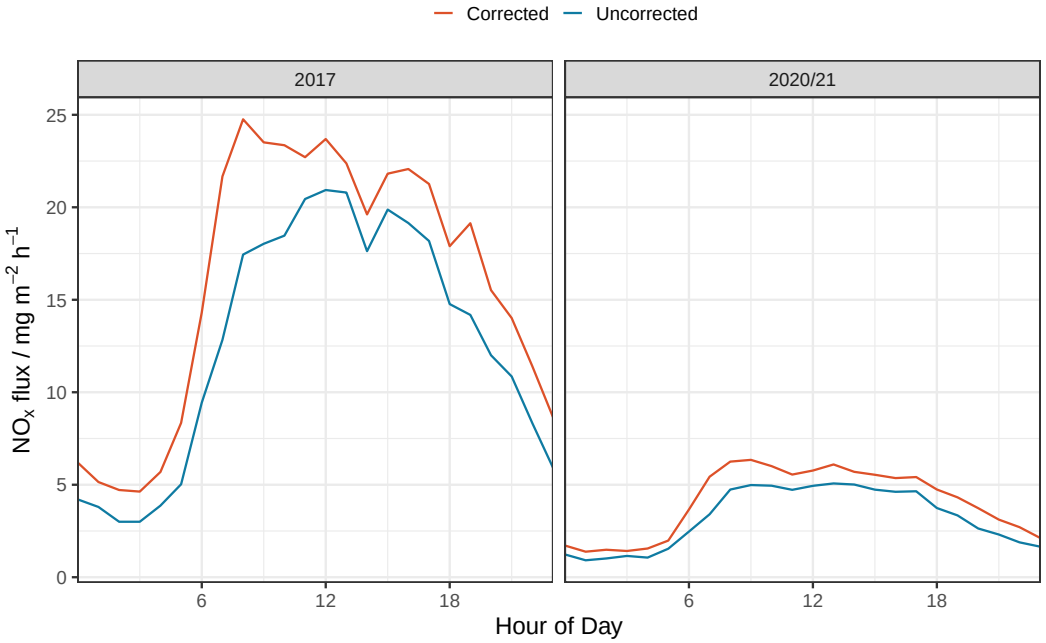

Figure 2.4: Diurnal profiles comparing uncorrected and vertical flux divergence corrected NO_x flux for the 2017 and 2020/21 measurement periods.

2.3.7 Footprint Modelling

A parameterised version of the backwards Lagrangian stochastic particle dispersion model implemented in eddy4R was used to estimate the footprint for each hourly flux measurement at the BT Tower. The model is described by Kljun et al. [32] and has been parameterised for a range of meteorological conditions and receptor heights to reduce the computational expense of running it. The original model aims to produce a cross-wind integrated footprint function as a function of its along-wind distance, which has now been further extended into two dimensions using a Gaussian distribution driven by the standard deviation in the cross-wind component.[33,34] Meteorology statistics from the eddy covariance calculations are used in combination with modelled boundary layer height from ERA5,[35] and a surface roughness length of 1.1 m to produce a weighted matrix of 100 m x 100 m grid cells. Each output weighted matrix was then scaled and aligned

to an appropriate coordinate reference system to allow each matrix to be plotted onto a map.

2.3.8 Traffic Data

Hourly traffic loads surrounding the BT Tower were calculated by summing the traffic load from each of the 24 Automatic Traffic Counters (ATCs) within the flux footprint, as shown in Figure 2.1. This gave an indication of the magnitude of traffic load for both measurement periods and allowed relative changes to be studied between the two years. In addition, daily vehicle length breakdown was examined from which vehicles were separated into three length classes: < 5.2 m, indicating the number of passenger cars, 5.2 m-12 m, indicating the number of vans and rigid lorries and > 12 m, indicating the number of buses and articulated lorries. As the LAEI estimates that almost all lorry emissions in central London are due to the rigid class, the >12 m class is assumed to solely be made up from buses. Data was provided by the Operational Analysis Department, Transport for London (TFL) via a freedom of information request.[36]

2.3.9 Emissions inventories

The London Atmospheric Emissions Inventory (LAEI) is a spatially disaggregated 1 km^2 gridded map of the annual emissions of various air pollutants for the London area up to the M25 motorway ring road.[37] Annual emissions are estimated using emission factors and activity factors for the different sources. For example, emissions from domestic combustion in (tonnes/year) would be calculated as Gas Consumption (GW.h/year) × Emission Factor (t poll/GW.h). The inventory is produced roughly every 3 years by TFL and the Greater London Authority (GLA). At the time of writing, there was no inventory estimates for the pandemic affected years of 2020 and 2021. We therefore use the most recent version produced in 2016,

which relates to a 'normal' year unaffected by lockdowns, to understand how emissions have changed since the 2017 measurements.

2.4 Results and Discussion

Of the 8760 hours in the year, 7034 hours of NO_x fluxes were calculated. Data loss was largely due to instrument or sample pump failure. Of these 7034 hours, a further 3621 were removed by the quality control flagging to leave 3413 hours of NO_x fluxes to be analysed. This data is displayed in Figure 2.5 along with measured CO_2 flux, traffic load around the tower and the UK's restrictions stringency index as calculated by the Oxford COVID-19 Government Response Tracker.[38] Traffic load around the tower was strongly anti-correlated with stringency index as expected. However, there was no obvious correlation of NO_x flux with traffic load. In fact, NO_x flux displays an anti-correlation with traffic flow and stringency index from April to August. This is likely due to a reduction in heat and power generation emissions due to the warmer weather, which is a first indication that traffic may not be the dominant source of NO_x flux during this period. Traffic loads had not recovered to pre-pandemic levels either (Figure 2.6) despite the fact all lockdown restrictions were fully removed on 21 June 2021, hinting at a more long-term change in behaviour. This is not unexpected as the stringency index remained at 40 %, mainly due to self-isolation requirements and international travel restrictions which were still present at this stage. In the absense of a long term time series from which a number of studies have used boosted regression models to predict normal emission scenarios, we compare data to that previously measured from March - August 2017 by Drysdale et al. [21]. This is an ideal time period for comparison since the measurement footprint was very similar (see Figure 2.7) and meteorological conditions meant minimal bias was expected between the years (see Sec. 2.3.6.2). Average diurnal NO_x fluxes were down 73 % (3.45 vs

12.88 mg m^{-2} h^{-1}). However, only a corresponding 20 % reduction in CO_2 flux (2455 vs 3062 mg m^{-2} h^{-1}) and 32 % reduction in traffic load (16540 vs 24405 vehicles day^{-1}) around the measurement site was observed. These changes can be clearly seen in the diurnal profiles in Figure 2.5. These % changes were calculated after application of the different vertical flux divergence corrections discussed in Section 2.3.6.2, and exhibited a negligible variation of < 1 %.

2.4.1 Calculation of inventory estimated emissions

Estimated emissions from the London Atmospheric Emissions Inventory (LAEI) for the measurement footprint were calculated to aid understanding of these observations. The hourly footprint weighted matrix output from eddy4R was used to select the relevant areas of the LAEI. The theoretical contribution to the flux was extracted from each footprint grid cell and scaled for hour of day, day of week and month of year for each emissions sector using a set of anthropogenic scaling factors described by Drysdale et al. [21]. An excellent agreement between the diurnal profiles and measurement footprint (shown in Figure 2.7) for the 2017 and 2020/21 measurement periods was seen. This gave us confidence that any changes in emissions were not to do with sampling in different times of year or sampling in different areas of central London. The source breakdown of the 2017 inventory generated time series for both CO_2 and NO_x is shown in Figure 2.8. Emissions of both species are almost entirely made up from combustion of fossil fuels to generate heat and power in the domestic, commercial and industrial sectors and the transport sector, which is dominated by various forms of road transport. However, each species has a significantly different relative contribution from each sector. 75 % of CO_2 emissions are estimated to arise from heat and power generation but only 42 % of NO_x emissions from the same source.

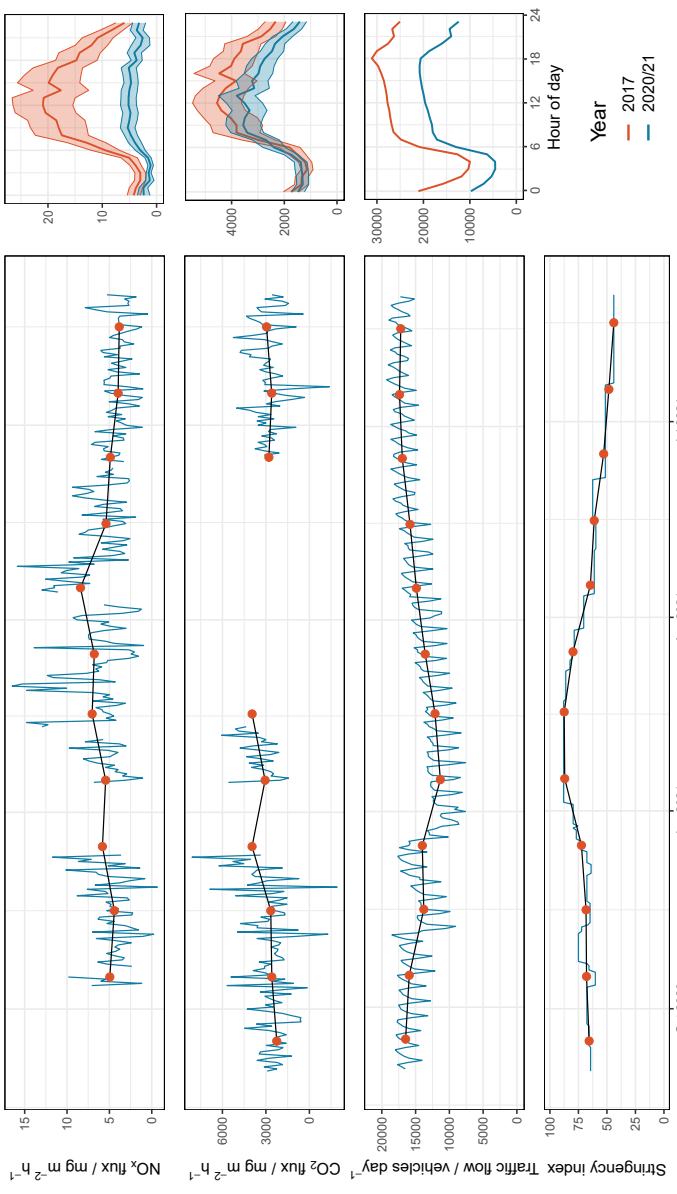

Figure 2.5: Time series from September 2020 to September 2021 for daily time averaged NO_x flux, CO_2 flux, traffic load around the tower and stringency index in the UK. Also shown are monthly averages for each variable as red dots centered around the center of each month. Average median diurnal profiles with error bars (calculated as the combination of random and systematic errors in the flux calculations, as described by Mann and Lenschow [39]) for the data are shown to the right in blue for 2020/21 in comparison to those generated from the 2017 data in red.

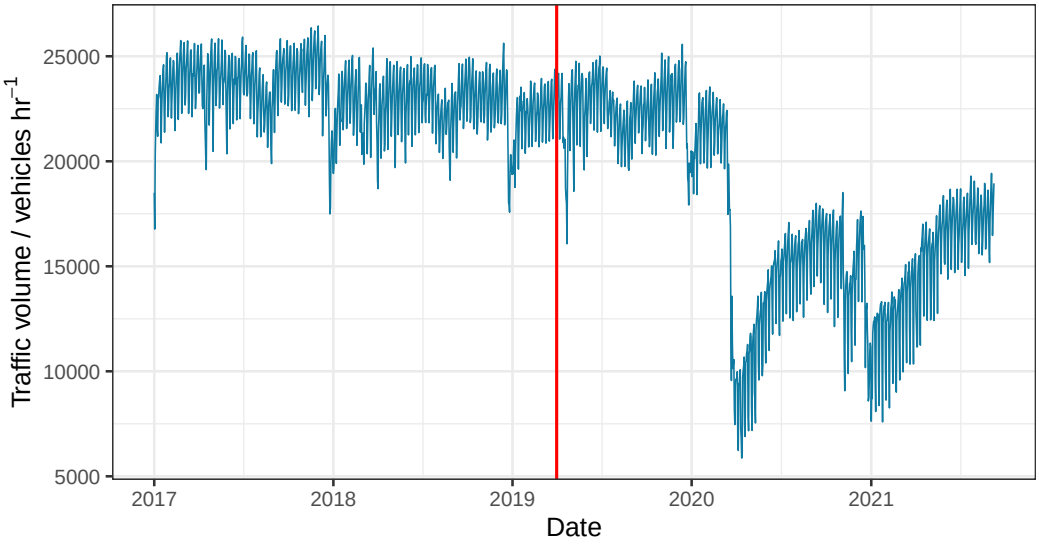

Figure 2.6: Daily average traffic load from 01/01/2017 - 01/09/2021. The date of the introduction of the ULEZ is marked as a vertical red line.

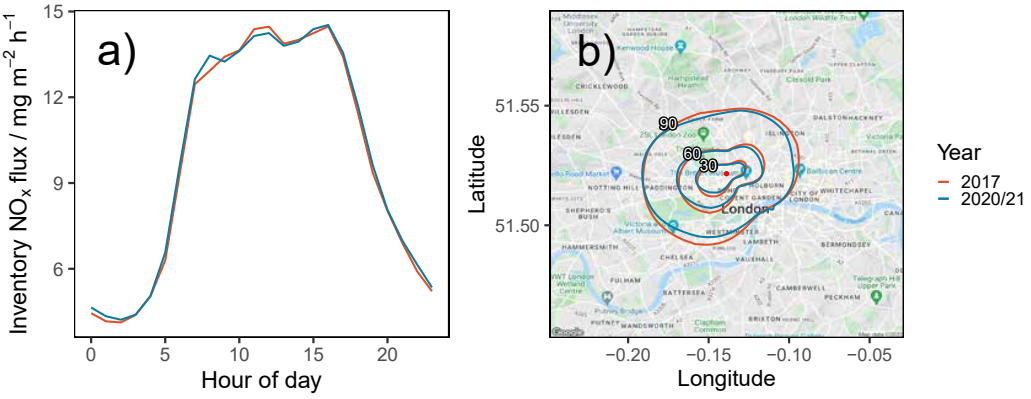

Figure 2.7: Comparison of a) the diurnal profile of the inventory generated time series and b) the 30, 60 and 90 % footprint contribution contours for the 2017 data set in black and the 2020/21 data set in red. Map in b) produced from Google Maps (© Google Maps 2021) accessed using an API in R.

2.4.2 Source apportionment of emissions reduction

The inventory breakdown for each species and the different percentage reductions in measured emissions since 2017 were used to disentangle changes in emissions of each sector. This was done simultaneously using a number of assumptions.

Table 2.1: A summary of the data used in the formation of simultaneous Eqs. (2.7) and (2.8).

	NO_x	CO_2
% measured reduction in emissions since 2017	73 %	20 %
% contribution from heat and power generation	0-50 % (α)	75 %
% contribution from transport	50-100 % (β)	25 %
% reduction in heat and power generation emissions	x	x
% reduction in transport emissions	y'	y

Helfter et al. [14] highlight the excellent agreement of CO_2 emissions measured at the BT Tower to those estimated by the LAEI and thus the source contributions of 75 % from heat and power generation and 25 % from transport for CO_2 are taken as accurate here. On the other hand, previous observations have shown a significant underestimation of NO_x emissions in central London.[16,21] This is most likely due to an underrepresentation of road transport NO_x emissions in line with a poor representation of diesel vehicle emissions and/or congestion. Therefore, rather than using the inventory predicted 42:58 split for heat and power generation:transport the relative contributions were varied. Labelled as $\alpha : \beta$, different scenarios between 50:50 and 0:100 (where $\alpha + \beta = 100\%$) were chosen to represent all possible levels of NO_x underestimation. The percentage reduction in heat and power generation emissions for both species is labelled as x with the assumption that any reduction in this sector's emissions would have the same reduction in measured flux for both species. With minimal legislation for

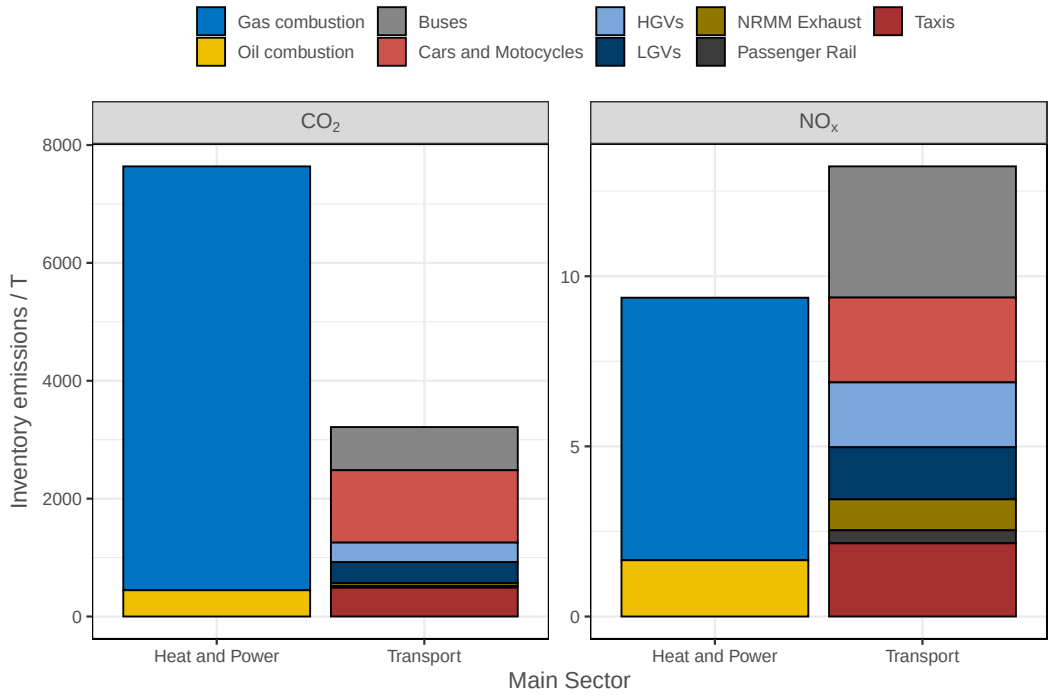

Figure 2.8: Inventory estimated breakdown of emissions for CO_2 (left) and NO_x (right) in Tonnes for March through August of 2017 as determined from the inventory emissions extraction for our hourly measurement footprint. LGV = Light Goods Vehicles, HGV = Heavy Goods Vehicles, NRMM = Non-Road Mobile Machinery.

the sector introduced between 2017 and 2020/21 and a failure to address NO_x emissions from boilers in the UK's Clean Air Strategy, this assumption is considered reasonable.[40] However, this is is likely to be untrue for transport. Policy implemented between the two measurement periods specifically targeted NO_x emissions and NO_x emissions are disproportionately higher in higher traffic loads due to the ineffectiveness of exhaust treatment systems in that environment. Additionally, the modernisation of the vehicle fleet will have introduced more vehicles with lower NO_x/CO_2 emission ratios. Therefore, the relative change in the emissions of NO_x and CO_2 from traffic sources may not have been the same, and different values are given here as y and y'. This information is all summarised in Table 2.1 with the two independent constraints displayed in Eq.'s (2.7) for CO_2 and (2.8) for NO_x:

$$\delta CO_2 = 0.75x + 0.25y_{[32,100]} = 20\% \tag{2.7}$$

$$\delta NO_x = \alpha x + \beta y'_{[73,100]} = 73\% \tag{2.8}$$

The different scenarios are visualised in Figure 2.9 to aid understanding of the possible solutions. Two bounding conditions drawn as hashed lines are applied to constrain the solutions. These are as follows: a) A reduction in transport emissions greater than 100 % is not possible and b) CO_2 emissions from transport must have decreased by at least 32 % in line with the 32 % reduction in traffic load. In reality, CO_2 emissions will have decreased by greater that 32% as a result of the fleet modernisation which has lead to a decrease in the average CO_2 emissions per new vehicle registration.[41]

Highlighted in green are all the resulting possible solutions where crucially, to achieve the observed reductions in NO_x flux, there must have been a 73-100 % reduction in transport NO_x emissions with transport contributing > 70 % to total NO_x emissions. This transport contribution percentage

demonstrates the underestimation in the inventory of transport emissions in agreement with Karl et al. [15] and Drysdale et al. [21]. However, the most interesting observation is that a 73-100 % decrease in transport NO_x emissions is seen for only a 32 % decrease in traffic load since 2017.

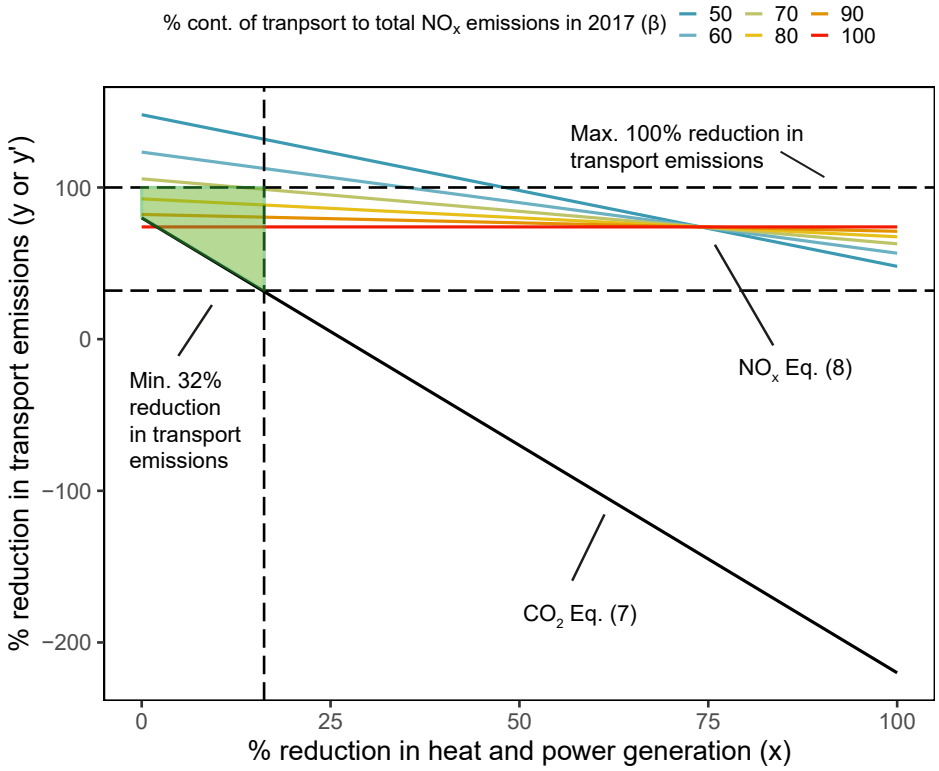

Figure 2.9: A plot showing the external constraints on NO_x and CO_2 emissions. Eq. (2.7) is shown as the solid black line and Eq. (2.8) as the coloured solid lines, with each colour reflecting a different value of β. The two horizontal hashed lines represent the two discussed constraints, and the vertical hashed line shows the constraint the minimum of 32 % reduction in traffic CO_2 emissions has on the NO_x scenarios. All possible solutions when the constraints are applied are highlighted by the shaded green area.

When compared to concentrations, we found that NO_x concentrations at Marylebone Road, a kerbside monitoring site within the flux footprint, had declined by 62 % between the two periods (248 vs 95 µg m^{-3}). This

is increased to 69 % (214 vs 67 µg m^{-3}) when looking at the roadside increment concentration (roadside – urban background) as determined from Marylebone Road and London North Kensington monitoring sites. Whilst this was slightly lower in magnitude than the measured change in flux, the concentration data will have been heavily influenced by meteorology and so some disagreement was expected. There are a number of plausible explanations for the large decrease in NO_x fluxes. The introduction of the ULEZ is thought to have resulted in a pre-pandemic 35 % reduction in NO_x emissions from road transport in central London;[42] this is likely to be an upper estimate for our measurements due to the fact a significant proportion of our flux footprint being situated outside of the ULEZ zone. With average traffic loads between April and November 2019 after the ULEZ was introduced only down 1.8 % on 2018 levels for the same period, the vast majority of the reduction is due to a clean-up of the fleet which reduces the emissions per vehicle per unit distance. The remaining emissions are further reduced by 32 % due there being 32 % less vehicles on the roads surrounding the BT tower during the pandemic. This leaves 16-41 % of unaccounted for emissions reduction. A small portion of this unaccounted for reduction may be due to a 40 % reduction in the number of buses on the roads surrounding the BT Tower during 2020/21. The >12 m class of the vehicle length breakdown in Figure 2.10 represents the bus classification. With buses making up 17 % of the total NO_x emissions from road transport, the decrease in relative proportion between 2017 and 2020/21 could result in a maximum of 7 % extra reduction in NO_x emissions. It is likely to be less than 7 % due to the small increase in the relative proportion of the 5.2 m-12 m class.

2.4.3 Flux correlations with traffic load

Examining how the NO_x flux correlated with traffic load for both measurement time periods gives further insight into the unaccounted emissions re-

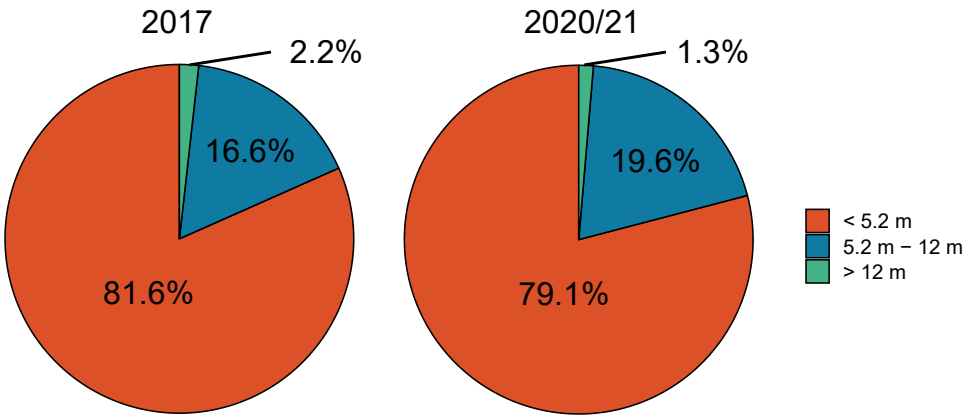

Figure 2.10: Pie chart for the 2017 and 2020/21 measurement periods displaying the distribution of vehicle length classes measured by the 24 ATC's surrounding the BT Tower.

duction. Figure 2.11 generally shows significantly enhanced NO_x emissions in 2017 above 25000 vehicles hr^{-1}. With road transport being the dominant source during these measurements it is highlighting what is thought to be the effect of congestion on NO_x emissions.

During periods of high congestion, increased emissions are expected due to increased length in journey time, a greater number of accelerations in the stop start nature of traffic and reduced effectiveness of exhaust gas NO_x treatment systems in diesel vehicles at low engine temperatures.[43] The effect of congestion on NO_x emissions is highly dependent on several variables including the fleet composition, type of exhaust treatment system and the actual level of congestion.[44] It is thought that for individual roads, excess emissions from congestion can be anything up to 75 % greater than non-congested roads.[45] Therefore, it is thought that reducing the peak traffic load below 25000 vehicles hr^{-1} has had a large impact on traffic NO_x emissions, more than accounting for the remaining emissions reduction.

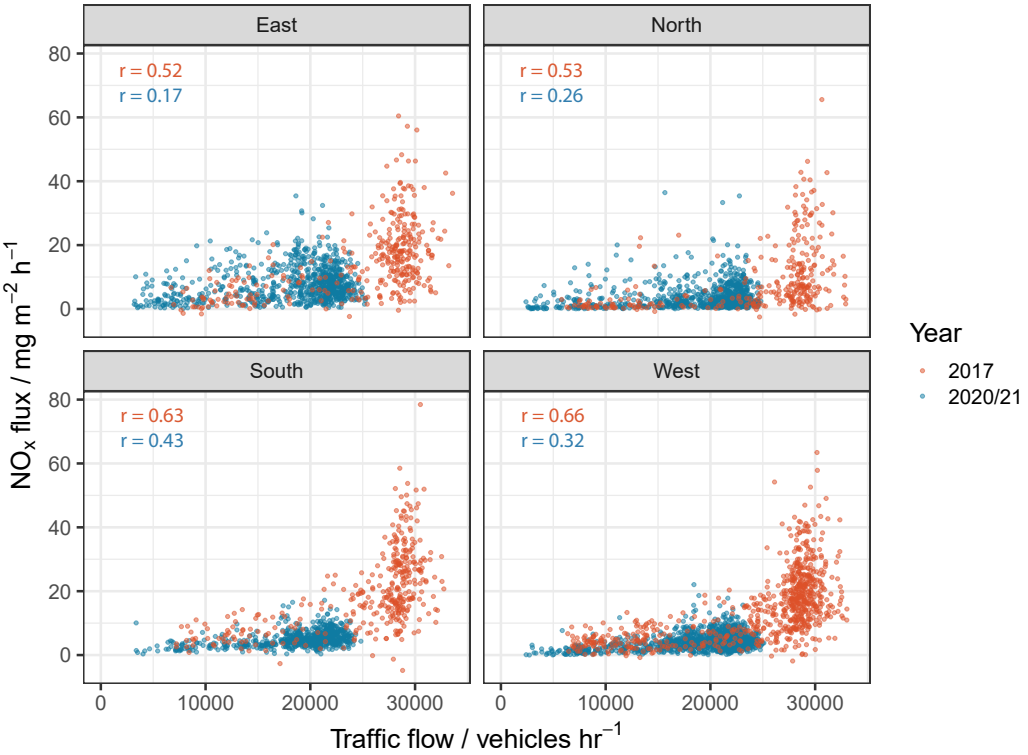

Figure 2.11: Comparison of the measured NO_x flux with hourly traffic load (sum of the 24 surrounding ATCs) for March through August 2017 (red) and Sept 2020 - Sept 2021 (blue). The data is split by wind direction: North (315°-45°), east (45°-135°), south (135°-225°) and west (225°-315°). In the top left of each facet is the Spearman correlation coefficient for each year for the corresponding wind direction.

2.4.4 Spatial Mapping

This change in emissions is clearly seen in the spatial mapping of the NO_x fluxes in Figure 2.12. Drysdale et al. [21] assigned the heightened emissions to the northeast of the BT Tower in Figure 2.12 a) to Euston station, including not only the train station, but also the large Euston bus station, taxi ranks and busy roads feeding the station. In addition, the high fluxes measured to the southwest are assigned to highly congested streets such as Oxford Street, Regent Street and Piccadilly. Both areas are associated with high traffic volumes and congestion and support the notion that road transport emissions dominate in central London in 2017. However, these areas have almost an order of magnitude smaller emissions and are barely visible for 2020/21 when shown on the same scale. This adds additional support to the conclusion that reduced traffic load and thus congestion in 2020/21 have been a major cause of the reduced NO_x flux.

The spatial map for 2020/21 in Figure 2.12 c) on its own scale identified a shift in the dominant NO_x emissions source between 2017 and 2020/21. Whilst Euston station and the previously congested southwesterly area are still noticeable, the major stand out area is to the east. Depicted as a white box is the outline of the University of London point source as documented by the National Atmospheric Emissions Inventory, a similar inventory to the LAEI but for the whole of the UK.[46] The University of London is the largest university in the UK and its Bloomsbury Campus appears directly under the heightened emissions area. This site is made up of much of the University College London (UCL) central administration, the UCL hospital and Bloomsbury Heat and Power, a number of combined heat and power (CHP) sites to power the university. CHP systems simultaneously generate heat and electrical power from a single source of energy. By capturing and utilising the heat that is generated as a by product of the electricity generation process, efficiency is increased which can reduce carbon emissions

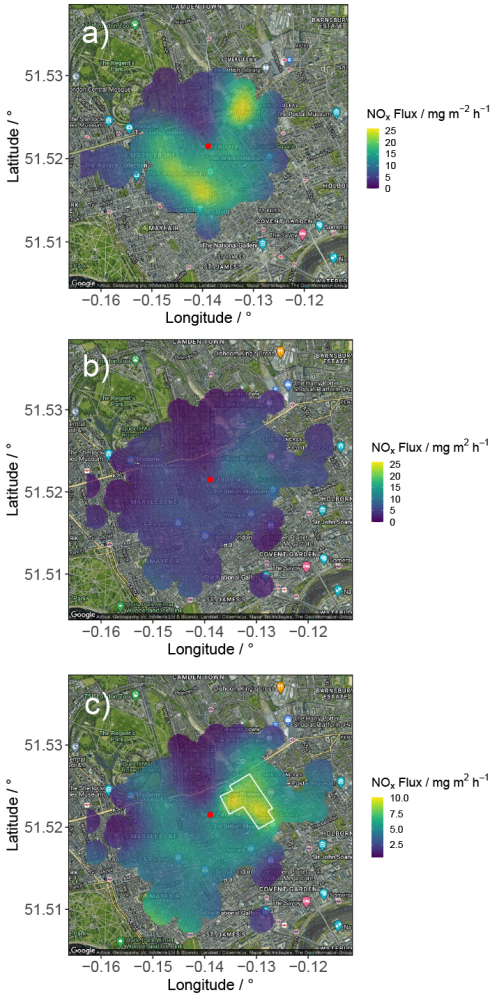

Figure 2.12: NO_x flux surfaces as a function of along-wind distance to the footprint maximum contribution and wind direction, as derived by Drysdale et al. [21], for a) March through August 2017 and b) September 2020 to September 2021, displayed on the same scale for ease of visual comparison. Also shown in c) September 2020 to September 2021 on it's own scale with the border for the University of London overlaid in white. The location of the BT Tower site is displayed as a red dot in each spatial map. Maps are produced using Google Maps (© Google Maps 2022) accessed using an API in R.

by up to 30 % compared to conventional separate generation.[47] However, the requirement for CHP to be in urban areas risks an increase in air pollution. Indeed it has been shown that CHP can "substantially" impact air quality due to NO_x, the highest criteria judged by Environment Protection UK and the Institute of Air Quality Management.[48] Here, the heat and power generation source stands out and dominates over transport but is only seen due to the drastic reduction in transport NO_x emissions during the period of pandemic reduced mobility. The Spearman Correlation coefficients presented in Figure 2.11 give further evidence that the dominant source between the two periods has changed. Correlations between NO_x flux and traffic load are reduced in 2020/21, in particular in the Easterly direction. Here, the lowest correlation is observed and high NO_x fluxes are seen even at low traffic loads. These observations are in agreement with the spatial mapping interpretation in that heat and power generation is the dominant source from this direction.

2.5 Conclusions

Eddy covariance emissions measurements at the unique BT Tower site in central London provide an opportunity to study the evolution of air pollutant emissions in a megacity and the part that policy and other external stimuli play in improving air quality. Here, the direct emissions measurements have shown that reducing congestion could be an even more effective way of reducing NO_x emissions from road transport than the ULEZ. However, this is not the direction in which the UK is heading. With much cheaper mileage, the continued uptake of electric vehicles is predicted to increase congestion. Reducing the number of vehicles on the road by improving infrastructure for other greener methods of travel such as cycling would not only achieve reduced congestion but give additional benefits to health further reducing costs of treatment at health services.[49] A more tar-

geted approach to simultaneously reduce congestion as well as emissions per vehicle per unit distance is therefore recommended to other cities looking to implement policies to tackle high traffic NO_x emissions.

The observation that NO_x emissions in central London during this continuing period of reduced mobility were thought to be dominated by heat and power generation is an important one. This is a transition which was expected to occur in the coming years but was brought forward in time by the pandemic, providing a glimpse into future air quality. As of 2020, there were 2659 CHP sites in the UK with additional widespread usage in Europe.[47] Due to their increased efficiency and the push towards NetZero economies, they are expected to increase in popularity. Despite this period of drastically reduced transport emissions, all air quality monitoring sites (urban background, urban traffic and curbside) in London far exceeded the new WHO NO_2 air quality target. To achieve these targets it is therefore clear that legislation is required to reduce NO_x emissions from heat and power generation. The heat and power generation source has been somewhat neglected due to the prominence of issues with diesel vehicle emissions. But with the planned use of hydrogen combustion in decarbonisation, which currently has major uncertainties due to a lack of experimental data, now is the critical time to start thinking about policy intervention for this sector.[50] This makes the lack of acknowledgement for gas combustion in boilers in the UK clean air strategy highly disappointing. This is the first indication from a megacity which shows heat and power emissions will need to be regulated to achieve the new air quality NO_x targets. As more and more of the world's population is expected to live in urban areas, it is essential that compliance with WHO targets is achieved to minimise health and economic impacts. The conclusions derived from this work will therefore be of interest to other nations, especially with air quality improvements being increasingly sought in the developing world.

Bibliography

[1] World Health Organisation. *Global health estimates 2016: deaths by cause, age, sex, by country and by region, 2000–2016*. https://www.who.int/health-topics/air-pollution#tab=tab_1, accessed October 2021. 2018.

[2] Ciencewicki, J. and Jaspers, I. Air Pollution and Respiratory Viral Infection. *Inhalation Toxicology* 19.14 (2007), pp. 1135–1146. DOI: 10.1080/08958370701665434.

[3] Zhang, J., Wei, Y., and Fang, Z. Ozone pollution: A major health hazard worldwide. *Frontiers in Immunology* 10 (2019), p. 2518. DOI: 10.3389/fimmu.2019.02518.

[4] Public Health England. *Estimation of costs to the NHS and social care due to the health impacts of air pollution: summary report*. https://assets.publishing.service.gov.uk/government/uploads/system/uploads/attachment_data/file/708855/Estimation_of_costs_to_the_NHS_and_social_care_due_to_the_health_impacts_of_air_pollution_-_summary_report.pdf, accessed June 2022. 2018.

[5] Imperial College London. *Investigating links between air pollution, COVID-19 and lower respiratory infectious diseases*. https://www.imperial.ac.uk/media/imperial-college/medicine/sph/environmental-research-group/ReportfinalAPCOVID19_v10.pdf, accessed November 2022. 2021.

[6] European Parliament. *Directive 2008/50/EC of the European Parliament and of the council of 21 May 2008 on ambient air quality and cleaner air for Europe*. https://eur-lex.europa.eu/legal-content/EN/TXT/?uri=CELEX:02008L0050-20150918, accessed October 2022. 2008.

[7] World Health Organisation. *WHO global air quality guidelines: particulate matter (PM2.5 and PM10), ozone, nitrogen dioxide, sulfur dioxide and carbon monoxide*. https://apps.who.int/iris/handle/10665/345329, accessed December 2022. 2021.

[8] Font, A., Guiseppin, L., Blangiardo, M., Ghersi, V., and Fuller, G. W. A tale of two cities: is air pollution improving in Paris and London? *Environmental Pollution* 249 (2019), pp. 1–12. DOI: 10.1016/j.envpol.2019.01.040.

[9] Baldocchi, D., Falge, E., Gu, L., Olson, R., Hollinger, D., Running, S., Anthoni, P., Bernhofer, C., Davis, K., Evans, R., Fuentes, J., Goldstein, A., Katul, G., Law, B., Lee, X., Malhi, Y., Meyers, T., Munger, W., Oechel, W., U, K., Pilegaard, K., Schmid, H., Valentini, R., Verma, S., Vesala, T., Wilson, K., and Wofsy, S. FLUXNET: A new tool to study the temporal and spatial variability of ecosystem-scale carbon dioxide, water vapor, and energy flux densities. *Bulletin of the American Meteorological Society* 82.11 (2001), pp. 2415–2434. DOI: 10.1175/1520-0477(2001)082<2415:FANTTS>2.3.CO;2.

[10] Griffis, T. J., Sargent, S. D., Baker, J. M., Lee, X., Tanner, B. D., Greene, J., Swiatek, E., and Billmark, K. Direct measurement of biosphere-atmosphere isotopic CO_2 exchange using the eddy covariance technique. *Journal of Geophysical Research: Atmospheres* 113.D8 (2008), p. D08304. DOI: 10.1029/2007JD009297.

[11] Butterbach-Bahl, K., Baggs, E. M., Dannenmann, M., Kiese, R., and Zechmeister-Boltenstern, S. Nitrous oxide emissions from soils: how well do we understand the processes and their controls? *Philosophical Transactions of the Royal Society B: Biological Sciences* 368.1621 (2013), p. 20130122. DOI: 10.1098/rstb.2013.0122.

[12] Langford, B., Nemitz, E., House, E., Phillips, G. J., Famulari, D., Davison, B., Hopkins, J. R., Lewis, A. C., and Hewitt, C. N. Fluxes and concentrations of volatile organic compounds above central London, UK. *Atmospheric Chemistry and Physics* 10.2 (2010), pp. 627–645. DOI: 10.5194/acp-10-627-2010.

[13] Lee, J. D., Helfter, C., Purvis, R. M., Beevers, S. D., Carslaw, D. C., Lewis, A. C., Møller, S. J., Tremper, A., Vaughan, A., and Nemitz, E. G. Measurement of NOx Fluxes from a Tall Tower in Central London, UK and Comparison with Emissions Inventories. *Environmental Science & Technology* 49.2 (2015), pp. 1025–1034. DOI: 10.1021/es5049072.

[14] Helfter, C., Tremper, A. H., Halios, C. H., Kotthaus, S., Bjorkegren, A., Grimmond, C. S. B., Barlow, J. F., and Nemitz, E. Spatial and temporal variability of urban fluxes of methane, carbon monoxide and carbon dioxide above London, UK. *Atmospheric Chemistry and Physics* 16.16 (2016), pp. 10543–10557. DOI: 10.5194/acp-16-10543-2016.

[15] Karl, T., Graus, M., Striednxig, M., Lamprecht, C., Hammerle, A., Wohlfahrt, G., Held, A., Heyden, L. von der, Deventer, M. J., Krismer, A., Haun, C., Feichter, R., and Lee, J. Urban eddy covariance measurements reveal significant missing NO_x emissions in central Europe. *Scientific Reports* 7.1 (2017), pp. 2536–2545. DOI: 10.1038/s41598-017-02699-9.

[16] Vaughan, A. R., Lee, J. D., Metzger, S., Durden, D., Lewis, A. C., Shaw, M. D., Drysdale, W. S., Purvis, R. M., Davison, B., and Hewitt, C. N. Spatially and temporally resolved measurements of NO_x fluxes by airborne eddy-covariance over Greater London. *Atmospheric Chemistry and Physics* 2021 (2021), pp. 1–27. DOI: 10.5194/acp-21-15283-2021.

[17] Metzger, S., Junkermann, W., Mauder, M., Butterbach-Bahl, K., Trancón y Widemann, B., Neidl, F., Schäfer, K., Wieneke, S., Zheng, X. H., Schmid, H. P., and Foken, T. Spatially explicit regionalization of airborne flux measurements using environmental response functions. *Biogeosciences* 10.4 (2013), pp. 2193–2217. DOI: 10.5194/bg-10-2193-2013.

[18] Vaughan, A. R., Lee, J. D., Shaw, M. D., Misztal, P. K., Metzger, S., Vieno, M., Davison, B., Karl, T. G., Carpenter, L. J., Lewis, A. C., Purvis, R. M., Goldstein, A. H., and Hewitt, C. N. VOC emission rates over London and South East England obtained by airborne eddy covariance. *Faraday Discussions* 200 (0 2017), pp. 599–620. DOI: 10.1039/C7FD00002B.

[19] Lamprecht, C., Graus, M., Striednig, M., Stichaner, M., and Karl, T. Decoupling of urban CO_2 and air pollutant emission reductions during the European SARS-CoV-2 lockdown. *Atmospheric Chemistry and Physics* 21.4 (2021), pp. 3091–3102. DOI: 10.5194/acp-21-3091-2021.

[20] United Nations. *World Urbanisation Prospects The 2018 Revision*. https://population.un.org/wup/publications/Files/WUP2018-Report.pdf, accessed January 2022. 2019.

[21] Drysdale, W. S., Vaughan, A. R., Squires, F. A., Cliff, S. J., Metzger, S., Durden, D., Pingintha-Durden, N., Helfter, C., Nemitz, E., Grimmond, C. S. B., Barlow, J., Beevers, S., Stewart, G., Dajnak, D., Purvis, R. M., and Lee, J. D. Eddy Covariance Measurements Highlight Sources of Nitrogen Oxide Emissions Missing from Inventories for Central London. *Atmospheric Chemistry and Physics Discussions* 2022 (2022), pp. 1–35. DOI: 10.5194/acp-2021-982.

[22] Squires, F. A., Nemitz, E., Langford, B., Wild, O., Drysdale, W. S., Acton, W. J. F., Fu, P., Grimmond, C. S. B., Hamilton, J. F., Hewitt, C. N., Hollaway, M., Kotthaus, S., Lee, J., Metzger, S., Pingintha-Durden, N., Shaw, M., Vaughan, A. R., Wang, X., Wu, R., Zhang, Q., and Zhang, Y. Measurements of traffic-dominated pollutant emissions in a Chinese megacity. *Atmospheric Chemistry and Physics* 20.14 (2020), pp. 8737–8761. DOI: 10.5194/acp-20-8737-2020.

[23] Lane, S., Barlow, J., and Wood, C. An assessment of a three-beam Doppler lidar wind profiling method for use in urban areas. *Journal of Wind Engineering and Industrial Aerodynamics* 119 (2013), pp. 53–59. DOI: 10.1016/j.jweia.2013.05.010.

[24] Hartmann, J., Gehrmann, M., Kohnert, K., Metzger, S., and Sachs, T. New calibration procedures for airborne turbulence measurements and accuracy of the methane fluxes during the AirMeth campaigns. *Atmospheric Measurement Techniques* 11.7 (2018), pp. 4567–4581. DOI: 10.5194/amt-11-4567-2018.

[25] Smith, D. and Metzger, S. *Algorithm Theoretical Basis Document: Quality Flags and Quality Metrics for TIS Data Products*. https://data.neonscience.org/api/v0/documents/NEON.DOC.001113vA, accessed June 2022. 2013.

[26] Metzger, S., Durden, D., Xu, K., Natchaya, P.-D., Hongyan, L., and Florian, C. *NEON Algorithm Theoretical Basis Document (ATBD): Eddy-Covariance Data Products Bundle*. https://data.neonscience.org/api/v0/documents/NEON.DOC.004571vF, accessed Jan 2023. 2022.

[27] Jet Propulsion Laboratory. *Chemical Kinetics and Photochemical Data for Use in Atmospheric Studies, Evaluation No. 19*. https://jpldataeval.jpl.nasa.gov/, accessed January 2022. 2020.

[28] Lee, J. D., Whalley, L. K., Heard, D. E., Stone, D., Dunmore, R. E., Hamilton, J. F., Young, D. E., Allan, J. D., Laufs, S., and Kleffmann, J. Detailed budget analysis of HONO in central London reveals a missing daytime source. *Atmospheric Chemistry and Physics* 16.5 (2016), pp. 2747–2764. DOI: 10.5194/acp-16-2747-2016.

[29] Barlow, J. F., Dunbar, T. M., Nemitz, E. G., Wood, C. R., Gallagher, M. W., Davies, F., O'Connor, E., and Harrison, R. M. Boundary layer dynamics over London, UK, as observed using Doppler lidar during REPARTEE-II. *Atmospheric Chemistry and Physics* 11.5 (2011), pp. 2111–2125. DOI: 10.5194/acp-11-2111-2011.

[30] Helfter, C., Famulari, D., Phillips, G. J., Barlow, J. F., Wood, C. R., Grimmond, C. S. B., and Nemitz, E. Controls of carbon dioxide concentrations and fluxes above central London. *Atmospheric Chemistry and Physics* 11.5 (2011), pp. 1913–1928. DOI: 10.5194/acp-11-1913-2011.

[31] Langford, B., Nemitz, E., House, E., Phillips, G. J., Famulari, D., Davison, B., Hopkins, J. R., Lewis, A. C., and Hewitt, C. N. Fluxes and concentrations of volatile organic compounds above central London, UK. *Atmospheric Chemistry and Physics* 10.2 (2010), pp. 627–645. DOI: 10.5194/acp-10-627-2010.

[32] Kljun, N., Calanca, P., and Rotach, M. W. A Simple Parameterisation for Flux Footprint Predictions. *Boundary-Layer Meteorology* 112 (2004), pp. 503–523. DOI: 10.1023/B:BOUN.0000030653.71031.96.

[33] Metzger, S., Junkermann, W., Mauder, M., Beyrich, F., Butterbach-Bahl, K., Schmid, H. P., and Foken, T. Eddy-covariance flux measurements with a weight-shift microlight aircraft. *Atmospheric Measurement Techniques* 5.7 (2012), pp. 1699–1717. DOI: 10.5194/amt-5-1699-2012.

[34] Kljun, N., Calanca, P., Rotach, M. W., and Schmid, H. P. A simple two-dimensional parameterisation for Flux Footprint Prediction (FFP). *Geoscientific Model Development* 8.11 (2015), pp. 3695–3713. DOI: 10.5194/gmd-8-3695-2015.

[35] Copernicus Climate Change Service Climate Data Store (CDS). *Copernicus Climate Change Service (C3S): ERA5: Fifth generation of ECMWF atmospheric reanalyses of the global climate.* https://cds.climate.copernicus.eu/cdsapp#!/home, accessed October 2021. 2021.

[36] Transport for London. *Transport for London: original source data provided by Operational Analysis department*. 2023.

[37] Greater London Authority. *London Atmospheric Emissions Inventory 2016, licensed under the Open Government Licence (OGL) v2.0, Crown Copyright 2020.* https://data.london.gov.uk/dataset/london-atmospheric-emissions-inventory--laei--2016, accessed March 2022. 2016.

[38] Hale, T., Angrist, N., Goldszmidt, R., Kira, B., Petherick, A., Phillips, T., Webster, S., Cameron-Blake, E., Hallas, L., Majumdar, S., and Tatlow, H. A global panel database of pandemic policies (Oxford COVID-19 Government Response Tracker). *Nature Human Behaviour* 5 (4 2021), pp. 529–538. DOI: 10.1038/s41562-021-01079-8.

[39] Mann, J. and Lenschow, D. H. Errors in airborne flux measurements. *Journal of Geophysical Research: Atmospheres* 99.D7 (1994), pp. 14519–14526. DOI: 10.1029/94JD00737.

[40] Department for Environment, Food and Rural Affairs (DEFRA). *Clean Air Strategy 2019*. https://www.gov.uk/government/publications/clean-air-strategy-2019, accessed December 2022. 2019.

[41] European Environment Agency. *CO_2 performance of new passenger cars in Europe*. https://www.eea.europa.eu/ims/co2-performance-of-new-passenger#ref-DNi82, accessed December 2022. 2022.

[42] Greater London Authority. *Central London ultra-low emission zone - ten month report*. https://www.london.gov.uk/programmes-and-strategies/environment-and-climate-change/environment-publications/central-london-ulez-ten-month-report#:~:text=This%20report%20evaluates%20the%20impact,reduction%20of%2044%20per%20cent., accessed November 2022. 2020.

[43] Carslaw, D. C. and Rhys-Tyler, G. New insights from comprehensive on-road measurements of NO_x, NO_2 and NH_3 from vehicle emission remote sensing in London, UK. *Atmospheric Environment* 81 (2013), pp. 339–347. DOI: 10.1016/j.atmosenv.2013.09.026.

[44] Ko, J., Myung, C.-L., and Park, S. Impacts of ambient temperature, DPF regeneration, and traffic congestion on NO_x emissions from a Euro 6-compliant diesel vehicle equipped with an LNT under real-world driving conditions. *Atmospheric Environment* 200 (2019), pp. 1–14. DOI: 10.1016/j.atmosenv.2018.11.029.

[45] Gately, C. K., Hutyra, L. R., Peterson, S., and Sue Wing, I. Urban emissions hotspots: Quantifying vehicle congestion and air pollution using mobile phone GPS data. *Environmental Pollution* 229 (2017), pp. 496–504. DOI: 10.1016/j.envpol.2017.05.091.

[46] Defra and BEIS. *National Atmospheric Emissions Inventory, licenced under the Open Government Licence (OGL), Crown Copyright 2020*. naei.beis.gov.uk/data/, accessed March 2022. 2019.

[47] Department for Business, Energy and Industrial Strategy (BEIS). *Digest of UK Energy Statistics*. https://www.gov.uk/government/collections/digest-of-uk-energy-statistics-dukes, accessed November 2022. 2021.

[48] Kings College London. *Urban air pollution from combined heat and power plants*. https://www.london.gov.uk/sites/default/files/urban_air_pollution_from_combined_heat_and_power_plants.pdf, accessed November 2022. 2018.

[49] Fishman, E., Schepers, P., and Kamphuis, C. B. M. Dutch cycling: Quantifying the health and related economic benefits. *American Journal of Public Health* 105.8 (2015), e13–e15. DOI: 10.2105/AJPH.2015.302724.

[50] Lewis, A. C. Optimising air quality co-benefits in a hydrogen economy: a case for hydrogen-specific standards for NO_x emissions. *Environmental Science: Atmospheres* 1 (5 2021), pp. 201–207. DOI: 10.1039/D1EA00037C.

Chapter 3

Commercial space heating is the largest source of NO_x in central London

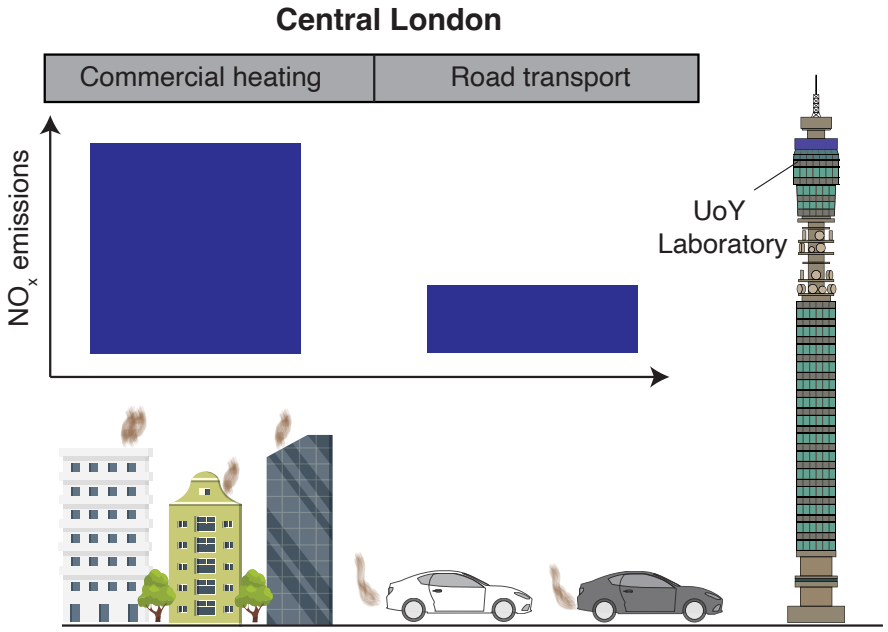

3.1 Abstract

While road transport NO_x emissions have steadily reduced due to improved exhaust after-treatment technology, ambient concentrations of NO_2 continue to exceed the World Health Organisation's (WHO) guideline values in many cities globally. The megacity of London has taken an international lead in mobility interventions through the use of low emissions zones with transport NO_x emissions reducing by > 73% over the period 2017 - 2021 in the central area. Using long-term air pollution flux measurements made from a 190 m communications tower in central London, we show that the largest source of NO_x emissions in central London has transitioned from road vehicles to commercial space heating. Observations and supporting consumption/mobility data indicate that natural gas combustion in boilers was responsible for 76 ± 17 % of NO_x emissions in the measurement footprint (average years 2021-2023). Additionally, we calculate that UK and European emissions inventories actually overestimate commercial NO_x emissions by 53% by reason of outdated emission factors and thus propose an updated NO_x: CO_2 emission ratio of 0.85×10^{-3} for the source. Since around 1990 road transport has dominated air quality policy thinking on NO_2. However, in densely populated urban environments that are reliant on natural gas, building heating may now be an effective sector to prioritise for future NO_x emissions intervention, should further lowering of ambient NO_2 be a policy objective. With system-wide changes in the heat and power sector expected in the coming decades as a result of net zero pledges, we project that very low future urban concentrations of NO_2 are technically possible. The trajectory for urban NO_2 will however depend in large part on choices made around urban buildings and their associated infrastructure and whether combustion or electrification pathways are delivered as part of urban decarbonisation.

3.2 Introduction

Nitrogen oxides (or NO_x) are one of the six criteria air pollutants that have a range of direct and indirect negative effects on human health.[1] In the urban environment, NO_x are formed via high-temperature combustion. The majority of the production occurs in what is commonly referred to as thermal NO_x.[2] This is when molecular nitrogen in the air is oxidised via the Zel'dovich mechanism in Eq. 3.1 - 3.3.[3]

$$N_2 + O \rightarrow NO + N \tag{3.1}$$

$$N + O_2 \rightarrow NO + O \tag{3.2}$$

$$N + OH \rightarrow NO + H \tag{3.3}$$

The reaction is strongly influenced by temperature and the air-fuel ratio giving different combustion sources different NO_x emissions rates. There are additional smaller fuel and prompt NO_x sources (related to nitrogen within the combusted fuel). Typically, developed urban environments contain two main sources of NO_x: road transport and heat and power generation. Road transport emissions vary by fuel type and are dominated by diesel vehicles. Heat and power generation emissions can be broken down into the domestic and commercial sectors. Here, emissions arise from the combustion of fuel (most commonly natural gas) in a boiler to heat water for supply to a central heating system and hot water taps. The difference between the two is the type of building that they heat and their size. Domestic boilers operate in residential homes and are small (typically < 50 kW). Commercial boilers heat commercial premises and are much larger (up to 50 MW) since they are required to heat larger spaces. In the past, it was generally assumed that the larger the boiler, the higher the operating

temperature, and thus the greater the NO_x emissions. However, 'ultra-low' NO_x burner technology for larger gas combustion appliances has been applied for at least a decade.[4]

Particularly in European countries, the fraction of diesel vehicles in the fleet has meant that road transport has been the dominant source of NO_x to urban areas for the past few decades.[5] As such, the sector has received the greatest amount of policy intervention. There have been continual increases in Euro Standard stringency for NO_x emissions and the number of traffic pollution and congestion charging zones is rising.[6,7] Heat and power generation emissions become more important the greater the population density. With an increasing percentage of the population expected to live in urban areas and an increasing global population, population density is expected to increase.[8] With this, and the progressing transition to electrically powered transport, it would be anticipated that urban NO_x emissions will at some point no longer be dominated by road transport. One question arising, however, is whether the reductions in transport emissions alone would be sufficient to achieve "safe" levels of NO_2, or whether emissions from other sectors would also require further abatement.

Eddy covariance is used in this study to directly quantify NO_x fluxes from the city centre; it is a measurement technique used for the top-down quantification of emissions. While its application for air pollutants in urban environments is challenging, an increasing number of studies are being reported.[9,10] Here, we build on previous research and present multi-year NO_x emissions measurements made in a megacity. Central London is an ideal location for the study of evolving urban NO_x sources due to a) the high population density resulting in historically high NO_x emissions and b) the proactive approach the local government has taken in reducing emissions from some sectors. London has had a congestion charging zone in place since 2003 and more recently implemented, then twice expanded, an ultra-low emissions zone (ULEZ). It has been previously reported that in

2021 road transport NO_x emissions in the city centre had reduced by > 73 % since 2017, albeit influenced by COVID-19 lockdowns.[11] Here, we present evidence that road transport emissions have not returned to pre-pandemic levels and now represent a minor source in the city centre. Urban NO_x emissions are now dominated by the heating sector.

3.3 Experimental

3.3.1 Measurement Site

Instruments for measuring fluxes of urban air pollutants and greenhouse gases are situated in a small lab atop the British Telecommunications Tower (BT Tower) located in central London, UK (51°31'17.4"N, 0°8'20.04"W). The measurement height is 190 m above street level, with a mean building height of 8.8 ± 3.0 m in the 10 km radius surrounding the tower.[12] The gas inlet and ultrasonic anemometer are attached to a mast that extends 3 m above the top of the tower. Air is pumped down a 45 m Teflon tube (3/8" OD) in a turbulent flow of 20-25 L min^{-1} to the gas instruments, which are situated in a small air-conditioned room inside the tower on the 35th floor.

3.3.2 Instrumentation

Concentrations of nitrogen oxides (NO and NO_2) were measured using a dual-channel chemiluminescence analyser (Air Quality Design Inc., Boulder Colorado, USA; 5 Hz). The number of photons measured by the photomultiplier tube was converted into a part per trillion (ppt) mixing ratio using a five-point calibration curve produced through dilutions of a 5 ppm NO in N_2 calibration standard (BOC Ltd., UK; traceable to the scale of the UK National Physical Laboratory, NPL) into NO_x free air. NO_2 was calculated by conversion of NO_2 into NO using a photolytic blue light converter (BLC). Here, both NO and NO_2 were measured, from which NO_2 can be

quantified by subtracting the NO mixing ratio and applying a correction factor for the conversion efficiency of the BLC. The instrument was calibrated every 37 hours in addition to an hourly zero measurement to subtract the temperature-dependent background signal of each channel.

Long-term measurements of CO_2 have been ongoing at the BT Tower since 2011 as part of UKCEH's National Capability program. Dry mass fractions were measured using a cavity ringdown spectrometer (Model 1301-f, Picarro Inc., Santa Clara, California, USA; 1 Hz) as described by Helfter et al. [13].

Meteorological measurements were made at the BT Tower as described by Lane et al. [14]. Wind speed, wind direction and sonic temperature were measured using an ultrasonic anemometer (Gill R3-50, Gill Instruments, Lymington, UK; 20 Hz), along with pressure and relative humidity measurements using a weather station (WXT520, Vaisala Corp. Helsinki, Finland; 1 Hz).

3.3.3 Flux Calculations

Fluxes were calculated via continuous wavelet transformation as described by the convolution of a time series, $x(t)$, with the complex conjugate of a wavelet function, $\psi^*_{a,b}(t)$

$$W(a,b) = \int_{-\infty}^{\infty} x(t) \cdot \psi^*_{a,b}(t) dt \tag{3.4}$$

where $W(a,b)$ is a matrix of the wavelet coefficients. The wavelet function can be written as

$$\psi^*_{a,b}(t) = \frac{1}{\sqrt{a}} \cdot \psi_0 \left(\frac{t-b}{a} \right) \tag{3.5}$$

which features a mother wavelet, ψ_0, scaled by parameter a and translated by parameter b. The scale parameter acts to either dilate or compress the mother wavelet. The translation parameter temporally shifts the wavelet

throughout the time series. There are a number of different mother wavelets that could be used. In the field of atmospheric turbulence, the Morlet wavelet has been found to be appropriate and has been extensively used in the literature for calculating turbulent fluxes.[15] As such, we use the Morlet wavelet defined as:

$$\psi_0 = \pi^{-1/4} \cdot e^{-i\omega_0\eta} \cdot e^{-\eta^2/2} \tag{3.6}$$

where ω_0 is the non-dimensional frequency given here as 6 for sufficient accuracy as previously done in the literature, and $\eta = \frac{t-b}{a}$.[16] For two simultaneously recorded time series $x(t)$ and $y(t)$, the covariance for a given averaging interval can be calculated from

$$\overline{x'y'} = \frac{\delta t}{C_\delta} \cdot \frac{\delta j}{N} \cdot \sum_{n=0}^{N-1} \sum_{j=0}^{J} \frac{\left[T_x(a,b) \cdot T_y^*(a,b)\right]}{a(j)} \tag{3.7}$$

using parameters

$$b_n = n\delta t \tag{3.8}$$

$$a_j = a_0 \cdot 2^{j\delta j} \tag{3.9}$$

Time domain scales are increased linearly at an increment of $\delta t = 0.2s$ which is the resolution between measurement data points and frequency domain scales are discretised using exponential scales of fractional powers of two where j is an integer and ν the number of voices per octave. The main factor in determining which ν is used is computational power. In this work, a value of 8, or δj of 0.125 is used after consideration of the resources available.

CWT was performed across 24-hourly data files with a wavelet maximum scale of 1 hour. Fluxes were averaged to 1-minute resolution using a 5-minute rolling averaging window. No cone of influence filter was applied as

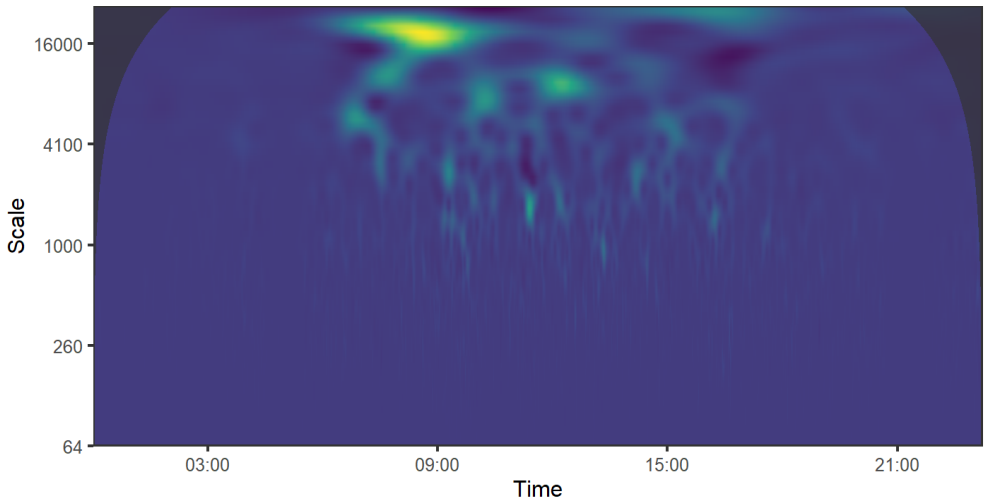

Figure 3.1: An example wavelet cross spectrum for 24 hours of NO_x data from the BT Tower. Yellow colours represent areas of high emission compared to blue colours of low emission. Shaded in black is the wavelet cone of influence.

previously discussed in the literature;[17] although performing CWT across 24-hourly data files places the greater uncertainty at night when minimal flux is measured (see Figure 3.1). All parameters used in the CWT processing are summarised in Table 3.1. CWT was chosen as the method of flux calculation to reduce previously reported high NO_x flux data loss at the BT Tower due to non-stationarity.[11] CWT does not require stationarity as an assumption and thus removes this issue.[16]

In addition, fluxes were corrected for both high-frequency loss and vertical flux divergence. High-frequency loss resulting from the long sampling line, closed-path instrumentation and insufficient instrument response time was corrected by matching normalized co-spectra of wNO, wNO_2 and wCO_2 to those of wT (see example spectra in Figure 3.2). Corrections were of the order of 2 % for NO, 6 % for NO_2 and 16 % for CO_2. Vertical flux divergence resulting from non-uniform turbulence properties in the boundary layer was accounted for using the correction presented in Drysdale et al. [18]. This assumes linear divergence of the vertical flux as a function of ef-

Table 3.1: Continuous wavelet transformation parameters used in eddy4R

Parameter	Value
δt	0.2 s
Zero padding	True
δj	0.125
J_{max}	110
Mother wavelet	Morlet
COI filter	No filter
Wavelet maximum scale	60 minutes
Averaging period	1 minute
Averaging window	5 minutes

fective measurement height and effective entrainment height. Here, hourly ERA5 modelled boundary layer height was used in addition to the measurement height of 190 m to produce an hourly correction.[19] This resulted in an average correction of 30 % per data point, although this was weighted to the nighttime data points when fluxes and boundary layer height were lowest. Fluxes were filtered such that sufficient turbulence was developed ($u^* > 0.2$), flux was greater than the limit of detection, and the measurement height was less than the entrainment height. Other potential uncertainties, particularly with reactive species such as NO_x, arise from chemical loss during transport to the measurement height. Previously conducted tracer experiments and calculations for the BT Tower site have estimated this as a typical 2 % loss rate, increasing up to a maximum of 11 % during stable atmospheric conditions.[11,20] No correction for chemical loss is applied here.

Fluxes were calculated using the eddy4R ecosystem within Docker.[21] Containers were run on the LOTUS Cluster within JASMIN, the UK's National Environmental Research Council's (NERC) supercomputer.

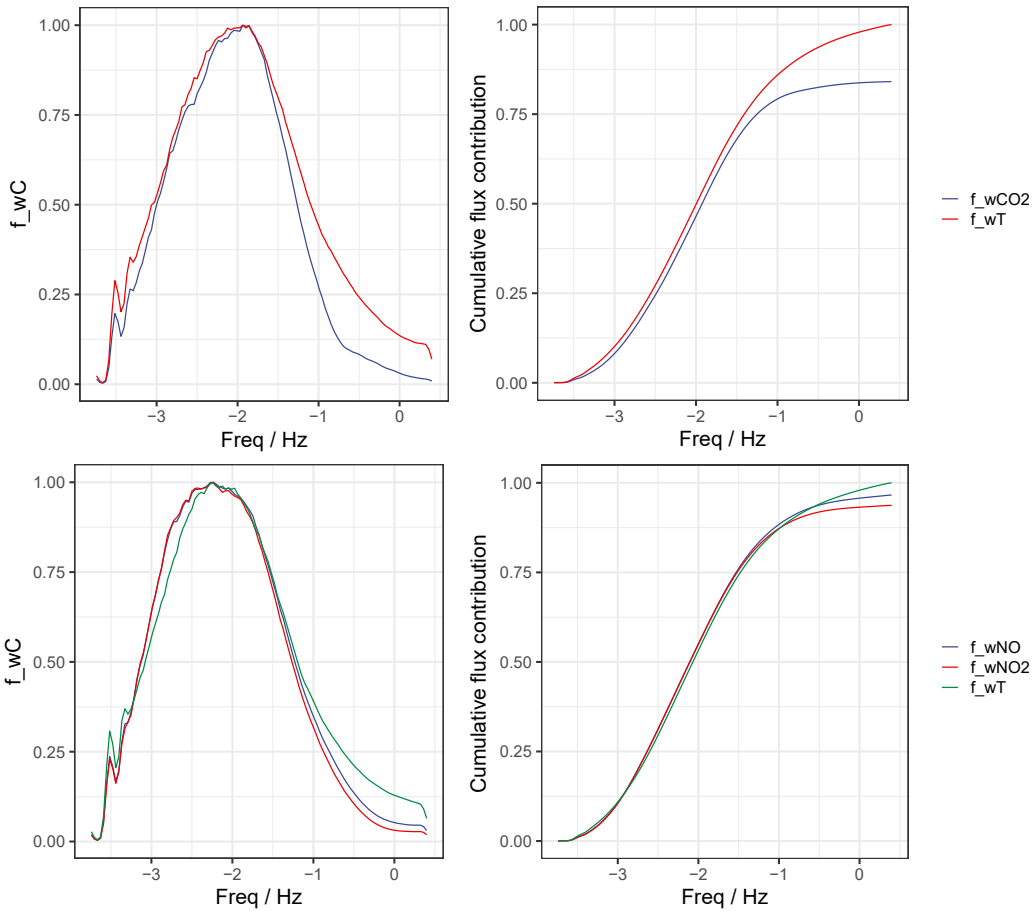

Figure 3.2: Normalised cospectra and their cumulative flux contribution by frequency for NO, NO_2, CO_2 and heat flux. Frequency is of $\log_{10}$ units.

3.3.4 Footprint Modelling

A parameterised version of the backward Lagrangian stochastic particle dispersion model implemented in eddy4R was used to estimate the footprint for each hourly flux measurement at the BT Tower. The model is described by Kljun et al. [22] and has been parameterised for a range of meteorological conditions and receptor heights to reduce the computational expense of running it. The original model aims to produce a cross-wind integrated footprint function as a function of its along-wind distance, which has now been further extended into two dimensions using a Gaussian distribution driven by the standard deviation in the cross-wind component.[23,24] Meteorology statistics from the eddy covariance calculations are used in combination with modelled boundary layer height from ERA5,[19] and a surface roughness length of 1.1 m to produce a weighted matrix of 100 m x 100 m grid cells. Each output weighted matrix was then scaled and aligned to the World Geodetic coordinate reference system.

3.3.5 Emissions inventories

The UK's annual National Atmospheric Emissions Inventory (NAEI) defines greenhouse gas and air pollutant emissions spatially (1 km x 1 km) by emissions source and sector.[25] The city of London has the additional London Atmospheric Emissions Inventory (LAEI) which largely uses the same methodology as the NAEI but with additional London-specific information.[26] The LAEI was produced for 2013, 2016 and 2019, and provides recent projections for emissions in 2025 and 2030. In these analyses, we study the LAEI for our specific measurement footprint. This is done by extracting the spatial inventory values using the footprint-weighted grid cells.

3.3.6 Additional data on emissions drivers

3.3.6.1 Traffic

Hourly traffic loads surrounding the BT Tower were calculated by summing the traffic load from each of the 24 Automatic Traffic Counters (ATCs) within the flux footprint. Data was provided by the Operational Analysis Department, Transport for London (TFL) via a freedom of information request.[27]

3.3.6.2 Natural gas usage

Natural gas demand for the North Thames (NT) local distribution zone (LDZ) (Demand, actual daily metered, LDZ (NT), D+1) which London resides in was collated from.[28] This data was available at a maximum temporal resolution of 1 day. Data for the diel use of natural gas in heating systems and their operating hours is scarce. However, access to utility meters within University College London, which is a key site within the measurement footprint, has been provided by their sustainability team. Data for a number of office buildings for the whole of 2022 was averaged and used in this study.

3.3.6.3 Building types

The 3DStock model was used to identify building use sectors within the BT Tower footprint. 3DStock is a method for modelling all buildings – domestic, non-domestic and mixed-use – in a locality, in three dimensions and located geographically.[29] The model was developed and is maintained by University College London.

3.3.6.4 Large heat sources

Consumption data for the production of heat for large buildings in central London was collated as part of the Decentralised Energy Master planning

program (DEMaP) for the Mayor of London and used in this study.[30]

3.4 Results and Discussion

3.4.1 Long-term flux time series

Three years of continuous NO_x flux data (in addition to two shorter term campaigns discussed by Lee et al. [12] and Drysdale et al. [18]) has now been collated from the BT Tower site. At the time of writing, this is the only long-term flux data set for NO_x in a megacity to our knowledge. The first year of flux data (Sept. 2020 - Sept. 2021) was heavily influenced by COVID-19 restrictions and has already been discussed in the literature.[11] Presented here are the subsequent two years of data (Sept. 2021 - Sept 2023) measured after the date on which all restrictions in the UK were lifted. Unlike the previous studies at the BT Tower, fluxes calculated here utilised wavelet-based processing rather than traditional eddy covariance methodology. CWT is typically only used in the calculation of airborne fluxes due to the requirement for higher time resolution outputs. The computational demand of the calculations means its use for tower-based studies is uncommon. However, CWT methodology negates the requirement for a stationarity filter,[16] for which NO_x fluxes at the BT Tower regularly fail.[11] Indeed, the transition from traditional to wavelet-based processing resulted in a 29 % increase (82 vs 53 %) in data coverage whilst maintaining an excellent agreement between the two methods (See Figure 3.3).

3.4.2 Temporal trends

In central London, NO_x and CO_2 share the same two major sources; these are road transport and fossil fuel combustion for space heating. The LAEI estimates that these two sectors make up > 91 % and > 95 % of NO_x and CO_2 emissions respectively. Comparing the emissions of both species is

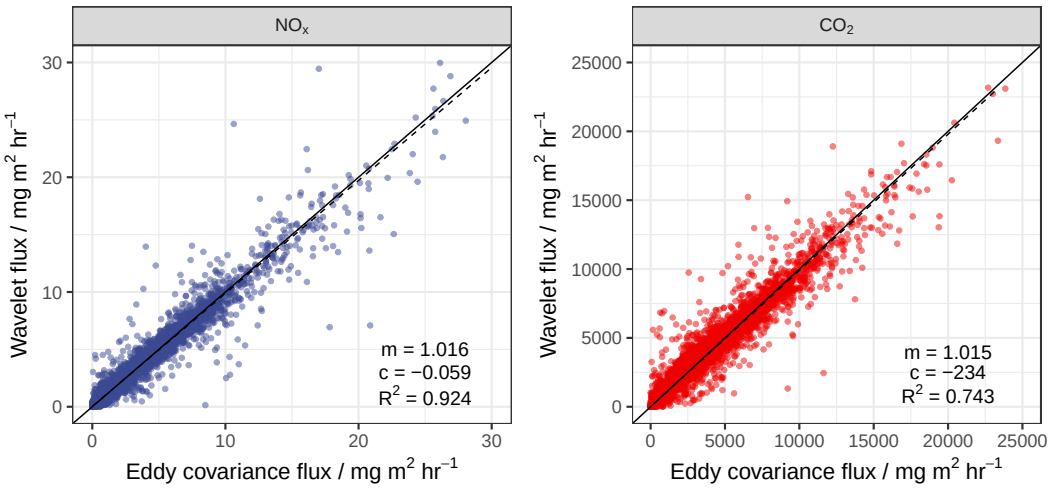

Figure 3.3: Traditional hourly eddy covariance flux compared with hourly averaged wavelet flux for NO_x and CO_2. The solid line represents the 1:1 ratio between the two methods and the dashed line the linear regression. Regression statistics are detailed in the bottom right of each facet.

often complementary and can provide insight into which sectors are dominant. Monthly and diel trends for NO_x and CO_2 flux are presented in Figure 3.4 along with the road transport (traffic flow) and energy consumption (natural gas combustion) data for the measurement footprint area in central London. Monthly variability of NO_x and CO_2 flux track each other closely. A similar winter maximum and summer minimum are seen in natural gas usage. Here, ambient temperature is the main driver with reduced combustion required to heat buildings during warmer months. This is in contrast to traffic flow which remains high throughout the year. The observations for CO_2 are unsurprising; it is well established that the heat and power generation sector dominates CO_2 emissions in European cities. The LAEI currently attributes around 80 % of CO_2 within our flux measurement footprint to the heat and power sector. By contrast, NO_x emissions in urban environments have been overwhelmingly dominated by road transport emissions for the past few decades. This has been demonstrated as recently as 2017 for cen-

tral London.[18,31]

3.4.3 Emission ratios

An emission ratio of pollutant-to-CO_2 is a useful metric in source apportionment, particularly here for NO_x since both species have the same two major sources. Due to the nature of the combustion processes that fuel these sources, in which differing temperature ranges/fuel types are present, the emitted NO_x/CO_2 ratio is distinct for each. The measured flux ratio at any given time therefore corresponds to the combination of the ratios of each given source, and their relative contributions. Therefore, the NO_x/CO_2 ratio diel profile can be used to generate some insight into which source dominates and at what times.

The NO_x/CO_2 emission ratios for each of the sources were taken from the LAEI and are discussed below. Emissions of CO_2 typically have a low uncertainty due to generally accurate national greenhouse gas emissions reporting. This has resulted in well-established emission factors from combustion applications and fuel activity statistics.[32] Emissions inventory estimates have been shown to agree well with flux measurements in London previously (Helfter et al. [13]) and later in this study (see Section 3.4.6). Although often unquantified, NO_x emissions have a higher uncertainty due to the variable role of different emissions control technologies. This level of uncertainty varies for different sectors. Traffic NO_x emissions have received extensive attention in recent years due to previous inventory inaccuracies arising from the underrepresentation of diesel vehicle emissions under real-world driving conditions. Many real-world remote sensing measurements have been conducted which help verify and improve the emissions inventories.[33,34] For London specifically, the Breathe London campaign (2018-2019) reported NO_x/CO_2 emission factors for road transport in good agreement with those in the LAEI.[35] Emission factors for 2017 also

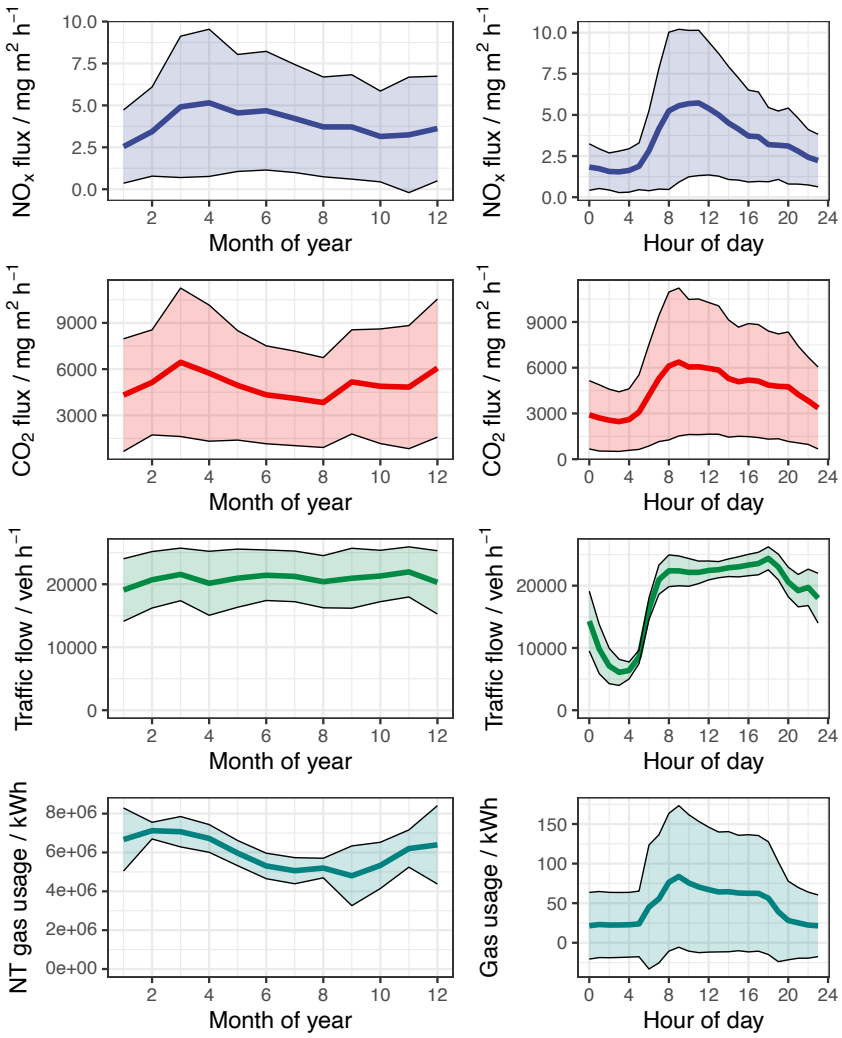

Figure 3.4: Median average monthly and diel profiles for NO_x flux, CO_2 flux, traffic flow and natural gas usage (2021-2023). The gas usage monthly profile uses data from the North Thames LDZ which includes central London consumption. Gas usage data has a maximum resolution of 24 hours, so the gas usage diel profile from UCL building utility meters (2022) discussed in Section 3.3.6.2, available at 1-hour resolution, is used as a representative commercial daily profile of consumption. Shaded regions represent the median absolute deviation of the measurements.

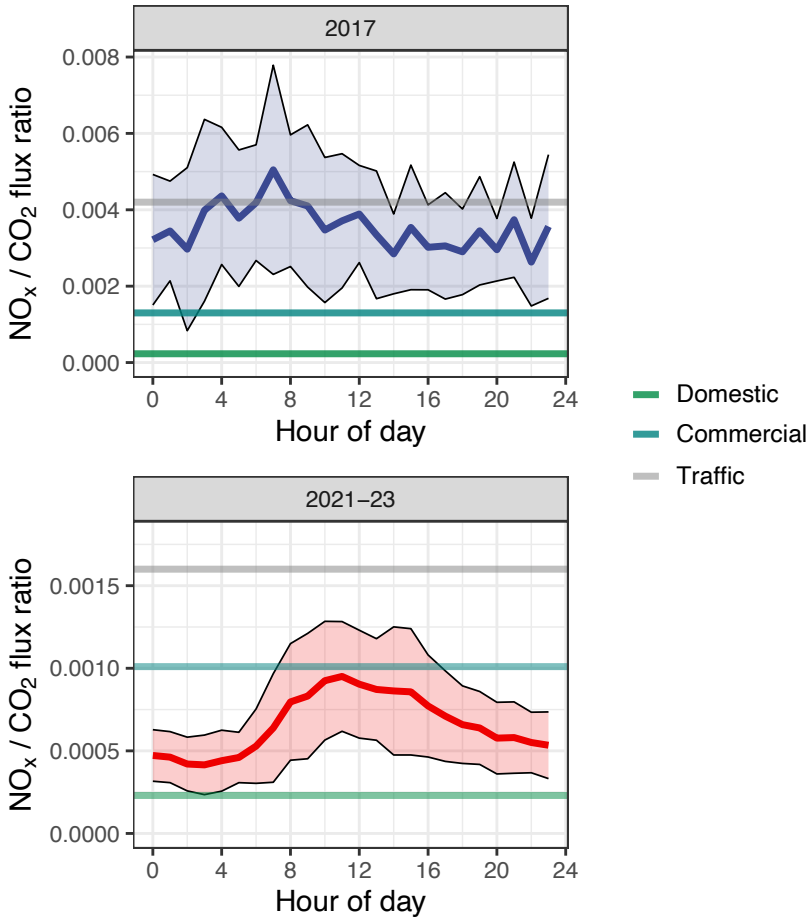

Figure 3.5: Median average NO_x/CO_2 emission ratio diel profiles at the BT tower in 2017 and 2021-23. The shaded region represents the median absolute deviation. Horizontal coloured lines are the sector emission ratios described in Table 3.2.

Table 3.2: NO_x/CO_2 emission ratios for different source sectors and year.

Year	Traffic	Residential	Commercial
2017	$4.2x10^{-3}$	$0.25x10^{-3}$	$1.3x10^{-3}$
2021-23	$1.6x10^{-3}$	$0.25x10^{-3}$	$0.84x10^{-3}$

agree well with those estimated from flux measurements made in Innsbruck during the same year; which at the time was a European city with a similar fleet fuel-type composition as London.[36] The ULEZ expansion since the Breathe London measurements will have reduced the emission factor further and is more likely now representative of that estimated in the 2025 LAEI. Domestic combustion emission factors have received some real-world verification in London and boiler age is considered in their calculation.[26,37] They also agree well with those estimated by Karl et al. [36]. On the other hand, commercial combustion has received little attention and has no real-world verification. Emissions factors used in the construction of the UK's emissions inventories (both the NAEI and the LAEI) are taken from European EMEP/EEA guidance based in turn on somewhat outdated reference materials (Italian Ministry for the Environment, 2005).[4] In the LAEI, an emission factor of 1.3×10^{-3} is given. However, this does not account for recent legislation in the UK which limits NO_x emissions from commercial boilers. The Ecodesign Directive (No 813/2013) limited all new natural gas boilers $\leq$ 400 kW to a NO_x emission level of 56 mg kW^{-1} (an emission ratio corresponding to approximately 0.23×10^{-3}) from September 2018.[38] Similarly, the 2018 Medium Combustion Plant (MCP) Directive limited plants $\geq$ 1 MW and $\leq$ 50 MW to 100 mg NM^{-3} of gas (an emission ratio corresponding to approximately 0.041×10^{-3}).[39]

The distribution of large boilers surrounding the BT Tower is shown in Figure 3.6. Fractions of total commercial heating (number of boilers multiplied by their size) for each boiler size group referred to in the legislation were extracted using the footprint model. The majority (71.4 %) are covered

by the Ecodesign Directive, with a smaller number by the MCP Directive (12.1 %) and some compliant with no Directive (16.5 %). We therefore use this distribution, the new Directive limits and an estimated boiler lifetime of 10 years (or fleet turnover of 50 % since 2018, to estimate an updated commercial combustion NO_x/CO_2 emission ratio of 0.85 $\times 10^{-3}$, or an over-estimation of 53 %. All emissions ratios used in the following analysis are presented in Table 3.2, and highlighted in relation to the measured data in Figure 3.5.

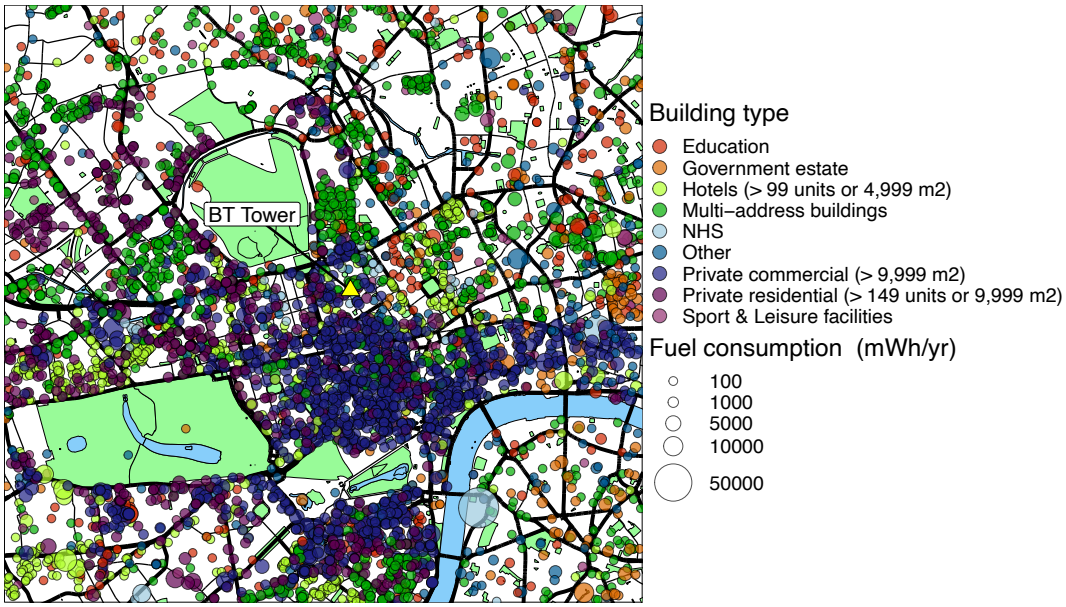

Figure 3.6: A map of large boilers in the area surrounding the BT Tower coloured by building type and sized based on fuel consumption in mWh yr^{-1}. Data obtained from London heat source data as collated during the Decentralised Energy Master Planning program (DEMaP) for the Mayor of London.

A useful example to initially discuss is the NO_x/CO_2 flux diel profile in Figure 3.5 for 2017 flux data. The measured ratio is high during the day and close to a ratio indicative of 100 % of NO_x emissions coming from traffic. Even at night, the ratio remains high due to the relatively high background traffic counts that central London experiences. This is as expected

and corroborates previous measurements which assign traffic as the overwhelmingly dominant source in central London.[18,31]

The situation changes however by the years 2021-23 (note the different y-axis scales). At night, the measured ratio indicates a dominant residential heating sector for NO_x. Despite traffic emissions having a lower ratio in 2021, that ratio is still around 6× that of residential combustion and thus highly distinguishable. Given that traffic flow remains relatively high during these hours, this suggests traffic has become a more minor NO_x source relative to heating. This is further supported by the diel profile now tracking typical commercial heating schedules as seen in Figure 3.4. Seasonal average emission ratios of 0.74×10^{-3}, 0.86×10^{-3}, 0.77×10^{-3}, 0.64×10^{-3} for spring, summer, autumn and winter respectively are consistent with natural gas usage driving the measured ratio. A higher proportion of gas usage in the cooler seasons results in more emissions from the heating sector and a lower measured ratio. These observations, including the monthly trends, are plausible given that emissions of NO_x from road transport within the measurement footprint are estimated to have reduced by 73 - 100 % since 2017.[11] Although these figures relate to measurements made during periods of COVID-19 restrictions, there has been a minimal increase in flux (see Figure 3.7) after restrictions were lifted in 2021. As such, it is suggestive that the reduction of traffic NO_x emissions may derive from some combination of the ULEZ effects, natural fleet turnover to better-performing vehicles, and a permanent change in commuting behaviour post-COVID-19.

The measured ratio during the day can be explained by a dominant commercial heating source with small contributions from traffic and residential combustion. However, the low emission ratio measured at night means that this commercial source must also have low activity during these hours. In general, heat use in buildings is expected to track building occupancy, although data availability in this area is scarce. Commercially occupied buildings, in particular offices and shops (as opposed to health facilities and some

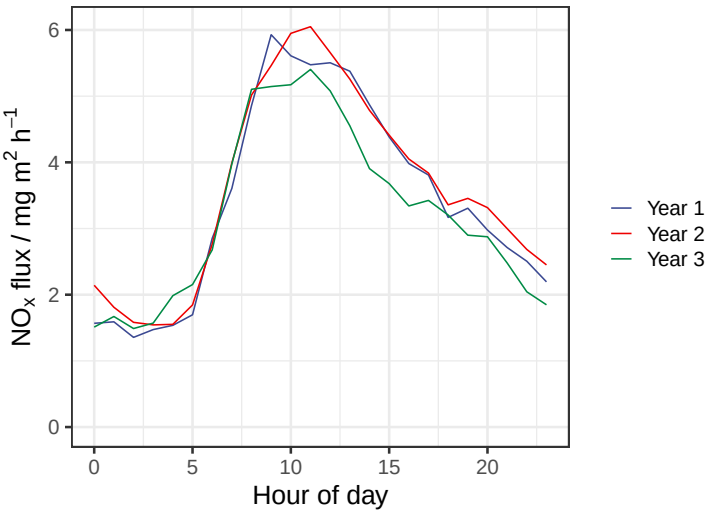

Figure 3.7: Diel comparison of NO_x flux for the different measurement years. The dates for each profile are one full year of data from the start date of September 2020.

forms of hospitality) have very low or no occupancy at night and high occupancy during typical working hours. As such, they would fit the profile described. Indeed, this is supported by the diel gas usage in UCL office buildings presented in Figure 3.4, and energy modelling in Johnston et al. [40]. A high density of commercial boilers is present in the measurement footprint (see Figure 3.6).

3.4.4 Building distribution by sector

The 3DStock building model was used to quantify the dominant building types within the measurement footprint. 3DStock is described in Section 3.3.6.3 and provides building use classification for floor space within each unique property reference number. Data from 3DStock are presented in Figure 3.8. To obtain a distribution representative of the measurement footprint, buildings were weighted by their location within the footprint-weighted contribution grid cells. This ensured that geographic areas sampled a greater proportion of the time were weighted appropriately. It was

calculated that 80 % of the weighted building floor space within the footprint was commercial-dominated with 20 % attributed to pure domestic. Table 3.3 presents the commercial building use activity distribution by floor space from this analysis. Offices dominate commercial buildings within the footprint at 62 %, with additional contributions by unclassified commercial buildings and shops at 18 % and 14 % respectively. Therefore, building heat schedules for the majority of building floor space are proposed to follow a diel variation similar to that seen in the measured ratio. This supports a dominant commercial heating source of NO_X.

Table 3.3: CaRB2 classification distribution of commercial building floor space weighted by location within the footprint.

Building use category	Percentage of commercial floor space in footprint (%)
Education	0.75
Factory	0.57
Health	1.02
Hospitality	1.84
Office	61.97
Other	0.97
Shop	14.29
Unclassified commercial	18.26
Warehouse	0.33

3.4.5 Quantification of the dominant source of NO_x emissions

The measured ratio between 10:00 and 14:00 (which is when peak NO_x emissions occur) can be simultaneously solved to calculate the relative contribution of different sectors to NO_x emissions, provided only two sectors are considered. An overall heating sector emissions ratio (commercial + domestic) of 0.73 $\times 10^{-3}$ was calculated for these hours using the 20:80 split of

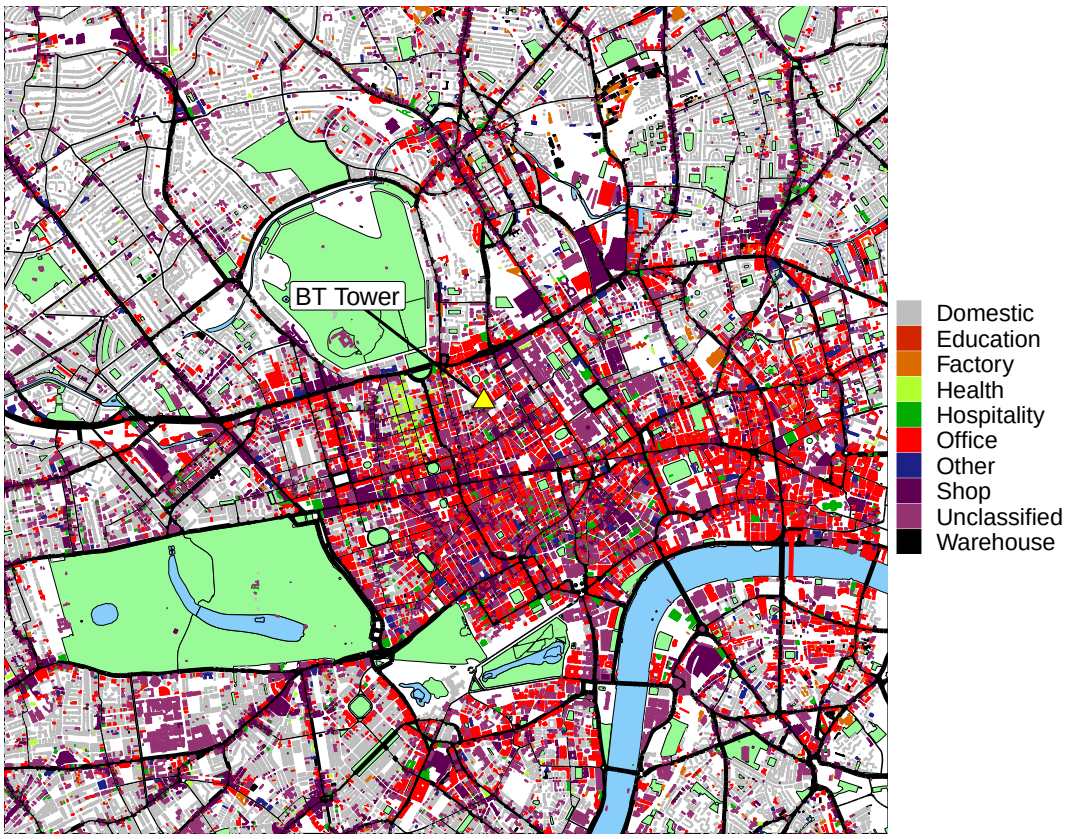

Figure 3.8: Building type distribution for CaRB2 classification in the area surrounding the BT Tower. Data was obtained from the London Building Stock Model (LBSM). Unclassified is unclassified commercial premises.

domestic to commercial floor space within the footprint (see Section 3.4.4) and the domestic and commercial emission ratios. This split agrees well with activity factors for domestic and commercial gas usage in the LAEI (23:77). We note that during the day this is likely to be a lower bound since domestic combustion can be higher in the morning and evening. From this, and the road transport emission ratio, we estimate that $76 \pm 17\%$ of NO_x emissions occurring during the day now arise from gas combustion within boilers for hot water and space heating. Here, the uncertainty is given as the standard error based on the monthly variation in the measured ratio. This is a substantial change in the dominant source from only five years previous and, as far as we know, the first observations of such in a city globally. The cause of this is a combination of effects that include active traffic management policies in central London and an ever-improving vehicle fleet with lower tailpipe NO_x emissions.

3.4.6 Emissions inventory comparison

In Section 3.4.3, we estimated that NO_x emissions for commercial combustion are likely overestimated by 53 % in the LAEI emissions inventory due to outdated emission factors. This is further verified when comparing measured vs inventory bulk annual emissions. Figure 3.9 compares emissions for 2022 vs. the different LAEI years. Here, measured values are calculated from the average measured flux in a day multiplied by the number of days in a year, to deal with small amounts of data loss. While top-down flux estimated CO_2 agrees well with the inventory bottom-up estimate, there appears to be an overestimation in the inventory NO_x emissions. The 2025 LAEI attributes an even larger proportion (78 %) of NO_x to the heating sector than seen in these measurements. If the updated commercial emission factor proposed here is used, a much better agreement for total NO_x emissions is achieved between measurements and inventory. The commercial

proportion is brought down to 70% which is well within the uncertainty of these measurements.

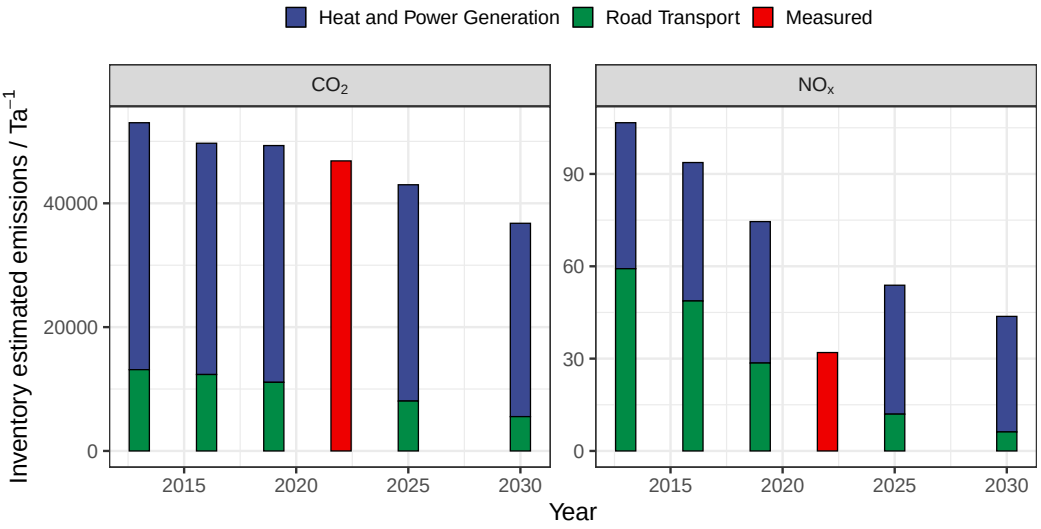

Figure 3.9: Comparison of measured and LAEI estimated annual emissions for NO_x and CO_2 for the measurement footprint. The LAEI emissions are split by sector and the measured data is for 2022.

The wider national impact of the apparent inventory NO_x overestimate from commercial buildings is however likely small. Commercial combustion is a relatively minor source when considering the whole of the UK (around 2 % of total UK NO_x emissions), where traffic still substantially dominates. Since NO_x from commercial heating will be lower than is currently reported, this may help modestly in supporting the UK in achieving international emissions ceilings set under CLRTAP. However, in city centres where commercial combustion becomes more of an important source, these effects are more significant, particularly when inventories are used to support the modelling of future NO_2 concentrations. Nevertheless, concentration modelling typically uses background concentration measurement sites to calibrate the dispersion model,[41] so inventory inaccuracies may already to a degree be accounted for. Since the LAEI/NAEI follow EMEP/EEA guidance, this will likely impact most European inventories that report commer-

cial heating NO_x.

3.4.7 A look into the future

Despite the large reductions in road transport NO_x emissions, all air quality sites in central London still exceed the 2021 WHO Air Quality Guidelines for NO_2 in 2022, although most do now meet national limit values which are higher. Time series concentration data for the two urban background monitoring sites within the BT Tower measurement footprint in London are shown in Figure 3.10. Current NO_2 concentrations at the sites are 2.5× that of the 2021 WHO guideline. Looking to the future, it is anticipated that the commercial heating sector will see a further drop in NO_x emissions as the boiler fleet transitions to one that fully complies with the 2018 Ecodesign and MCP Directives. Assuming a full boiler fleet transition to the new regulations by 2028 (due to the boiler lifetime of 10 years), a further 35 % reduction in commercial combustion NO_x from 2018 levels is expected. The magnitude of this reduction is shown as a red arrow with the time period highlighted as a green box, where total NO_x emissions are reduced by 21 % due to commercial combustion only making up 61 % of the emissions. Meeting 2018 Ecodesign and MCP Directives for all heating in the footprint would be insufficient to achieve 2021 WHO air quality guidelines for NO_2, including if road transport NO_x emissions were reduced to zero (a further 6.3 μg m^{-3}).

The UK Government has committed to overall Net-Zero greenhouse gas emissions by 2050, and this has profound long-term implications for the road transport and the heating sectors in which both will transition away from fossil fuel combustion as their primary energy source. The UK Climate Change Committee has a number of projections for how each sector may be decarbonised.[42] Figure 3.11 shows the balanced projection for the non-residential buildings sector as an example. While reductions would be

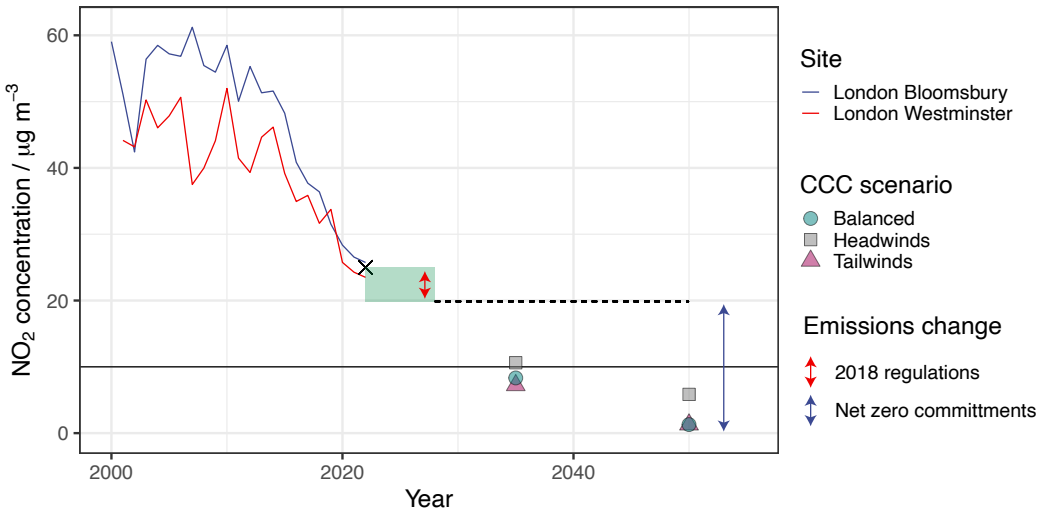

Figure 3.10: AURN NO_2 concentration data for the two urban background sites within the BT Tower footprint. The cross displays the average concentration of the two sites in 2022 which acts as a baseline scenario. The red arrow represents the reduction in concentration that would solely occur from full compliance with 2018 boiler emission directives, and the green box highlights the time period in which this is expected to occur. The dashed line highlights the baseline concentration used for the 2035 and 2050 projections. Other shapes are a result of emissions changes from CCC scenarios as described in the text, with the blue arrow spanning their magnitude.

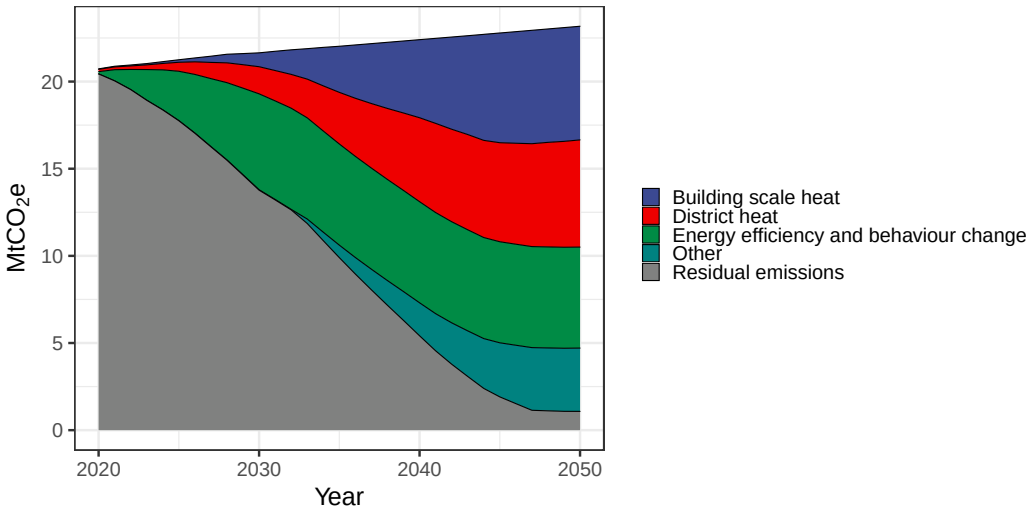

Figure 3.11: The UK's Climate Change Committee (CCC) CO_2 abatement pathways for non-residential buildings to achieve net zero carbon emissions by 2050. Data is taken from The Climate Change Committee [42].

expected in heat demand due to improved energy efficiency of buildings and behaviour change, there would still be NO_x emissions occurring should "low-carbon" fuels be combusted. The relevant sectors here where combustion might be retained include building scale heat, low-carbon district heating schemes and residual point-of-use boilers. Combustion of Hydrogen, solid biomass or bio-methane for heating may be acceptable from a carbon budget standpoint (provided they are produced in a low-carbon way), however, all would lead to continued emissions of NO_x in urban centres unless abated. Therefore, the degree to which combustion is used to heat buildings compared to full electrification (direct or via heat pumps) will play a defining role in setting future urban NO_2 concentrations.

Future concentrations at the London urban background sites based on CCC scenarios are estimated for 2035 and 2050 in Figure 3.10. These projections all assume that the urban background concentrations of NO_2 will decrease linearly with emissions of NO_x in the central area, and that there is a full compliance with the 2018 boiler regulations by 2035 (dashed line).

They have been calculated based on the relative proportions of the heating and transport sectors calculated in this study, and changes in fuel source detailed in the CCC scenario relative to the 2020 baseline. For residential and non-residential buildings, NO_x emissions are scaled linearly with projected H_2 and natural gas usage in the sector, assuming no further changes are made to boiler NO_x emissions regulations post-2018, or the requirement for after-treatment systems (e.g. SCR) on H_2 of bio-gas fueled boilers. Similarly, for the road transport sector, emissions changes have been calculated based on reductions in petroleum demand.

Very low urban concentrations (below 2021 WHO guidelines) for NO_2 are possible for 2035 and beyond, even in the net zero "headwind" scenarios where there is a higher uptake of H_2 boilers. This is largely dependent however on the successful delivery of a very high proportion of space heating from heat pumps, a key assumption in all scenarios. Should some substantial fraction of heating be retained instead using combustion appliances, either fossil fuels or low carbon fuels, then the attainment of 2021 WHO guidelines for NO_2 (for these selected locations) seems unlikely, even with a full electric road transport fleet.

3.5 Conclusions

This work presents a unique long-term NO_x and CO_2 flux data set in a large modern megacity. Long-term measurements have shown that a transition from road transport-dominated to commercial-heating-dominated NO_x emissions occurred in central London after 2020. This is likely a result of policies implemented at the city level that focused on traffic pollution and congestion charging, and natural technological evolution towards cleaner vehicles. It is notable however that should the revised 2021 WHO guidelines for annual average concentrations of NO_2 be an aspiration, then much of London continues to experience concentrations above that recommendation. This

research indicates that in the central area of London 76 ± 17 % of NO_x emissions arise from building heating and that road transport is no longer the largest source. Assuming a full replacement of all older commercial boilers that do not meet the 2018 Ecodesign and MCP Directive limits, NO_2 concentrations in two representative background locations in the central area would be 21 % lower than in 2023. However, this would still be in excess of the 2021 WHO recommended annual average concentration of 10 μg m^{-3}.

Pathways and timelines to lower NO_2 concentrations in London in the 2030s and beyond will now depend on a successful transition to cleaner forms of building heating. The type of technology replacing natural gas boilers in the transition to net zero greenhouse gas emissions will play a central role in this. Using projections from the UK Committee on Climate Change, under all scenarios future central London NO_2 concentrations below 10 μg m^{-3} do appear feasible, although this is critically dependent on a high fraction of heating (assumed in all CCC scenarios) being delivered by heat pumps. The rate at which heat pumps replace gas boilers in London may become a controlling factor in further lowering NO_2 in the city centre. Recent reports suggest the UK is behind on most net zero targets, including the installation of heat pumps for building heat.[43] Should instead some fraction of central London space heating be supplied using combustion sources, for example burning hydrogen, bio-methane of solid biomass, all processes that emit NO_x, then central London NO_2 would inevitably be higher.

Finally, this research highlights that NO_x emission factors applied to commercial combustion within the UK's emissions inventories, taken from EMEP/EEA guidance, may need updating. A value 35 % lower than the guidebook reference, or a NO_x: CO_2 emission ratio of 0.85×10^{-3}, is suggested from this work based on top-down measurement. However, this should be further verified using appliance-level real-world verification, as has been recently undertaken with domestic boilers.

Bibliography

[1] World Health Organisation. *WHO global air quality guidelines: particulate matter (PM2.5 and PM10), ozone, nitrogen dioxide, sulfur dioxide and carbon monoxide*. https://apps.who.int/iris/handle/10665/345329, accessed December 2022. 2021.

[2] United States Environmental Protection Agency. *Nitrogen Oxides (NOx), why and how they are controlled*. https://www3.epa.gov/ttncatc1/dir1/fnoxdoc.pdf, accessed August 2023. 1999.

[3] Zel'dovich, Y. B. The Oxidation of Nitrogen in Combustion Explosions. *Acta Physicochimica U.R.S.S* 11 (1946), pp. 577–628. DOI: 10.1515/9781400862979.364.

[4] European Environment Agency. *EMEP/EEA air pollutant emission inventory guidebook, Report. No 13/2019*. https://www.eea.europa.eu/publications/emep-eea-guidebook-2019, accessed August 2023. 2019.

[5] Jonson, J. E., Borken-Kleefeld, J., Simpson, D., Nyíri, A., Posch, M., and Heyes, C. Impact of excess NOx emissions from diesel cars on air quality, public health and eutrophication in Europe. *Environmental Research Letters* 12.9 (2017), p. 094017. DOI: 10.1088/1748-9326/aa8850.

[6] European Parliament. *Regulation (EC) No 715/2007 of the European Parliament and of the Council of 20 June 2007 on type approval of motor vehicles with respect to emissions from light passenger and commercial vehicles (Euro 5 and Euro 6) and on access to vehicle repair and maintenance information*. https://eur-lex.europa.eu/legal-content/EN/ALL/?uri=celex%3A32007R0715, accessed August 2023. 2007.

[7] European Parliament. *Directive 70/220/EEC of 20 March 1970 on the approximation of the laws of the Member States relating to measures to be taken against air pollution by gases from positive-ignition engines of motor vehicles*. https://\/?uri=CELEX%3A31970L0220, accessed August 2023. 2023.

[8] Ritchie, H. and Roser, M. Urbanization. *Our World in Data* (2018). URL: https://ourworldindata.org/urbanization.

[9] Joshi, R., Liu, D., Nemitz, E., Langford, B., Mullinger, N., Squires, F., Lee, J., Wu, Y., Pan, X., Fu, P., Kotthaus, S., Grimmond, S., Zhang, Q., Wu, R., Wild, O., Flynn, M., Coe, H., and Allan, J. Direct measurements of black carbon fluxes in central Beijing using the eddy covariance method. *Atmospheric Chemistry and Physics* 21.1 (2021), pp. 147–162. DOI: 10.5194/acp-21-147-2021.

[10] Karl, T., Lamprecht, C., Graus, M., Cede, A., Tiefengraber, M., Arellano, J. V.-G. de, Gurarie, D., and Lenschow, D. High urban NOx triggers a substantial chemical downward flux of ozone. *Science Advances* 9.3 (2023), eadd2365. DOI: 10.1126/sciadv.add2365.

[11] Cliff, S. J., Drysdale, W., Lee, J. D., Helfter, C., Nemitz, E., Metzger, S., and Barlow, J. F. Pandemic restrictions in 2020 highlight the significance of non-road NO_x sources in central London. *Atmospheric Chemistry and Physics* 23.4 (2023), pp. 2315–2330. DOI: 10.5194/acp-23-2315-2023.

[12] Lee, J. D., Helfter, C., Purvis, R. M., Beevers, S. D., Carslaw, D. C., Lewis, A. C., Møller, S. J., Tremper, A., Vaughan, A., and Nemitz, E. G. Measurement of NOx Fluxes from a Tall Tower in Central London, UK and Comparison with Emissions Inventories. *Environmental Science & Technology* 49.2 (2015), pp. 1025–1034. DOI: 10.1021/es5049072.

[13] Helfter, C., Tremper, A. H., Halios, C. H., Kotthaus, S., Bjorkegren, A., Grimmond, C. S. B., Barlow, J. F., and Nemitz, E. Spatial and temporal variability of urban fluxes of methane, carbon monoxide and carbon dioxide above London, UK. *Atmospheric Chemistry and Physics* 16.16 (2016), pp. 10543–10557. DOI: 10.5194/acp-16-10543-2016.

[14] Lane, S., Barlow, J., and Wood, C. An assessment of a three-beam Doppler lidar wind profiling method for use in urban areas. *Journal of Wind Engineering and Industrial Aerodynamics* 119 (2013), pp. 53–59. DOI: 10.1016/j.jweia.2013.05.010.

[15] Thomas, C. and Foken, T. Detection of long-term coherent exchange over spruce forest using wavelet analysis. *Theoretical and Applied Climatology* 80 (2006), pp. 91–104. DOI: 10.1007/s00704-004-0093-0.

[16] Schaller, C., Göckede, M., and Foken, T. Flux calculation of short turbulent events – comparison of three methods. *Atmospheric Measurement Techniques* 10.3 (2017), pp. 869–880. DOI: 10.5194/amt-10-869-2017.

[17] Metzger, S., Junkermann, W., Mauder, M., Butterbach-Bahl, K., Trancón y Widemann, B., Neidl, F., Schäfer, K., Wieneke, S., Zheng, X. H., Schmid, H. P., and Foken, T. Spatially explicit regionalization of airborne flux measurements using environmental response functions. *Biogeosciences* 10.4 (2013), pp. 2193–2217. DOI: 10.5194/bg-10-2193-2013.

[18] Drysdale, W. S., Vaughan, A. R., Squires, F. A., Cliff, S. J., Metzger, S., Durden, D., Pingintha-Durden, N., Helfter, C., Nemitz, E., Grimmond, C. S. B., Barlow, J., Beevers, S., Stewart, G., Dajnak, D., Purvis, R. M., and Lee, J. D. Eddy Covariance Measurements Highlight Sources of Nitrogen Oxide Emissions Missing from Inventories for Central London. *Atmospheric Chemistry and Physics Discussions* 2022 (2022), pp. 1–35. DOI: 10.5194/acp-2021-982.

[19] Copernicus Climate Change Service Climate Data Store (CDS). *Copernicus Climate Change Service (C3S): ERA5: Fifth generation of ECMWF atmospheric reanalyses of the global climate.* https://cds.climate.copernicus.eu/cdsapp#!/home, accessed October 2021. 2021.

[20] Barlow, J. F., Dunbar, T. M., Nemitz, E. G., Wood, C. R., Gallagher, M. W., Davies, F., O'Connor, E., and Harrison, R. M. Boundary layer dynamics over London, UK, as observed using Doppler lidar during REPARTEE-II. *Atmospheric Chemistry and Physics* 11.5 (2011), pp. 2111–2125. DOI: 10.5194/acp-11-2111-2011.

[21] Metzger, S., Durden, D., Sturtevant, C., Luo, H., Pingintha-Durden, N., Sachs, T., Serafimovich, A., Hartmann, J., Li, J., Xu, K., and Desai, A. R. eddy4R 0.2.0: a DevOps model for community-extensible processing and analysis of eddy-covariance data based on R, Git, Docker, and HDF5. *Geoscientific Model Development* 10.9 (2017), pp. 3189–3206. DOI: 10.5194/gmd-10-3189-2017.

[22] Kljun, N., Calanca, P., and Rotach, M. W. A Simple Parameterisation for Flux Footprint Predictions. *Boundary-Layer Meteorology* 112 (2004), pp. 503–523. DOI: 10.1023/B:BOUN.0000030653.71031.96.

[23] Metzger, S., Junkermann, W., Mauder, M., Beyrich, F., Butterbach-Bahl, K., Schmid, H. P., and Foken, T. Eddy-covariance flux measurements with a weight-shift microlight aircraft. *Atmospheric Measurement Techniques* 5.7 (2012), pp. 1699–1717. DOI: 10.5194/amt-5-1699-2012.

[24] Kljun, N., Calanca, P., Rotach, M. W., and Schmid, H. P. A simple two-dimensional parameterisation for Flux Footprint Prediction (FFP). *Geoscientific Model Development* 8.11 (2015), pp. 3695–3713. DOI: 10.5194/gmd-8-3695-2015.

[25] Defra and BEIS. *National Atmospheric Emissions Inventory, licenced under the Open Government Licence (OGL), Crown Copyright 2020*. naei.beis.gov.uk/data/, accessed March 2022. 2019.

[26] Greater London Authority. *London Atmospheric Emissions Inventory 2016, licensed under the Open Government Licence (OGL) v2.0, Crown Copyright 2020*. https://data.london.gov.uk/dataset/london-atmospheric-emissions-inventory--laei--2016, accessed March 2022. 2016.

[27] Transport for London. *Transport for London: original source data provided by Operational Analysis department*. 2023.

[28] National Grid. *National Gas Transmission Data Portal*. https://data.nationalgas.com/, accessed February 2023. 2023.

[29] Evans, S., Liddiard, R., and Steadman, P. 3DStock: A new kind of three-dimensional model of the building stock of England and Wales, for use in energy analysis. *Environment and Planning B: Urban Analytics and City Science* 44.2 (2017), pp. 227–255. DOI: 10.1177/0265813516652898.

[30] Greater London Authority. *London Heat Map*. https://data.london.gov.uk/dataset/london-heat-map, accessed August 2023. 2012.

[31] Vaughan, A. R., Lee, J. D., Metzger, S., Durden, D., Lewis, A. C., Shaw, M. D., Drysdale, W. S., Purvis, R. M., Davison, B., and Hewitt, C. N. Spatially and temporally resolved measurements of NO_x fluxes by airborne eddy-covariance over Greater London. *Atmospheric Chemistry and Physics* 2021 (2021), pp. 1–27. DOI: 10.5194/acp-21-15283-2021.

[32] Solazzo, E., Crippa, M., Guizzardi, D., Muntean, M., Choulga, M., and Janssens-Maenhout, G. Uncertainties in the Emissions Database for Global Atmospheric Research (EDGAR) emission inventory of greenhouse gases. *Atmospheric Chemistry and Physics* 21.7 (2021), pp. 5655–5683. DOI: 10.5194/acp-21-5655-2021.

[33] Davison, J., Rose, R. A., Farren, N. J., Wagner, R. L., Murrells, T. P., and Carslaw, D. C. Verification of a National Emission Inventory and Influence of On-road Vehicle Manufacturer-Level Emissions. *Environmental Science & Technology* 55.8 (2021), pp. 4452–4461. DOI: 10.1021/acs.est.0c08363.

[34] Carslaw, D. C. and Rhys-Tyler, G. New insights from comprehensive on-road measurements of NO_x, NO_2 and NH_3 from vehicle emission remote sensing in London, UK. *Atmospheric Environment* 81 (2013), pp. 339–347. DOI: 10.1016/j.atmosenv.2013.09.026.

[35] Cambridge Environmental Research Consultants. *D2.1 Pollutant:CO_2 Ratio Analysis*. https://globalcleanair.org/wp-content/blogs.dir/95/files/2021/01/Breathe-London-CERC-CO2-Ratio-Analysis-Report.pdf, accessed August 2023. 2021.

[36] Karl, T., Graus, M., Striednxig, M., Lamprecht, C., Hammerle, A., Wohlfahrt, G., Held, A., Heyden, L. von der, Deventer, M. J., Krismer, A., Haun, C., Feichter, R., and Lee, J. Urban eddy covariance measurements reveal significant missing NO_x emissions in central Europe. *Scientific Reports* 7.1 (2017), pp. 2536–2545. DOI: 10.1038/s41598-017-02699-9.

[37] Greater London Authority. *Domestic Boiler Emission Testing*. https://www.london.gov.uk/sites/default/files/domestic_boiler_emission_testing_report.pdf, accessed August 2023. 2018.

[38] European Parliament. *Directive 2009/125/EC of the European Parliament and of the Council with regard to ecodesign requirements for space heaters and combination heaters*. https://eur-lex.europa.eu/legal-content/EN/TXT/?uri=CELEX%3A32013R0813, accessed August 2023. 2009.

[39] European Parliament. *Directive (EU) 2015/2193 of the European Parliament and of the Council on the limitation of emissions of certain pollutants into the air from medium combustion plants*. https://eur-lex.europa.eu/legal-content/EN/TXT/?uri=CELEX:32015L2193, accessed August 2023. 2015.

[40] Johnston, D., Bentley, E., Narayana, M., Jiang, T., Suwanapingkarl, P., and Putrus, G. Electric vehicles as storage devices for Supply-Demand management. *2010 IEEE Vehicle Power and Propulsion Conference*. 2010, pp. 1–6. DOI: 10.1109/VPPC.2010.5729237.

[41] Rittner, R., Gustafsson, S., Spanne, M., and Malmqvist, E. Particle concentrations, dispersion modelling and evaluation in southern Sweden. *SN Applied Sciences* 2 (2020), p. 1013. DOI: 10.1007/s42452-020-2769-1.

[42] The Climate Change Committee. *Sixth Carbon Budget*. https://www.theccc.org.uk/publication/sixth-carbon-budget, accessed August 2023. 2021.

[43] The Climate Change Committee. *2023 Progress Report to Parliament*. https://www.theccc.org.uk/publication/2023-progress-report-to-parliament, accessed August 2023. 2023.

Chapter 4

Unreported VOC emissions from road transport including from electric vehicles

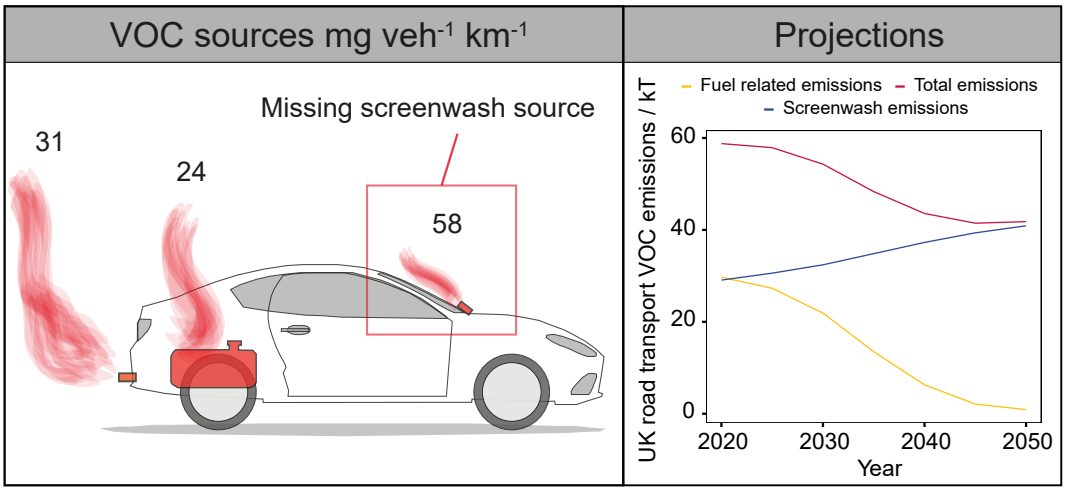

4.1 Abstract

There are widespread policy assumptions that the phase-out of gasoline and diesel internal combustion engines will over time lead to much reduced emissions of Volatile Organic Compounds (VOCs) from road transport and related fuels. However, the use of real-world emissions measurements from a new mobile air quality monitoring station demonstrated a large underestimation of alcohol-based species in road transport emissions inventories. Scaling of industry sales statistics enabled the discrepancy to be attributed to the use of ancillary solvent products such as screenwash and deicer which are not included in internationally applied vehicle emission methodologies. A fleet average non-fuel non-exhaust VOC emission factor of 58 ± 39 mg veh^{-1} km^{-1} was calculated for the missing source, which is greater than the total of all VOCs emitted from vehicle exhausts and their associated evaporative fuel losses. These emissions are independent of the vehicle energy/propulsion system and therefore applicable to all road vehicle types including those with battery-electric powertrains. In contrast to predictions, vehicle VOC emissions may actually increase given a predicted growth in total vehicle kilometers driven in a future electrified fleet and will undergo a complete VOC respeciation due to the source change.

Synopsis: Measurements show that screenwash application dominates vehicular VOC emissions and is missing from road transport inventories.

4.2 Introduction

Road traffic has long been an important source of air pollution to urban environments both directly, and indirectly, contributing to five classes of major air pollutants (NO_x, particulate matter (PM), O_3, VOCs and CO). However, with increasingly stringent emissions legislation and continued uptake

of air pollution abatement strategies, the dominant sources are changing.[1] A wealth of research has been dedicated to understanding non-exhaust PM (e.g. brake and tyre wear), since these are sources that will be present despite fleet electrification.[2] However, very little consideration has been given to non-exhaust VOC emissions.

There have been large decreases in both emissions and some concentrations of VOCs since the mid-1990s in Europe and North America following the universal implementation of the three-way catalytic converter (exhaust control) and the carbon canister (evaporative control).[3] Light duty vehicle regulated emissions standards for NMHC + NO_x have decreased by 97% in the US (Tier 1-3) and by 80-85% in the EU (Euro 1-6),[4] with further improvement planned.

VOC emissions are unusual compared to other gaseous air pollutants because they are a summed group of thousands of different compounds rather than a single chemical. Different VOC species play different roles in atmospheric chemistry depending on their reactivity and functionality. For example, short chain alkenes have a low secondary organic aerosol formation potential, but a high ozone formation potential resulting from their high reactivity with the hydroxyl radical. Aromatic species exhibit different properties being both precursors to ozone and particulate matter.[5] To fully understand atmospheric and potential health implications of VOCs, it is not sufficient to solely monitor the change in total VOC burden to the atmosphere, but also to accurately determine the change in composition.

Typically, only a small number of VOC species are monitored routinely, and many oxygenated VOCs are not measured at all despite comprising an increasing fraction of emissions.[1] In the UK only 4 of the 10 most abundant VOCs are now being measured by national air quality monitoring networks.[6] Current observations in Europe focus on those VOCs that are distinctive of fossil fuels and combustion and have convincedly tracked the downward trends in concentrations related to gasoline vehicles (Figure 4.1).

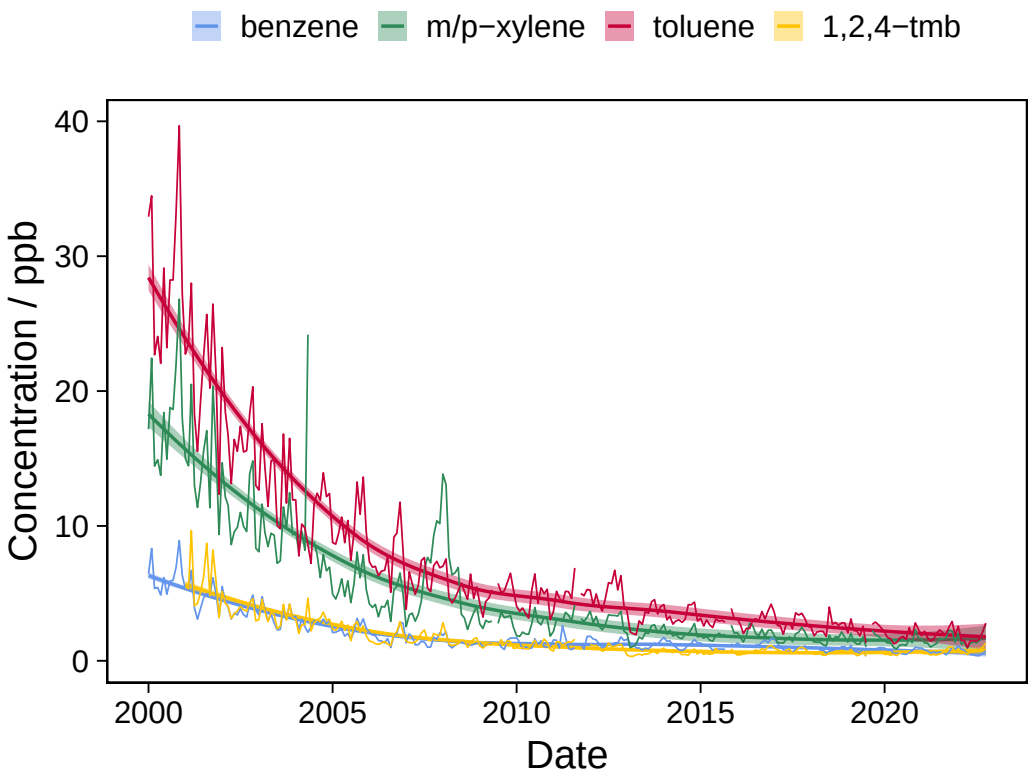

Figure 4.1: Time series benzene, m/p-xylene, toluene and trimethylbenzene at the Marylebone road, central London air quality monitoring station.

Policy projections for the future of VOC emissions in high income countries show downward trends in VOC emissions as older vehicles leave the fleet to be replaced in the medium to long term by electric vehicles. It appears intuitive that vehicles without fuels and combustion will be VOC-free in terms of their operating emissions.

The United Kingdom has a detailed National Atmospheric Emissions Inventory (NAEI) for VOCs which is constructed bottom up, often using industry supplied sales statistics for solvent containing products. It is speciated into more than 600 different individual VOCs. A curious observation from that inventory is that there are industry reported classes of solvent-containing products, labelled as 'car care', that appear to give rise to a larger mass of emissions than that from fuel evaporation and tailpipe exhaust.[7]

A large fraction of this is thought to be the application of screenwash which contains VOCs in the form of alcohol content for their antifreeze properties. Screenwash has in the past received some attention and consideration, in particular in the US, as an important source of air pollution. California, for example, limits their summer formula to 1% VOC content with only certain areas allowed to sell winter blends up to 25% VOC content.[8] This group of products, at least in the UK NAEI, appears to contribute 6% of all UK VOC emissions. However, only a very small number of countries, namely the Netherlands and parts of Scandinavia, produce inventories with this degree of speciation and product granularity.[9] Moreover, the presence of this apparently large VOC source has never been experimentally verified in the field. Here we utilise a new mobile measurement platform to calculate real-world road transport VOC emission factors via a roadside increment-type analysis in Manchester, UK. This methodology has previously been used for studies of non-exhaust particulate matter emissions,[10] and accommodated the quantification of non-fuel related VOC emissions at the roadside. We compare measurements to inventory estimated emissions and outline the potential implications of the findings on future emissions scenarios, policy, and atmospheric chemistry.

4.3 Materials and Methods

4.3.1 Measurement locations

The locations of the two measurement sites are shown in Figure 4.2. The roadside site was situated on Upper Brook Street (53°27’59.9"N, 2°13’44.9"W), which is a key arterial road for transport into and out of Central Manchester and at the location of the roadside site consisted of four lanes. The Manchester Air Quality Supersite (MAQS) is located at the Firs Botanical Gardens (53°26’38.9"N, 2°12’51.1"W) on the University of Manchester Fallowfield

Campus, and is representative of urban background air. Two, three-week measurement periods took place during the Observation System for Clean Air project (OSCA) in July 2021 and February 2022.

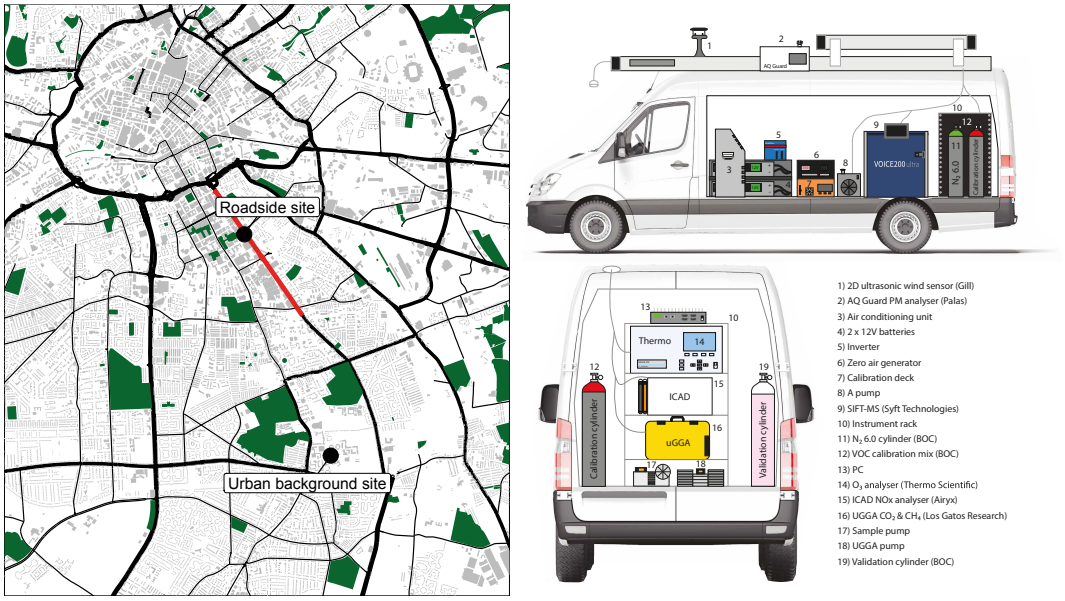

Figure 4.2: Left: Locations of the roadside and urban background measurement sites (black dots) and Upper Brook Street (red line) in Manchester, UK. Map reproduced with permission in R using data from © OpenStreetMap contributors, available under the Open Database License. Right: A schematic of the WASP instrumentation configuration during OSCA. At the top is a side profile with each piece of kit numbered and labeled below. Below is a back profile of the black instrument rack **10**.

4.3.2 Instrumentation

The WACL Air Sampling Platform (WASP) was deployed as the roadside measurement site. The WASP has been previously described in detail,[11] with an updated suite of instrumentation presented in Figure 4.2. The Manchester Air Quality Supersite (MAQS) used as the urban background site carries out long-term measurements of gases, aerosols, and meteorol-

ogy.[12–14] The instrumentation used to measure each atmospheric species is described below.

4.3.2.1 VOCs

At the roadside, a Voice 200 Ultra Selected-Ion Flow Tube Mass Spectrometer (SIFT-MS) (Syft Technologies Ltd., New Zealand) was used to quantify VOC mixing ratios. The theory of operation is described in detail elsewhere in the literature,[15] with the instrument being operated using a flow tube pressure of 460 mTorr. Sampling from an in-house built palladium alumina-based zero air generator assessed the instrument background for five minutes of each hour. The five-minute average background mixing ratio was subtracted from the ambient mixing ratio measurements of the corresponding hour. Sensitivities for the compounds detected by SIFT-MS were determined every 3 days from automated multi-point calibrations performed using an in-house developed dilution unit. This used a 1 ppm gravimetrically prepared standard of different VOCs in ultrahigh purity nitrogen (National Physics Laboratory, UK) diluted with ambient humidity zero air.

At the background MAQS, VOCs were measured using Thermal Desorption-Gas Chromatography coupled with Flame Ionisation Detection (TD-GC-FID) (Agilent Technologies Inc., USA). Air was drawn down a 2 m 1/4" Silonite (Entech Instruments Inc., USA) coated heated stainless steel tube at 20-30 slpm using a MB-158 metal bellows compressor (Senior Aerospace BWT., UK) and back pressure regulated to maintain a 25 sccm sampling flow through a custom built pre-concentration unit. Calibration gas was provided from a working standard cylinder comprising a sample of NMVOCs (material number: 177664-AL-HC, BOC Special Gases) diluted to 1.2 ppb per component in purified nitrogen (cylinder number: D035781, Air Liquide S.A., France), linked to an NPL30 primary calibration standard (National Physical Laboratory, UK). VOC free blanks were created from compressed air, through a bed of 1 % Pt on Alumina beads at 375 °C. Air, cal-

ibration and blanks were de-humidified with a -40 °C water trap and 500 mL samples were pre-concentrated on a multi-bed sorbent trap at around -120 °C, flow controlled by a downstream MC mass flow controller (Alicat Scientific Inc., USA). After removal of CO_2 and other permanent gases at -80 °C, the preconcentration trap was desorbed and refocused before final desorption in a H_2 carrier gas flow onto a VF-WAX-MS GC column (60 m, 0.25 mm I.D. 150 μm film, Agilent Technologies Inc., USA). Analytes not retained on the WAX column (C2-C6 aliphatics) were diverted by Deans Switch and separated on a PLOT column ($A1_2O_3/Na_2SO_4$ 50 m, 0.32 mm I.D. 5 μm film, Agilent Technologies Inc., USA). Oxygenates, > C6 aliphatic, and aromatics were not diverted and analytes eluting from each column were detected by flame ionisation detectors.

4.3.2.2 Nitrogen Oxides

NO_x (NO + NO_2) was measured at the roadside using the Iterative CAvity enhanced Differential optical absorption spectroscopy system (ICAD) (Enviro Technology Services Ltd., UK).[16] Urban background NO_x was calculated via the sum of two separate measurements of NO and NO_2. NO was measured using a Thermo 42i- (Thermo Fisher Scientific Inc., USA), and NO_2 using a T500U Cavity Attenuated Phase Shift (CAPS) analyser (Teledyne API., USA).

4.3.2.3 Carbon Dioxide

An Ultra-portable Greenhouse Gas Analyser (UGGA) (Los Gatos Research Inc., USA) was used to quantify mixing ratios of CH_4, CO_2 and H_2O (1 Hz data acquisition) at the roadside. The instrument utilises Off-Axis Integrated-Cavity Output Spectroscopy (OA-ICOS) to directly quantify mixing ratios of the three species.[17,18] The instrument was linearly calibrated using a three-point calibration curve, using standards traceable to the WMO scale.

Table 4.1: A list of the compounds measured by the SIFT-MS during the OSCA experiments, their corresponding product ion and molar mass, a flag to indicate the calibration status, all grouped by the reagent ion used.

Reagent Ion	Compound	Product ion	Molar Mass g mol^{-1}	Calibrated?
H_3O^+	Methanol	CH_5O^+	33	Y
	Ethanol	$C_2H_7O^+$	47	Y
	Acetonitrile	$CH_3CN{\cdot}H^+$	42	Y
	Acetaldehyde	$C_2H_4O{\cdot}H^+$	45	N
	Nitrous acid	$H_2NO_2{}^+$	48	N
	Nonane	$C_9H_2O{\cdot}H_3O^+$	147	Y
	Decane	$C_{10}H_{22}{\cdot}H_3O^+$	161	Y
	Formaldehyde	CH_3O^+	31	N
NO^+	Benzene	$C_6H_6{}^+$	78	Y
	Toluene	$C_7H_8{}^+$	92	Y
	M-xylene	$C_8H_{10}{}^+$	106	Y
	1,2,4-trimethlybenzene	$C_9H_{12}{}^+$	120	Y
	Acetone	$C_3H_6O{\cdot}NO^+$	88	Y
	Butadiene	$C_4H_6{}^+$	54	Y
	Isoprene	$C_5H_8{}^+$	68	Y
	3-buten-2-one	$C_4H_6O{\cdot}NO^+$	100	Y
	Butanone	$C_4H_8O{\cdot}NO^+$	102	Y
	Acetic acid	$CH_3COOH{\cdot}NO^+$	90	N
	Methyl tert-butyl ether	$C_4H_9{}^+$	57	N
	Octane	$C_8H_{17}{}^+$	113	Y
$O_2{}^+$	Isoprene	$C_5H_7{}^+$	67	Y
	Acetylene	$C_2H_2{}^+$	26	N
	Propane	$C_2H_4{}^+$	28	N
	Nitrogen dioxide	$NO_2{}^+$	46	N

CO_2 was measured at the supersite using a Multi-gas Carbon Emissions Analyser (MGCEA) (Los Gatos Research Inc., USA), capable of simultaneous measurements of CO_2, CH_4, CO, and H_2O. The MGCEA operates using the same measurement principles as the UGGA.

4.3.2.4 Traffic Data

To gather insight into the type and number of vehicles traveling by the measurement site, traffic counts, vehicle type, and hourly average speed data were gathered by a Vivacity traffic camera. The traffic sensor uses machine learning algorithms to enable accurate detection, classification, and analysis of different transport modes and traffic movement. Vehicle type was broken down into the following categories: buses and coaches, cars and vans, cars with a trailer, Heavy Goods Vehicles (HGVs), motorcycles and rigids. The camera is owned by Transport for Greater Manchester (TfGM), and the data was provided by Manchester-i, a data solution that collects, hosts, and exposes city open data to a broad set of researchers and end-users operating / interested in urban-related disciplines. Across the two periods, emissions from a total of 754519 vehicles were measured.

4.3.3 Emission Factor Calculation

4.3.3.1 Real World Emission Factors

Fleet average emission factors for different VOC species were calculated from hourly speed-dependent emission factors of a tracer species, the incremental concentrations of the tracer species and VOCs at the roadside in comparison with an urban background site, and an assumption that the emitted tracer and VOC species were transported and diluted in the same way in the atmosphere, as has been done previously in the literature.[10,19,20] In this study, both CO_2 and NO_x were used as tracers. The following three steps show how this was done.

1) The roadside increment of a tracer species (ΔC_T) with well-known emission factors was calculated. This was done using Eq. 4.1, where the roadside concentration ($C_{TRoadside}$) was measured by the WASP, and the background ($C_{TBackground}$) was measured at the MAQS urban background location.

$$\Delta C_T = C_{TRoadside} - C_{TBackground} \tag{4.1}$$

2) Hourly emission factors for the tracer species were calculated and combined with the roadside increment in part a) to calculate a correction factor for the dilution of the emissions between the two sites. Hourly tracer species speed-dependent emission factors (EF_T) were obtained from the Department for Environment, Food, and Rural Affairs (Defra) Emission Factor Toolkit (V11.0).[21] Due to the nearby location of the TfGM Vivacity traffic camera, an hourly detailed breakdown of traffic counts (n) and type (i) was able to be used as an input, along with hourly average speed, the Urban (not London) road-type setting and the appropriate year of measurement (2021 or 2022 depending on the measurement campaign period). The hourly dilution correction (dT) was then calculated from Eq. 4.2 using the tracer emission factor for each vehicle type and the dry roadside increment concentration.

$$dT = \frac{\sum_i EF_{T,i} \times n_i}{\Delta C_T} \tag{4.2}$$

3) The fleet average emission factor for a species x ($\mathrm{EF}_{fleet,x}$), was then calculated from the roadside increment of that species (ΔC_x), the dilution factor of the tracer species and the total number of vehicles on the road during the hour (n_{tot}) in Eq. 4.3.

$$EF_{fleet,x} = \frac{\Delta C_x \times dT}{n_{tot}} \tag{4.3}$$

4.3.3.2 Inventory Estimated Emission Factors

Inventory estimated emissions were calculated using the international reference methods of COPERT (Calculation Of air Pollutant Emissions from Road Transport) following UK-specific guidance presented in the "Methodology for the UK's Road Transport Emissions Inventory" report.[22] The UK road transport emissions inventory in turn follows the methodology outlined in the EMEP/EEA "Air Pollutant Emission Inventory Guidebook",[23] which uses emission factors in COPERT. A full description of the data used for the COPERT calculations is given below.

To calculate emissions in COPERT, various data inputs are required. These were taken from the Ricardo handbook, or, if unavailable or Manchester specific, sourced elsewhere.[22] The data used is described below.

- Year: 2021 was used for the summer experiments and 2022 was used for the winter experiments.
- Environmental information (min temperature, max temperature and humidity): obtained from weather data archives for the different measurement periods. All months are filled with the same values so that the annual emissions represent conditions during the desired month. Summer: 12 °C, 20 °C and 80 %. Winter: 2 °C, 8 °C and 87 %.
- Trip length: 10 km, as described in the Ricardo handbook.
- Fuel advanced specifications = 2009 fuel year (the most recent).
- Reid Vapour Pressure = Summer: 70 kPa, Winter: 90 kPa, as described in the Ricardo handbook.

Stock configuration and activity data was obtained from the nearby traffic camera but required some additional processing for input into COPERT. COPERT requires a high level of granularity in the stock configuration and activity input. Vehicles should be broken down into the various vehicle

technologies by vehicle category (e.g. passenger car, HGV, bus etc.), Euro Standard, fuel type and size. Unfortunately, the traffic camera data available to us only breaks down the traffic into vehicle category. In order to further break this down into the required granularity, each vehicle category counts was multiplied by the 2021 or 2022 corresponding UK average Euro Standard, fuel type and vehicle size fractions taken from the NAEI fleet composition projections (2019),[24] as shown in Eq. 4.4.

$$n_{c,e,f,s} = n_c \times e_c \times f_c \times s_c \tag{4.4}$$

Where:

- $n_{c,e,f,s}$ is the number of vehicles of category c, Euro Standard e, fuel type f and size s.
- n_c is the number of vehicles of category c, measured at the roadside site
- e_c is the fraction of vehicles of category c that are of Euro Standard e
- f_c is the fraction of vehicles of category c that are of fuel type f
- s_c is the fraction of vehicles of category c that are of size s

Here, the assumption that the traffic measured in Manchester is representative of the whole UK fleet is made. In addition to fleet breakdown and vehicle counts, mean annual activity and lifetime cumulative mileage is required. Mean annual activity for the UK is ~ 12000 km and the average age of a car is ~ 8.4 year old. Therefore, lifetime cumulative mileage is given as 100000 km (the product of the two). Lifetime cumulative activity is largely required for degradation parameters, and it was found that it has minimal impact on the emissions outputted by COPERT. Mean activity is used for the calculation of annual bulk emissions. However, the actual magnitude is not important as we divide through by it later during conversion to an

EF. Finally, circulation activity was divided into a 100 % share for urban driving to represent our Manchester site, using urban peak/off peak traffic speeds obtained from the nearby traffic camera ($\sim$ 40/50 km h^{-1}).

All other data was kept as standard in the COPERT database. This includes fuel evaporation data such as fuel tank size, carbon canister size and % fuel injection. In the NAEI handbook, it is assumed "that all pre-Euro 1 cars would be with carburettor and that all Euro 1 onward cars would use fuel injection, but with fuel return systems, hence, having high emission factors". There is no input for % fuel return/returnless fuel systems in this version of COPERT so this impact can not be studied here.

COPERT outputs hot, cold and evaporative bulk NMVOC emissions for each vehicle technology. Evaporative emissions consist of a number of sources that we do not want to include in this analysis. As mentioned earlier, diurnal and hot soak emissions occur when the engine is turned off and so are not present at the roadside site. Therefore, rather than use the bulk evaporative emissions, the EFs in COPERT used for running emissions calculation are used instead. A fleet average running evaporative emissions factor is calculated using Eq. 4.5:

$$EF_{r,fa} = \frac{\sum_x EF_{r,x} \times n_x}{n_{total} \times 10\ km} \tag{4.5}$$

Where:

- $EF_{r,fa}$ is the fleet average running emissions factor in g vh^{-1} km^{-1}
- $EF_{r,x}$ is the running emissions factor for vehicles of technology x in g $trip^{-1}$
- n_x is the number of vehicles of technology x
- n_{total} is the total number of vehicles measured
- 10 km is the average trip length and thus division by it converts the emissions factor from g $trip^{-1}$ to g km^{-1}.

Exhaust emissions are calculated using Eq. 4.6:

$$EF_{e,fa} = \frac{E_{a,hot} + E_{a,cold}}{\sum_x n_x \times d_{a,x}} \tag{4.6}$$

Where:

- $EF_{e,fa}$ is the fleet average exhaust emission factor in g vh^{-1} km^{-1}
- $E_{a,hot}$ is the annual hot NMVOC emissions in g
- $E_{a,cold}$ is the annual cold NMVOC emissions in g
- n_x is the number of vehicles of technology x
- $d_{a,x}$ is the annual distance travelled per vehicle of technology x in km

The evaporative and exhaust NMVOC EFs are separately speciated based on their corresponding speciation fractions in COPERT, also displayed in the EMEP/EEA guidebook, in Eq. 4.7:

$$EF_{x,i} = EF_i \times s_x \tag{4.7}$$

Where:

- $EF_{x,i}$ is the emission factor for species x of emission type i (exhaust or evaporative) in g vh^{-1} km^{-1}
- EF_i is the emission factor for emission type i in g vh^{-1} km^{-1}
- $s_{x,i}$ is the percentage fraction of species x in emissions of type i

It should be noted that in COPERT ethanol is not included as a fraction in either exhaust or evaporative emissions. However, it can be calculated as the remaining fraction once all other species have been subtracted from 100 %. The 6 % given for evaporative emissions and 0 % given for exhaust emissions is consistent with that given in the EMISIA/EEA handbook.

Finally, the total EF for a NMVOC species is calculated from the sum of the speciated exhaust and evaporative EFs in Eq. 4.8:

$$EF_x = \sum_i EF_{x,i} \tag{4.8}$$

Where:

- EF_x is the emission factor for species x in g vh^{-1} km^{-1}
- $EF_{x,i}$ is as above

4.4 Screenwash composition

The alcohol composition of 10 different screenwash products ordered online (available UK market, October 2022) were determined by gas chromatography time of flight mass spectrometry. A headspace analysis was conducted, with the results shown in Table 4.2.

4.5 Results and discussion

4.5.1 Roadside vs background atmospheric concentrations

Ethanol and methanol were consistently the most abundant VOCs measured at both the roadside and the urban background site (Figure 4.3, see Table 4.1 for the full list of VOC species measured at the roadside). Throughout the day, concentrations an order of magnitude higher than the aromatic species were observed as is in agreement with previous measurements made in London, UK.[25] All species showed a positive roadside increment apart from methanol in the summer; methanol at the urban background site was greater than at the roadside due to the influence of biogenic emissions from the botanical gardens where the MAQS is located in. There was a notable

Table 4.2: The headspace composition of 10 different screenwash products as determined in the laboratory.

Product	Methanol %	Ethanol %
1	25.1	3.41
2*	4.95	17.5
3*	4.54	7.75
4	4.53	0.00
5	4.50	8.12
6	4.11	18.3
7	0.00	0.00
8*	1.95	7.29
9*	4.58	22.8
10	0.00	22.5
Average	5.42	10.8

*Diluted, 'ready to use' blends

contrast in diurnal shape between the seasons due to the impact of meteorology in the summer. Summer diurnals were driven by boundary layer height where a decrease in concentration after the morning rush hour is observed in line with increasing boundary layer height, before rising again in the evening as the boundary layer height begins to fall. Roadside winter diurnal profiles for all VOCs presented consistently tracked traffic flow (Figure 4.4), and the tracer species (NO_x and CO_2), with a peak in the morning and evening in line with rush hour increases in traffic. The urban background concentrations remained low and stable with minimum influence from traffic.

4.5.2 Emission factors

Emission factors were calculated using both NO_x and CO_2 as the tracer species due to their high degree of emissions regulation and therefore relatively well-known emission factors. Calculations using both enabled a useful comparison to be made as most previous roadside increment-type analyses have used NO_x only as a tracer.[19,20] However, the accuracy of NO_x emission factors in emissions inventories has been questioned as a result of the diesel-gate scandal and the ineffectiveness of exhaust treatment systems under real-world driving conditions, especially in urban areas.[10] Dilution factors were reasonably consistent with those measured previously in London and can be seen diurnally in Figure 4.5, with summer dilution factors being 21% and 24% larger than winter for CO_2 and NO_x respectively.[10] Figure 4.6 shows that in general, there is a good level of agreement between the two tracer methods; using NO_x as a tracer gave VOC emission factors that were on average 5% lower in summer and 16% lower in winter. This is due to a likely underestimation of NO_x in the emissions used in the calculations with the temperature-related performance of NO_x emissions control technologies explaining the seasonal variability. For the remainder of this

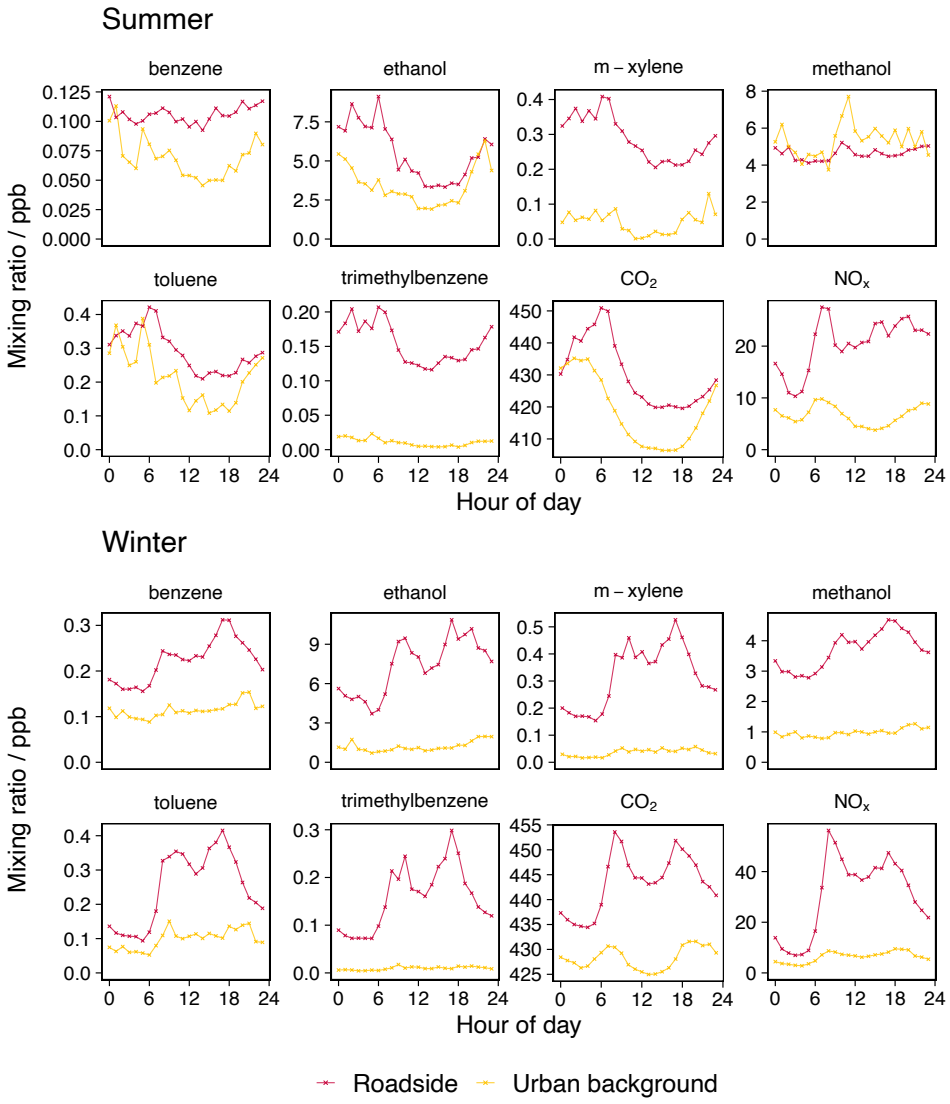

Figure 4.3: Median average diurnal profiles for six VOC species (benzene, ethanol, m-xylene, methanol, toluene, and trimethylbenzene) and both tracer species (CO_2 and NO_x) for the summer and winter at both measurement sites.

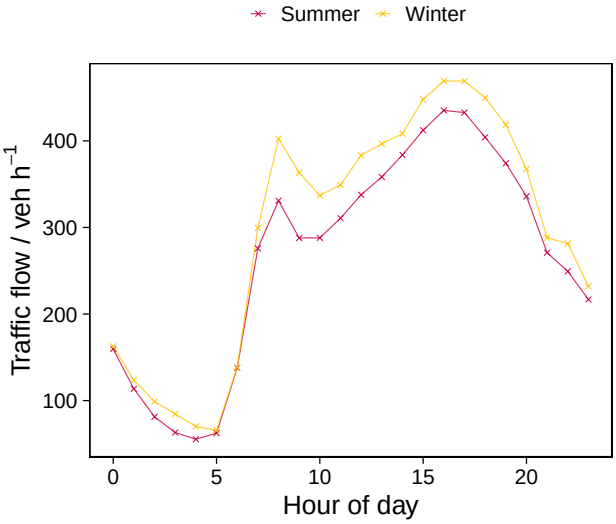

Figure 4.4: Median average diurnal profiles for traffic counts at the roadside site during the summer and winter measurement periods.

analysis, only the CO_2 emission factors will be discussed.

The aromatic species had emission factors in the range of 1-6 mg vh^{-1} km^{-1} and were similar across the seasons as a result of the competition between increased fuel evaporative emissions in the summer and increased cold exhaust emissions in the winter. The measured emission factors agreed well with COPERT-derived values with small discrepancies between the species arising due to variability in the speciation of VOC emissions from road transport in the inventory, itself influenced by fuel blends. Winter aromatic emission factors were slightly overestimated in COPERT due to greater cold exhaust emissions, all of which would not be captured at the roadside site. Nevertheless, the general agreement between in-field measured emission and COPERT for aromatics is very encouraging, but perhaps not surprising given the long intensive focus that regulations have had on VOCs of this type and exhaust emissions.

Emission factors for ethanol and methanol were much higher at 68 ± 42 and 18 ± 7 mg vh^{-1} km^{-1} respectively for winter, and 24 ± 19 and 12 ± 10 mg vh^{-1} km^{-1} for summer. Since a summer methanol emission factor

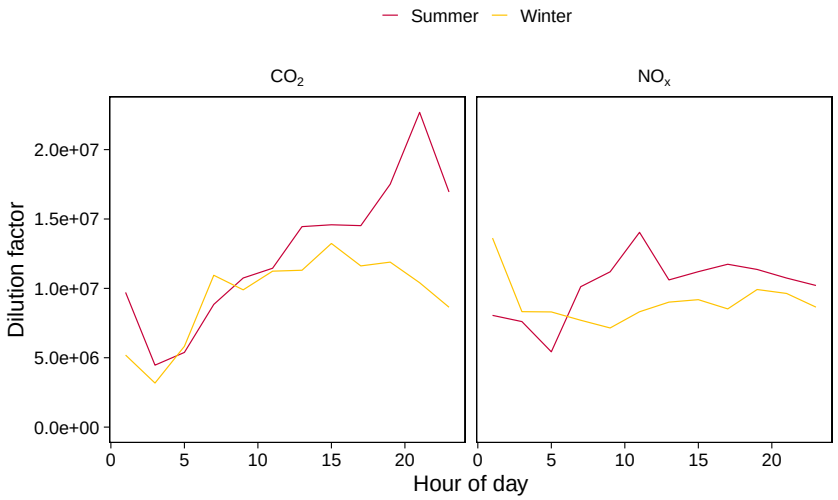

Figure 4.5: Diurnal profiles of the dilution factors measured for NO_x and CO_2 during the summer and winter measurement periods.

Table 4.3: Measured summer VOC emission factors calculated using CO_2 and NO_x as tracer species, listed as median and upper and lower quartiles.

Species	Measured emission factor (mg vh^{-1} km^{-1})					
	CO_2			NO_x		
	median	Q1	Q3	median	Q1	Q3
trimethlybenzene	3.367	2.564	5.401	3.307	2.471	5.002
benzene	0.5527	0.2633	0.8936	0.4344	0.2282	0.7525
ethanol	23.69	11.82	38.57	21.24	12.14	41.45
m-xylene	5.406	3.759	7.500	6.069	3.335	10.10
toluene	2.636	1.979	4.096	2.653	1.740	4.129

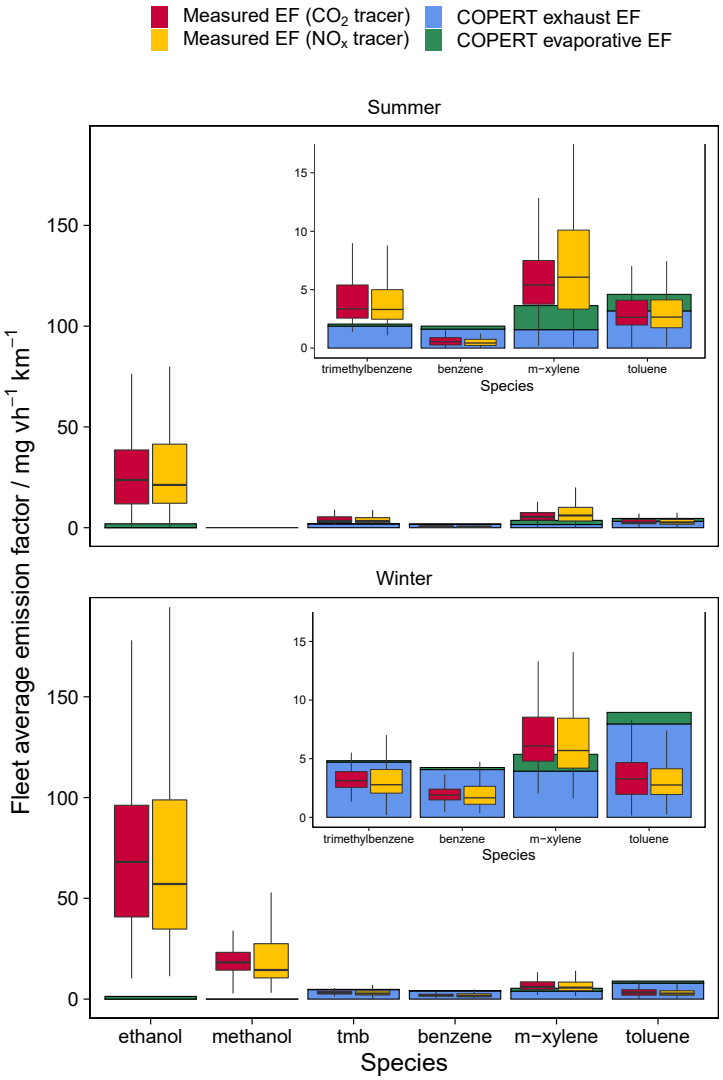

Figure 4.6: Box plots of measured VOC emission factors at the Manchester roadside using CO_2 and NO_x as tracer species, compared to COPERT calculated exhaust and evaporative emission factors as bars, faceted by season. In the top right of each facet is an expanded view of the aromatic emission factors to improve clarity.

Table 4.4: Measured winter VOC emission factors calculated using CO_2 and NO_x as tracer species, listed as median and upper and lower quartiles.

Species	Measured emission factor (mg vh^{-1} km^{-1})					
	CO_2			NO_x		
	median	Q1	Q3	median	Q1	Q3
1,2,4-trimethlybenzene	3.121	2.552	3.899	2.780	2.060	4.077
benzene	1.895	1.483	2.402	1.663	1.112	2.642
ethanol	68.08	40.78	96.19	57.11	34.75	101.7
m-xylene	6.075	4.792	8.543	5.695	4.195	8.451
methanol	18.22	14.37	23.21	14.45	10.55	27.51
toluene	3.287	1.959	4.667	2.755	1.946	4.139

was unavailable from the roadside increment methodology due to the urban background interference, an estimate was calculated from the average speciation of screenwash blends on the market in the UK and the summer ethanol emission factor. Since the composition of major sources such as screenwash are not well-known, and variable between products, we conducted laboratory headspace analysis of a range of products to evaluate the relative speciation between ethanol and methanol. This is shown in Table 4.2, indicating that an apportionment of 67:33 ethanol: methanol would be reasonable at this time. This is, within error, in agreement with the relative proportions of the ethanol and methanol emission factors measured for summer in this study. (We note that whilst methanol is now regulated and limited as an additive in Europe, online retailers appear to sell materials that continue to contain high methanol content). Assuming the speciation at the measurement site was the same as that measured in the lab and applying it to the ethanol emission factor gave the summer methanol emission factor of 12 ± 10 mg vh^{-1} km^{-1}. The emissions of the two alcohol species were substantially underestimated by the COPERT methodology.

Table 4.5: COPERT calculated total, exhaust and evaporative emission factors for the studied VOC species, separated by season.

Species	COPERT emission factor / mg vh^{-1} km^{-1}					
	Summer			Winter		
	Total	Exhaust	Evaporative	Total	Exhaust	Evaporative
trimethlybenzene	2.059	1.882	0.1771	4.831	4.708	0.1233
benzene	1.884	1.627	0.2576	4.249	4.069	0.1794
ethanol	1.932	0.000	1.932	1.345	0.000	1.345
m-xylene	3.635	1.574	2.061	5.374	3.939	1.435
methanol	0.000	0.000	0.000	0.000	0.000	0.000
toluene	4.601	3.184	1.417	8.951	7.964	0.9866

The discrepancy can be rationalised and the VOC budget closed by also including an emission of non-fuel, non-exhaust (NFNE) VOC deriving from what are classified as 'car care' solvents in the NAEI.[24] A large fraction of this is thought to be screenwash leading to a release of ~35 kT of VOCs in 2018. Dividing through by the total number of vehicle kilometers traveled in 2018 in the UK (537 billion km, DfT Road Transport Statistics) gives an estimated emission factor based on solvent inventories for screenwash of 64 mg vh^{-1} km^{-1}; a figure that agrees remarkably well with the seasonal average of the combined ethanol and methanol median emission factors measured in this study (60 ± 39 mg vh^{-1} km^{-1}). The increased winter emission factor is then explained by increased screenwash usage in wetter and dirtier conditions.

4.5.3 Implications

4.5.3.1 For future emissions and policy

A large source of vehicle emissions not captured by international emissions methodologies such as COPERT is surprising but reflects that the historical focus has been overwhelmingly on fuel-related exhaust and evaporative emissions. It is a measure of the success of abatement technologies that

these are now so reduced that other NFNE sources become visible. Real-world observations of NFNE are, in practice, in good agreement with separate industry solvent use statistics, so to a degree have been 'hiding in plain sight'. An important feature of car care product emissions is that they are independent of fuel type, meaning the emissions are applicable to all vehicles including those powered by battery electric powertrains. Therefore, we use this information to propose the need for a direct VOC emission factor for electric vehicles in international methodologies that are used to quantify the impacts of road transport on air quality. Subtracting the COPERT-estimated ethanol and methanol emissions (arising from exhaust and evaporative losses of ethanol-blended fuel use in the UK) from the measured sum of the alcohol emission factors gives the NFNE-related emission factor. We propose a value of 58 ± 39 mg vh^{-1} km^{-1} for UK vehicles which assumes all emissions can be apportioned as a combination of ethanol and methanol with an apportionment of 67:33 ethanol: methanol as derived from the laboratory headspace analysis of screenwash blends.

A NFNE emission factor of 58 mg vh^{-1} km^{-1} is 1.8 x greater than total exhaust VOC emissions in the UK (32 mg vh^{-1} km^{-1}). Looking to the future, NFNE emissions from solvent products may actually increase, should overall vehicle mileage increase, as is indicated in some projections of future electrified transport fleets. Annual vehicle kilometers driven in the UK have steadily increased over the last three decades and are predicted to increase by up to 51% on 2015 levels by 2050.[26] This is a consequence of increased population and an anticipated reduction in the cost of travel in electric vehicles. Assuming that NFNE emissions are simply proportional to total vehicle distance traveled, and that fuel-related emissions are inversely proportional to the % of electric vehicles in the UK fleet, future road transport emissions can be estimated. Figure 4.7 shows this projection; because of fleet electrification there is initially a fall in total road transport VOC emissions but due to increasing vehicle km and the related scaling

in NFNE emissions, road transport VOC emissions begin to increase after 2045. NFNE emissions would represent ~ 40 kT of VOC emissions in 2050 which is around 6% of the UK's 2030 National Emission Ceilings Directive (NECD) ceiling. Although only UK figures are presented here, this is a transition of global significance. The main driver for the rate of fleet electrification is transport decarbonisation and the policy to ban new sales of petrol and diesel vehicles. Current ICE ban commitments are highlighted in Figure 4.7 and span all the major continents, with further pledges, particularly in Asia, expected soon.

4.5.3.2 For atmospheric chemistry

The transition from fuel-related VOC emissions to non-fuel-related VOC emissions represents a notable change in the VOC speciation of the emissions. Fuel-related VOC emissions contain a complex mixture of aliphatics and aromatics whereas NFNE emissions typically only contain ethanol and methanol. On average, the ozone formation potential of ethanol and methanol is lower than a similar overall mass emission of fuel related VOCs.[27] However, increasing concentrations of ethanol in the atmosphere and even screenwash-related methanol emissions have been associated with increased formation of tropospheric ozone.[28,29] A useful comparison can be drawn with bioethanol use in Brazil. Ozone and PM levels have been shown to increase during periods where more ethanol is combusted in vehicles compared to gasoline, despite ethanol combustion typically reducing VOC emissions.[30,31] Here, the cause is thought to be reduced NO_x emissions in a VOC limited ozone regime. During fleet electrification, a similar scenario could occur in which VOC emissions remain high as a result of NFNE emissions with reductions in NO_x increasing ozone and PM formation. Whilst the transition could, at least initially, reduce the urban VOC burden, models which do not include NFNE emissions may underestimate future urban ozone concentrations due to the size of the missing source.

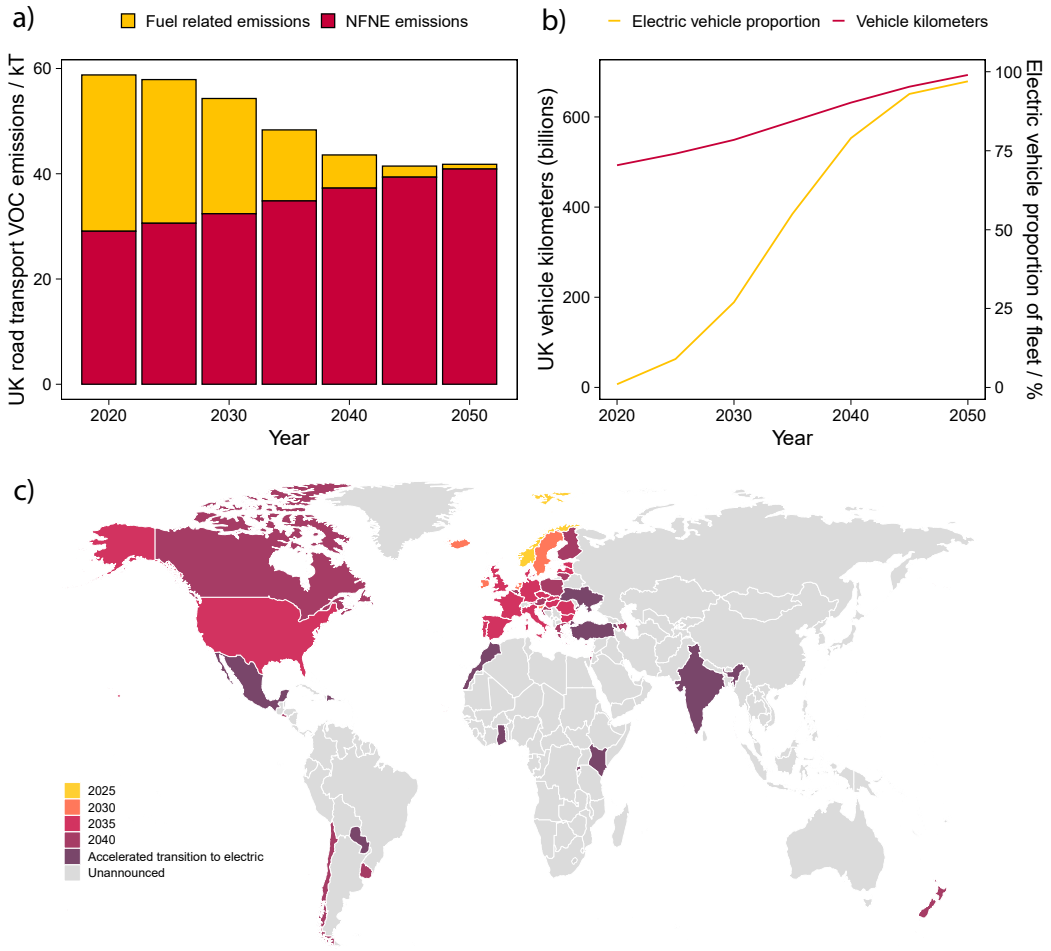

Figure 4.7: a) VOC emission projections for road transport for fuel-related and NFNE sources. Fuel-related emissions are proportionally reduced from 2020 estimates using projected electric vehicle fleet percentage. NFNE emissions are generated by multiplying the derived emission factor in this work (58 mg vh^{-1} km^{-1}) by projected vehicle kilometers traveled in the UK. b) Electric vehicle proportion and UK annual vehicle kilometers traveled predictions used to produce a) from DfT (Road Traffic Forecasts 2018). c) A global timeline of commitments to the banning of new petrol and diesel vehicle sales. Data were mainly taken from COP 26 signatory list, but also from the EU 'Fit for 55' proposal and the US Executive Order on Catalysing Clean Energy Industries and Jobs through Federal Sustainability.

In addition to its role in ozone formation, ethanol is a key precursor to the formation of acetaldehyde which is a highly reactive compound that is also a suspected carcinogen and is associated with various respiratory conditions.[32] Increasing ethanol concentrations in the atmosphere have been associated with increased production of peroxyacetyl nitrate (PAN) under high NO_x conditions.[28] PAN is an important species for the atmospheric transport of NO_x with implications for the global distributions of ozone and OH.[33] However, there is uncertainty surrounding future emissions scenarios of NO_x due to a poor quantification of the impact of congestion and the proposed transitions from natural gas to hydrogen combustion in heating systems.[34,35] As such, the ramifications of increasing ethanol concentrations are currently unknown but potentially important. Methanol plays an important atmospheric role through involvement in hydroxyl radical cycling and thus the tropospheric oxidative capacity.[36] It is also a precursor for formaldehyde and CO.

Looking forward, we recommend the inclusion of NFNE emissions within road transport emissions methodologies and within the COPERT framework. Road transport activity statistics are much more commonly reported worldwide than industrial sales of screenwash. This emission factor in a per kilometer form makes the calculation accessible for all. Moreover, road transport is a unique VOC source due to the co-emission of NO_x and the emission location largely occurring in heavily populated areas. Assignment of emissions via COPERT and vehicle mileage geolocates the VOC emissions where they actually occur, whereas the spatial desegregation of emissions of VOC in the industrial solvents class can often be represented as a uniform emission. This may help improve the performance of local to regional air pollution models. With bans on the sale of petrol and diesel vehicles starting as early as 2025 in some countries, it is crucial the atmospheric impacts of this transition are properly represented and monitored. For this, there is a clear benefit to having emissions associated with the correct sector. It

is possible, however, that the NFNE emission could be relatively straightforwardly reduced through policies (or voluntary schemes) that required product reformulation to remove VOCs of air pollution significance. Current approaches to VOC emissions control under EMEP and CLRTAP do not discriminate by VOC reactivity or photochemical ozone creation potential. Whilst this may not necessarily appear to be an optimal regulatory response, control of methanol and ethanol could be a potentially effective mechanism for a country to reduce overall mass emissions in response to further lowering of emission ceilings.

Bibliography

[1] McDonald, B. C., Gouw, J. A. de, Gilman, J. B., Jathar, S. H., Akherati, A., Cappa, C. D., Jimenez, J. L., Lee-Taylor, J., Hayes, P. L., McKeen, S. A., Cui, Y. Y., Kim, S.-W., Gentner, D. R., Isaacman-VanWertz, G., Goldstein, A. H., Harley, R. A., Frost, G. J., Roberts, J. M., Ryerson, T. B., and Trainer, M. Volatile chemical products emerging as largest petrochemical source of urban organic emissions. *Science* 359.6377 (2018), pp. 760–764. DOI: 10.1126/science.aaq0524.

[2] Timmers, V. R. and Achten, P. A. Non-exhaust PM emissions from electric vehicles. *Atmospheric Environment* 134 (2016), pp. 10–17. DOI: 10.1016/j.atmosenv.2016.03.017.

[3] Lewis, A. C., Hopkins, J. R., Carslaw, D. C., Hamilton, J. F., Nelson, B. S., Stewart, G., Dernie, J., Passant, N., and Murrells, T. An increasing role for solvent emissions and implications for future measurements of volatile organic compounds. *Philosophical Transactions of the Royal Society A* 378 (2020), p. 20190328. DOI: 10.1098/rsta.2019.0328.

[4] Winkler, S. L., Anderson, J. E., Garza, L., Ruona, W. C., Vogt, R., and Wallington, T. J. Vehicle criteria pollutant (PM, NO_x, CO, HCs) emissions: how low should we go? *npj Climate and Atmospheric Science* 1.25 (2018), pp. 1–5. DOI: 10.1038/s41612-018-0037-5.

[5] Li, J., Deng, S., Li, G., Lu, Z., Song, H., Gao, J., Sun, Z., and Xu, K. VOCs characteristics and their ozone and SOA formation potentials in autumn and winter at Weinan, China. *Environmental Research* 203 (2022), p. 111821. DOI: 10.1016/j.envres.2021.111821.

[6] Air Quality Expert Group. *Non-methane Volatile Organic Compounds in the UK*. https://uk-air.defra.gov.uk/library/reports.php?report_id=1003, accessed January 2023. 2020.

[7] Harrison, R. M., Allan, J., Carruthers, D., Heal, M. R., Lewis, A. C., Marner, B., Murrells, T., and Williams, A. Non-exhaust vehicle emissions of particulate matter and VOC from road traffic: A review. *Atmospheric Environment* 262 (2021), p. 118592. DOI: 10.1016/j.atmosenv.2021.118592.

[8] California Environmental Protection Agency Air Resources Board. *The California Consumer Products Regulations*. https://downloads.regulations.gov/EPA-R03-OAR-2018-0153-0009/content.pdf, accessed January 2023. 2010.

[9] National Institute for Public Health and the Environment. *Methodology for the calculation of emissions from product usage by consumers, construction and services*. https://www.rivm.nl/bibliotheek/rapporten/2021-0002.pdf, accessed January 2023. 2021.

[10] Hicks, W., Beevers, S., Tremper, A. H., Stewart, G., Priestman, M., Kelly, F. J., Lanoisellé, M., Lowry, D., and Green, D. C. Quantification of Non-Exhaust Particulate Matter Traffic Emissions and the Impact of COVID-19 Lockdown at London Marylebone Road. *Atmosphere* 12.2 (2021), pp. 1–19. DOI: 10.3390/atmos12020190.

[11] Wagner, R. L., Farren, N. J., Davison, J., Young, S., Hopkins, J. R., Lewis, A. C., Carslaw, D. C., and Shaw, M. D. Application of a mobile laboratory using a selected-ion flow-tube mass spectrometer (SIFT-MS) for characterisation of volatile organic compounds and atmospheric trace gases. *Atmospheric Measurement Techniques* 14.9 (2021), pp. 6083–6100. DOI: 10.5194/amt-14-6083-2021.

[12] NERC EDS Centre for Environmental Data Analysis. *NO and NO_y Abundance Data from Thermo Model 42i-Y NO_y Analyzer Instrument at the Manchester Air Quality Site, 2019 onwards*. https://catalogue.ceda.ac.uk/uuid/1d58f2f5e7874e55a83ca57311dcfb9a, accessed November 2022. 2022.

[13] NERC EDS Centre for Environmental Data Analysis. *Nitrogen Dioxide Abundance Data from Teledyne Model T500U Instrument at the Manchester Air Quality Site, 2019 onwards*. https://catalogue.ceda.ac.uk/uuid/f60761f3279042859e5c2902dfa0f2ef, accessed November 2022. 2022.

[14] NERC EDS Centre for Environmental Data Analysis. *Methane, Carbon Monoxide, Carbon Dioxide and Water Abundance Measurements from a Los Gatos Research Ammonia Analyzer Instrument at the Manchester Air Quality Site, 2019 onwards*. https://catalogue.ceda.ac.uk/uuid/671628b8f4474599ba074607e65c4bcc, accessed November 2022. 2022.

[15] Smith, D. and Španěl, P. Selected ion flow tube mass spectrometry (SIFT-MS) for on-line trace gas analysis. *Mass Spectrometry Reviews* 24.5 (2005), pp. 661–700. DOI: 10.1255/ejms.843.

[16] Horbanski, M., Pohler, D., Lampel, J., and Platt, U. The ICAD (iterative cavity-enhanced DOAS) method. *Atmospheric Measurement Techniques* 12.6 (2019), pp. 3365–3381. DOI: 10.5194/amt-12-3365-2019.

[17] Paul, J. B., Lapson, L., and Anderson, J. G. Ultrasensitive absorption spectroscopy with a high-finesse optical cavity and off-axis alignment. *Applied Optics* 40 (2001), pp. 4904–4910. DOI: 10.1364/AO.40.004904.

[18] Baer, D., Paul, J., Gupta, M., and O'Keefe, A. Sensitive absorption measurements in the near-infrared region using off-axis integrated-cavity-output spectroscopy. *Applied Physics B* 75.2 (2002), pp. 261–265. DOI: 10.1007/s00340-002-0971-z.

[19] Bukowiecki, N., Lienemann, P., Hill, M., Furger, M., Richard, A., Amato, F., Prévôt, A., Baltensperger, U., Buchmann, B., and Gehrig, R. PM10 emission factors for non-exhaust particles generated by road traffic in an urban street canyon and along a freeway in Switzerland. *Atmospheric Environment* 44.19 (2010), pp. 2330–2340. DOI: 10.1016/j.atmosenv.2010.03.039.

[20] Ferm, M. and Sjöberg, K. Concentrations and emission factors for PM2.5 and PM10 from road traffic in Sweden. *Atmospheric Environment* 119 (2015), pp. 211–219. DOI: 10.1016/j.atmosenv.2015.08.037.

[21] Department for the Environment Food and Rural Affairs. *Emissions Factor Toolkit (EFT) v11.0*. https://laqm.defra.gov.uk/air-quality/air-quality-assessment/emissions-factors-toolkit, accessed January 2023. 2021.

[22] Ricardo Energy & Environment. *Methodology for the UK's Road Transport Emissions Inventory, version for the 2016 National Atmospheric Emissions Inventory*. https://naei.beis.gov.uk/reports/reports?report_id=957, accessed January 2023. 2018.

[23] European Environment Agency. *EMEP/EEA air pollutant emission inventory guidebook, Report. No 13/2019*. https://www.eea.europa.eu/publications/emep-eea-guidebook-2019, accessed January 2023. 2019.

[24] Defra and BEIS. *National Atmospheric Emissions Inventory 2019 licenced under the Open Government Licence (OGL), Crown Copyright 2020*. naei.beis.gov.uk/data/, accessed Janurary 2023. 2020.

[25] Whalley, L. K., Stone, D., Dunmore, R., Hamilton, J., Hopkins, J. R., Lee, J. D., Lewis, A. C., Williams, P., Kleffmann, J., Laufs, S., Woodward-Massey, R., and Heard, D. E. Understanding in situ ozone production in the summertime through radical observations and modelling studies during the Clean air for London project (ClearfLo). *Atmospheric Chemistry and Physics* 18.4 (2018), pp. 2547–2571. DOI: 10.5194/acp-18-2547-2018.

[26] Department for Transport. *Road Traffic Forecasts*. https://www.gov.uk/government/publications/road-traffic-forecasts-2018, accessed January 2023. 2018.

[27] Jia, L., Xu, Y., and Shi, Y. Investigation of the ozone formation potential for ethanol using a smog chamber. *Chinese Science Bulletin* 57.34 (2012), pp. 4472–4481. DOI: 10.1007/s11434-012-5375-9.

[28] Willey, J. D., Avery, G. B., Felix, J. D., Kieber, R. J., Mead, R. N., and Shimizu, M. S. Rapidly increasing ethanol concentrations in rainwater and air. *npj Climate and Atmospheric Science* 2.3 (2014), pp. 1–5. DOI: 10.1038/s41612-018-0059-z.

[29] Carrière, A., Kaufmann, C., Shapiro, J., Paine, P., and Prinsen, J. H. The Contribution of Methanol (VOC) Emissions from Windshield Washer Fluid Use to the Formation of Ground-Level Ozone. *SAE Transactions* 109 (2000), pp. 227–234. DOI: 10.4271/2000-01-0663.

[30] Scovronick, N., França, D., Alonso, M., Almeida, C., Longo, K., Freitas, S., Rudorff, B., and Wilkinson, P. Air Quality and Health Impacts of Future Ethanol Production and Use in São Paulo State, Brazil. *nternational Journal of Environmental Research and Public Health* 13 (2016), pp. 1–13. DOI: 10.3390/ijerph13070695.

[31] Salvo, A. and Geiger, F. M. Reduction in local ozone levels in urban São Paulo due to a shift from ethanol to gasoline use. *Nature Geoscience* 7.6 (2014), pp. 450–458. DOI: 10.1038/ngeo2144.

[32] Dunmore, R. E., Whalley, L. K., Sherwen, T., Evans, M. J., Heard, D. E., Hopkins, J. R., Lee, J. D., Lewis, A. C., Lidster, R. T., Rickard, A. R., and Hamilton, J. F. Atmospheric ethanol in London and the potential impacts of future fuel formulations. *Faraday Discussions* 189 (2016), pp. 105–120. DOI: 10.1039/C5FD00190K.

[33] Fischer, E. V., Jacob, D. J., Yantosca, R. M., Sulprizio, M. P., Millet, D. B., Mao, J., Paulot, F., Singh, H. B., Roiger, A., Ries, L., Talbot, R. W., Dzepina, K., and Pandey Deolal, S. Atmospheric peroxyacetyl nitrate (PAN): a global budget and source attribution. *Atmospheric Chemistry and Physics* 14.5 (2014), pp. 2679–2698. DOI: 10.5194/acp-14-2679-2014.

[34] Wright, M. L. and Lewis, A. C. Emissions of NOx from blending of hydrogen and natural gas in space heating boilers. *Elementa: Science of the Anthropocene* 10.1 (2022). DOI: 10.1525/elementa.2021.00114.

[35] Cliff, S. J., Drysdale, W., Lee, J. D., Helfter, C., Nemitz, E., Metzger, S., and Barlow, J. F. Pandemic restrictions in 2020 highlight the significance of non-road NO_x sources in central London. *Atmospheric Chemistry and Physics* 23.4 (2023), pp. 2315–2330. DOI: 10.5194/acp-23-2315-2023.

[36] Bates, K. H., Jacob, D. J., Wang, S., Hornbrook, R. S., Apel, E. C., Kim, M. J., Millet, D. B., Wells, K. C., Chen, X., Brewer, J. F., Ray, E. A., Commane, R., Diskin, G. S., and Wofsy, S. C. The Global Budget of Atmospheric Methanol: New Constraints on Secondary, Oceanic, and Terrestrial Sources. *Journal of Geophysical Research: Atmospheres* 126.4 (2021), e2020JD033439. DOI: 10.1029/2020JD033439.

Chapter 5

Summary and conclusions

Outdoor air pollution is currently attributed to the premature mortality of 4.5 million people, the loss of 1.2 billion working days and $3.3 trillion in welfare costs every year globally. The reduction of air pollutant emissions has a clear benefit to society and is an area of international interest. Although some progress has been made, the WHO continues to reduce guideline values for air pollution exposure and the majority of the global population breathes air that exceeds these values. The 2020s mark a critical decade for the control of emissions. Decisions made over the next few years will determine the pathways followed in response to the Paris Agreement and international pledges to achieve net zero greenhouse gas emissions. Greenhouse gas and air pollutant emissions sources are closely related meaning these pathways will have a significant impact on air quality. It is a common opinion in air pollution research that the adoption of a pathway which does not also maximise air quality improvements would be a missed opportunity.

Policy decisions for the reduction of emissions rely on accurate data of the magnitude and location of emissions sources, commonly collated in an emissions inventory. However, emissions inventories have uncertainties and require continuous updating and verification as emissions sources change. As emissions from the dominant sources are reduced, previously minor

sources increase in their relative importance. However, by nature of being minor in the past, these other sources have usually received less attention and are prone to larger uncertainties. Having a good understanding of what sources will be important in the future is a crucial part of identifying strategies for air quality improvement.

Direct emissions measurements represent an effective way to verify and improve the accuracy of the emissions inventories used to inform current and future air quality policy decisions. This thesis describes the measurement and analysis of two unique data sets characterising real-world emissions of air pollutants that address uncertainties in sources of emerging importance. Since fossil fuel combustion in the road transport sector has dominated air quality issues in the European context, this research focuses on sources that remain following the control of emissions from that sector.

5.1 Contributions

The first emissions measurement application is a long-term NO_x flux data set discussed in Chapters 2 and 3. The data set is from an urban flux location from a tall tower in central London. At the time of writing, the number of long-term urban flux measurements is small, and those which measure air pollutant fluxes are even fewer. This data set is unique in that its location is within a megacity. With an increasing percentage of the population living in densely populated urban environments, the measurement location is perhaps what makes this data valuable and of potential international interest. This is especially the case with London being a world leader in road transport air quality policy. Generating an understanding of the effectiveness of such policies, and what sources dominate in the absence of road transport emissions, will help inform mitigation strategies in other cities.

A theme across these two chapters is the use of NO_x and CO_2 emissions together as a way of source apportioning emissions of NO_x. Measurements

during the 2020 and 2021 coronavirus pandemic mobility restrictions were used as a way of studying a likely future emissions scenario in which road transport emissions are significantly reduced. It was calculated that road transport NO_x emissions reduced by > 73 % since 2017 in the central area of London despite traffic flow reducing by only 32 %, and CO_2 emissions reducing by 20 %. In addition to the reduction caused by the ULEZ and natural fleet transition, a possible congestion-related factor was identified. Much enhanced NO_x flux was observed above $\sim$ 25000 vehicles hr^{-1}. This suggested that the incentivisation of public transport and green methods of travel (e.g. walking and cycling) to reduce congestion may be an even more effective way of reducing transport NO_x emissions than low emissions zones.

Following the large reduction in road transport emissions, the first indication of a now dominant heat and power generation sector was presented through spatial mapping. This was further investigated in the following two years of data. NO_x/CO_2 emission ratios were used to calculate that 76 ± 17 % of NO_x emissions in the measurement footprint came from the heat and power generation sector. For the measurement footprint, this was mostly due to natural gas combustion in commercial boilers for space heating. This was the first evidence of such a transition occurring in a city globally. International emissions inventories were shown to overestimate NO_x emissions from commercial gas boilers by reason of outdated emission factors. A NO_x/CO_2 emission ratio of 0.85 $\times 10^{-3}$, or 35% lower than that in the emissions inventories was calculated by taking into account recent legislation controlling NO_x emissions from boilers. Crucially, during the measurement period, all urban background sites within the measurement footprint vastly exceeded the WHO guidelines for ambient NO_2 concentrations. It was shown that even if all commercial boilers achieved current regulations, and road transport emissions were reduced to zero, WHO annual guidelines for NO_2 would not be achieved in the central area. This is the first indica-

tion that the heat and power generation sector would require policy consideration if WHO guidelines were to be achieved in densely populated urban environments with a similar climate to London. Future projections of fuel usage in UK urban environments required to meet net-zero pledges suggest that very low urban NO_2 concentrations are technically possible. However, the trajectory for urban NO_2 will depend in large part on choices made around urban buildings and their associated infrastructure and whether combustion or electrification pathways are delivered as part of urban decarbonisation.

The second emissions measurement application was a targeted approach to a specific source. Non-fuel-related air pollution emissions from road transport have received little attention in the past due to the prominence of fuel-related emissions. A pool of research studying non-exhaust PM from tyre and brake wear, and road dust resuspension is increasing in size since these emissions will be present despite fleet electrification. However, very little consideration has been given to non-exhaust VOC emissions. VOC emissions from road transport were quantified using a roadside increment-type methodology which identified a large source of alcohol species missing from international road transport emissions inventories. This was assigned to the application of screenwash with an emission of 58 ± 39 mg veh^{-1} km^{-1}, almost twice that of total exhaust VOC emissions. In contrast to widespread policy assumptions that the phase-out of gasoline and diesel internal combustion engines will over time lead to much reduced emissions of VOCs, these findings suggest that vehicle VOC emissions may actually increase given a predicted growth in total vehicle kilometers driven in a future electrified fleet. An improvement to road transport emissions inventories and the COPERT framework is recommended via the inclusion of this non-fuel-related emission factor. The research also highlights the source as a potentially interesting area for policy intervention for the achievement of emissions ceilings since it is responsible for around 6% of total UK VOC

emissions.

5.2 Future directions

The work presented here could be improved and extended in a number of ways. From the flux measurement perspective, continuing the NO_x and CO_2 measurements at the BT Tower would mean progress in reducing emissions could be tracked. The value of long-term data sets has been seen with concentration and indeed CO_2 flux measurements. An extension that includes NO_x flux measurements would facilitate the study of emissions changes that result from heat pump technology installation and the impact this has on NO_2 air quality. This is information that would be useful to those making decisions on which technology to adopt for the future heating of buildings that is not currently captured by national monitoring techniques. In this respect, an extension of the number of NO_x flux monitoring sites would give information on the spatial variability of urban air pollution emissions. This study only describes the situation in central London which is not necessarily applicable to other populated urban environments. Another obvious extension would be the measurement of additional flux species, such as O_3, VOCs and PM. This way the impact of the work could be broadened to the wider air quality issue rather than just NO_2. Measurements of additional species would also improve the source apportionment analysis capabilities, especially with PM and VOC speciation fingerprints. It is important to note, however, that this would significantly increase the data collection intensity. Finally, the verification of commercial boiler NO_x emissions in the field, as has been done previously with domestic boiler emissions, would be a nice addition to further verify this study. Their direct study would reduce the uncertainty associated with these measurements in which data is noisy and relies on a number of assumptions.

From the screenwash emissions work, there are a number of improve-

ments which could be made. The measurements would benefit from an increased time series length so that the emission factor uncertainty can be reduced and the seasonal variation better quantified. A better understanding of the spatial variability could be determined by measurements at different locations and road types. Factors such as the influence of weather on emissions could be studied as has been done previously with non-exhaust particulate matter. A greater VOC speciation through the use time of flight detection (as opposed to the SIFT-MS quadrupole) and other techniques such as gas chromatography may identify other non-fuel-related VOC emissions or screenwash components not detected in this analysis. Finally, atmospheric modelling studies which look at the impact of this source missing from road transport emissions inventories on atmospheric chemistry would help quantify the importance of these findings.

5.2.1 Final remarks

Air pollution and climate change continue to be a contentious political topic. At the time of writing, there is pushback on green policies such as the ULEZ, the banning of new sales of fossil fuel-powered vehicles, and the replacement of natural gas boilers. It is essential to continue to verify and update emissions data such that policy decisions are effective and backed up by evidence supported by accurate science. It is hoped that the benefit of these kinds of measurements has been highlighted in this thesis and that future research can build on them.